UNIVERSITY OF SOUTHAMPTON

EVALUATION OF BED SHEAR STRESS UNDER TURBID FLOWS THROUGH MEASURES OF FLOW DECELERATION

by

Maria Angelaki

A thesis submitted in partial fulfillment of the requirements for the degree of

Master of Philosophy

Faculty of Science, School of Ocean and Earth Science

June 2006

UNIVERSITY OF SOUTHAMPTON

ABSTRACT

FACULTY OF SCIENCE

SCHOOL OF OCEAN AND EARTH

SCIENCE

Master of Philosophy

EVALUATION OF BED SHEAR STRESS UNDER TURBID FLOWS THROUGH MEASURES OF FLOW DECELERATION

by Maria Angelaki

In previous work it has been observed that the direct application of the law-of-the-wall in flows of high concentrations of cohesive sediments, results in overestimation of the bed shear stress. In this experimental work the effect of various turbidity levels on the drag coefficient and shear stress over a smooth bed is investigated. For this purpose, turbid flows were simulated in a laboratory annular flume (the Lab Carousel), using kaolinite suspensions of different concentrations, varying from 0 to 60 g/l. Flow velocity measurements were taken in the turbulent boundary layer of hydraulically smooth flows and the values of bed drag coefficient and shear stress were calculated using the method of Flow Deceleration. The results obtained after the processing of the velocity time-series and the application of the Flow Deceleration method indicate that there is no evidence of shear stress modification for suspended sediment concentrations below 3 g/l. However, at higher concentrations the flow in the Lab Carousel exhibited different boundary layer characteristics. Therefore, the bed drag coefficient showed a significant response to the increase of the suspended clay concentration by decreasing up to ~ 50% from the clear water value over the range 3-60 g/l under a flow speed range of 0.8 m/s. The equivalent decrease in bed shear stress was calculated as ~ 40%. These results are in accordance with earlier findings of various researchers, thus confirming the validity of the Flow Deceleration method, used in accurate estimations of the bed drag coefficient and shear stress within the Lab Carousel.

Contents

List of Figures

List of Tables

Acknowledgements

This work was partially funded by the A. Papadakis grant of University of Athens, Greece. First of all I would like to express my thanks and appreciation to my supervisor, Prof. Carl Amos, for the valuable direction, advice and continued support he provided throughout this project, but most of all for his patience. I would also like to thank Prof. Mike Collins and Dr. Doug Masson for their help during an initial stage of the project. The laboratory work could not have been undertaken without technical support by Chris Mullen and John Davis, I really thank them. Dr. Charlie Thompson with her valuable experience provided necessary support during the start of the experimental measurements and also in the data processing. I am also deeply grateful to Dr. Valeria Quaresma for her continuous encouragement and support, but most of all for her friendship. Last but not least, I would like to thank Dr. P. Lappas for the appreciable advice he provided during the data processing. Finally, I would like to thank my mother, who was always behind me although suffering hard from her illness. I dedicate this thesis to her.

To my mother

1 Introduction

It is widely recognised that the boundary shear stress and the corresponding shear velocity are two very important parameters, used in many problems in river engineering. Such problems include determination of the resistance of a channel and its sediment-carrying capacity, bank erosion prediction, tractive force design for irrigation canals and also sidewall correction procedures for laboratory flume studies. On the other hand, the distribution of boundary shear stress around the wetted perimeter of a natural or artificial channel is influenced by various factors. Among them we can distinguish the cross-section of the channel, the boundary roughness and the sediment concentration. All of these factors act in combination and control the boundary shear stress distribution. This fact makes the prediction of the local shear stress at a particular point on a channel boundary a very difficult task. Many researchers have worked on the shear stress determination problem, considering various types of flows and channels (e.g. prismatic and non-prismatic open channels under sediment-free conditions, compound trapezoidal channels which are often typical of river cross-sections, etc.) and taking into account as many controlling factors as possible (Akan, 2001; Jin et al., 2004; Khiadani et al., 2005).

Furthermore, the drag coefficient is another key parameter, used both in the determination of the fluid drag force acting on a subaqueous boundary and in the estimation of the shear stress induced on the sea bottom by waves and currents. The latter has many applications in the study of erosion and sedimentation processes, including bed stability evaluation and sediment transport rate prediction (Grant & Madsen, 1979; Grant et al., 1984). Thus, it is widely recognised that the accurate knowledge of the boundary shear stress is necessary in the determination of initiation of sediment movement and the subsequent transport rates (Allen, 1977). The drag coefficient and the local boundary shear stresses are estimated by various techniques (Velocity Profile Method, Quadratic Stress Law, Reynolds Stress or Eddy Correlation Method, Turbulent Kinetic Energy Method, Pressure Gradient Method, Inertial

Dissipation Method) (Dyer, 1986; Thompson et al., 2003). However, all of these methods exhibit various problems when used in field applications, requiring more sophisticated measurements and analytical procedures and, therefore, they are considered as impractical. The drag coefficient is dependent on the boundary roughness and flow Reynolds number (Nikuradse, 1950). It also depends on the presence of suspended load (McCave, 1973; Ludwick, 1975) and large-scale bedforms. In some cases a constant value of the drag coefficient is considered, regardless the hydrodynamic roughness and flow strength (Sternberg, 1968; 1972). This fact makes the estimated values of shear stress less accurate. The present work is focussed on the determination of the shear stress exerted on a smooth boundary by flows transporting cohesive sediments in suspension.

Flows carrying clay material in suspension are common in a wide range of marine, fluvial and terrestrial environments, wherever a sufficient supply of sediment exists. They can be observed as river flows, subaerial mudslides and lahars, tidal currents in estuaries and on tidal flats, turbidity currents in marine basins, etc (Simpson, 1997; Leeder, 1999). Such flows and their characteristics have been experimentally studied by various researchers (Grant et al., 1984; Komar, 1985; Pantin & Leeder, 1987). From previous work it has been observed that turbulent seawater flows with low concentrations of suspended clay (<10 g/l) exhibit dramatically different boundary layer characteristics from clear water flows (Best & Leeder, 1993; Gust, 1976; Gust & Walger, 1976; Amos et al., 2003). In particular they show the phenomenon of drag reduction, which causes significantly lower friction factors and higher erosion thresholds than predicted by experimental data, obtained from clear water flows using the law of the wall for bed shear stress estimations.

This work aims to present the results of experiments on the effect of fine suspended sediment on the bed drag coefficient and bed shear stress, to interpret these results and compare them to the results obtained by other researchers. The laboratory simulations undertaken within this project deal with the determination of the drag coefficient of high density flows. It should be emphasized that the method used in the experiments is the flow deceleration method, which is based on Newton's second law and has been successfully used in clear water measurements by Thompson et al., (2004). It has been proven that with the use of the flow deceleration method, the estimation of the drag

coefficient over a wide range of Reynolds numbers can be accurate and fast. The experimental work was carried out in a laboratory annular flume – the Lab Carousel, and it consisted of flow velocity measurements of clay suspensions of various concentrations over a smooth flat bed.

In the following paragraphs a brief overview of each chapter of the thesis is given. In Chapter 2 a brief introduction in the fluid dynamics theory is given, concerning the motion of fluids. It aims to provide some theoretical background to the work described in chapters 4, 5 and 6. Chapter 3 contains a review on field and laboratory studies of sediment-laden flows, including complications due to the presence of the transported solid phase within the flow. The role of the drag reduction phenomenon is stressed, while emphasis is placed on the use of annular flumes in the investigation of turbid flows. In chapter 4 an overview of the laboratory procedure followed in this investigation is given, including description of the laboratory equipment and instrumentation used in the measurements, associated calibration curves, and detailed description of the undertaken series of experiments. The Flow Deceleration method is also presented, which forms the theoretical base further applied in the estimation of fundamental parameters (drag coefficient and shear stress). Chapter 5 contains the results obtained from the experimental runs in the Lab Carousel for the clear water flows and also the clay-water mixtures. The experimental results of chapter 5 are further discussed in chapter 6 and the conclusions are summarised in the subchapter 6.1. Finally, some certain directions to which the present work could be further extended are suggested, while Appendix A contains a published paper which is based on the work described in this thesis.

2 Fluid dynamics definitions

This chapter is focused on the background theory concerning the motion of fluids. Some basic aspects of fluid dynamics are presented, including physical properties of fluid phase, the boundary layers and the associated flow structures, flow regimes, friction factors and shear stress, sediment transport modes. The presence of suspended sediment in the flow is accordingly stressed, as it modifies the properties of the pure fluid phase.

2.1 Physical properties of fluids

Only the bulk properties of fluids, which depend on their molecular structure, are of great sedimentological interest. The **density (ρ)** is defined as mass (m) per unit volume and the units in SI are kg/m^3. The fluid density is a fundamental property as quantities like fluid momentum and effective (immersed) weight of solids immersed in fluids, depend on the mass per unit volume of the moving fluid. The density of a pure fluid phase is a function of temperature and pressure. For example, the density of fresh water is 1000 kg/m^3 at 4^{o}C, 999.0 kg/m^3 at 16^{o}C, 995.7 kg/m^3 at 30^{o}C, etc. However, in the case of most natural flows some complications arise due to the presence of the transported particulate matter. In such a case the effective bulk density (ρ_b) for unit volume is given by:

$$\rho_b = (1-c)\rho + c\sigma \qquad \text{Eq 2.1}$$

where ρ is the density of the pure fluid phase, c is the fractional concentration of the suspended sediments and σ is the density of the transported solids.

Dynamic or **absolute viscosity (μ)** is a physical property expressing the ease of deformation of a fluid or in other words it measures the resistance of a fluid to a change in shape. Viscosity controls the rate of deformation by an applied shear stress because the initiation and maintenance of relative motion between fluid layers requires some work against the resistive forces. Therefore, μ is a distinct property of a fluid and varies for different fluids. Dynamic viscosity is defined by Newton's relationship:

$$\tau = \mu \frac{du}{dy} \qquad \text{Eq 2.2}$$

where τ is the shear stress and du/dy is the velocity gradient (or strain rate). Thus, dynamic viscosity is the constant of proportionality, which relates shear stress to the strain rate. The SI units for dynamic viscosity are kg/ms or Ns/m^2 $(= Pas)$. Also $1\, g/cms = 1\, poise$ is often used as a dynamic viscosity unit. For example, at 15°C the absolute viscosity of fresh water is 1.14 centipoises while that of seawater is 1.22 centipoises (assuming $S = 35‰$). The viscosity of magmas is quite variable and some orders of magnitude higher than that of water. Obviously, a fluid of high dynamic viscosity will be 'thicker' than another fluid of a lower viscosity.

The fluid dynamic viscosity expresses the difficulty of the fluid molecules in moving fast relative to each other because of the mutual hindrance and the attractive forces, developed by the hydrogen bonding phenomenon. Dynamic viscosity is a function of temperature, while the effect of pressure is negligible. For example, the dynamic viscosity of water decreases with increasing temperature. This happens because the attractive forces among the water molecules decrease with increasing temperature. Furthermore, the addition of fine suspended material in a pure fluid phase can increase the viscosity of the sediment-water mixture (Figure 2.1). A possible explanation is that each solid surface within a fluid acts as a potential slip surface that increases the internal resistance to shear. Besides, the presence of suspended sediment load within a fluid flow has been extensively studied by many researchers, as the subsequent effect on the flow structure is of great sedimentological interest. Such aspects will be discussed in chapter 3.

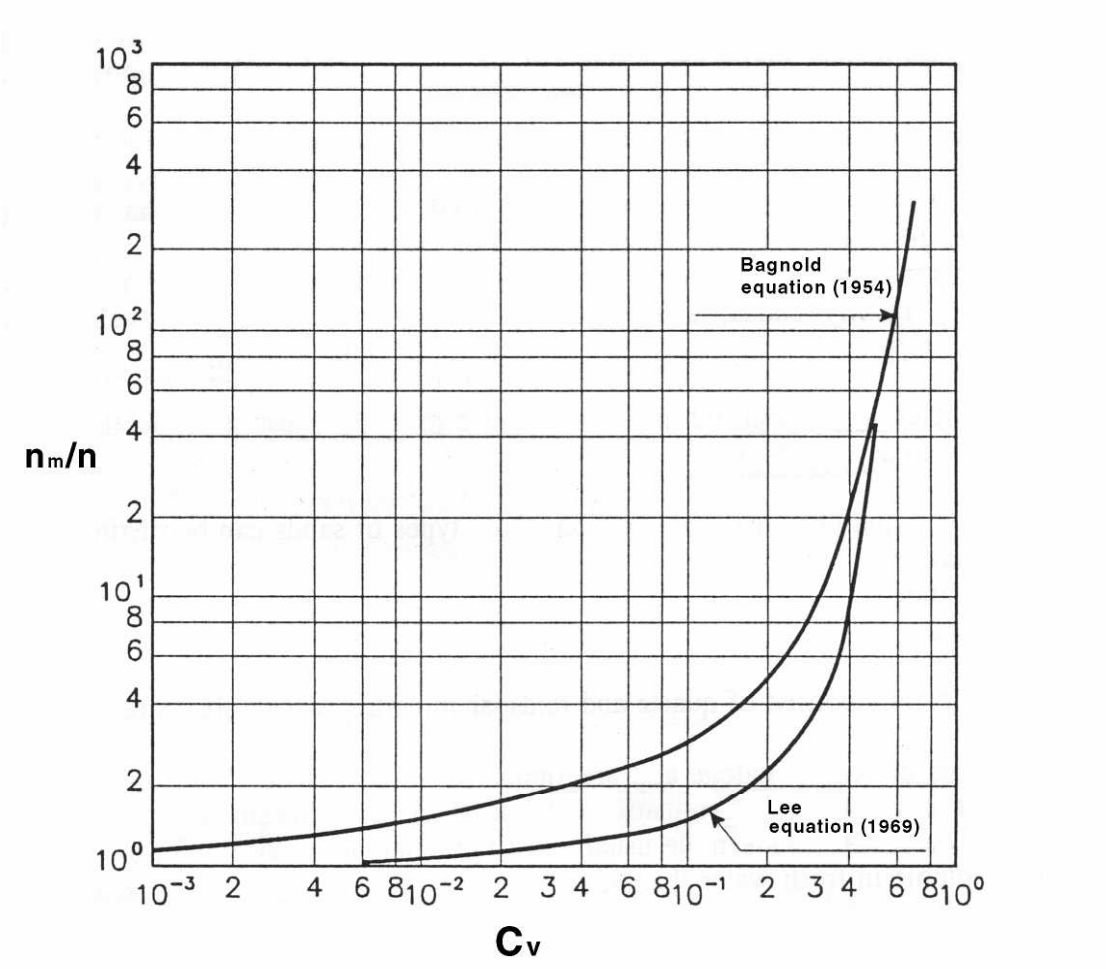

Figure 2.1 The dependence of dynamic viscosity coefficient (n_m / n) on the concentration of fine suspended sediment (n_m and n are the viscosity values of sediment-water mixture and clear water respectively, C_v is the volumetric concentration of suspended sediment) (Van Rijn, 1993).

The **kinematic viscosity (ν)** is another expression of viscosity and is derived by dividing the dynamic viscosity by fluid density:

$$\nu = \frac{\mu}{\rho} \qquad \text{Eq 2.3}$$

As it is known, there is a continuous transfer of fluid momentum from faster to slower moving layers within the flow. Thus there is a momentum flux toward the boundary, manifested by the shear stress in Eq 2.2. This momentum transfer is described by the ratio μ / ρ, which expresses the diffusivity of fluid momentum. In SI the units are

m^2/s. The dependence of kinematic viscosity on the temperature is illustrated in Figure 2.2.

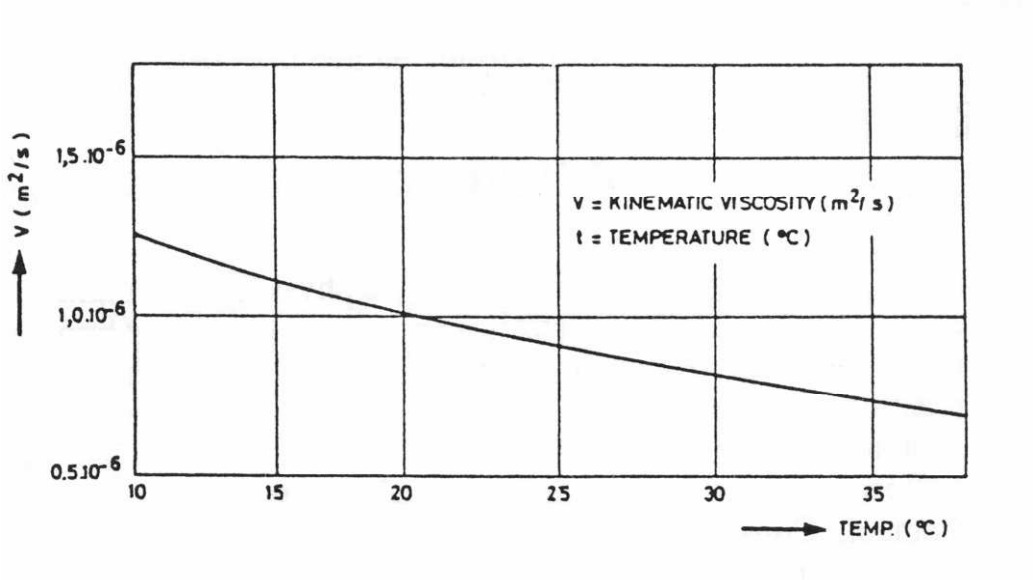

Figure 2.2 Kinematic viscosity (v) as a function of temperature (T) (Van Rijn, 1993).

2.2 Newtonian and non newtonian fluids

When a newtonian fluid moves then the shear stress due to viscous resistance in the flow is proportional to the gradient of the flow speed. Therefore, a newtonian fluid (e.g. clear-water) exhibits a dynamic viscosity which is constant at a constant temperature and is not affected by the shear rate, or in other words, the rate at which the newtonian fluid is strained does not influence the resistance to shear. This is depicted in Figure 2.3, where the shear stress-shear rate curve for a newtonian fluid is a straight line passing through the origin of the axes. The slope of the straight line equals to the dynamic viscosity of the fluid. Fluids containing a certain amount of suspended quartz particles show a similar behaviour, but their viscosity increases with the concentration of suspended particles. On the other hand, non-newtonian fluids exhibit a dynamic viscosity which varies with shear or strain rate (Figure 2.3). For example, fluids containing clay minerals in suspension are known to diverge from the newtonian response for clay concentrations above a certain value and for a proportion of clay minerals above 20 per cent (James and Williams, 1982) (Figure 2.4). Non-

newtonian rheologies are typical of many natural flows, such as water-saturated muds (fluid muds), while this non-newtonian response plays an important role in the processes of slumping, sliding and avalanching.

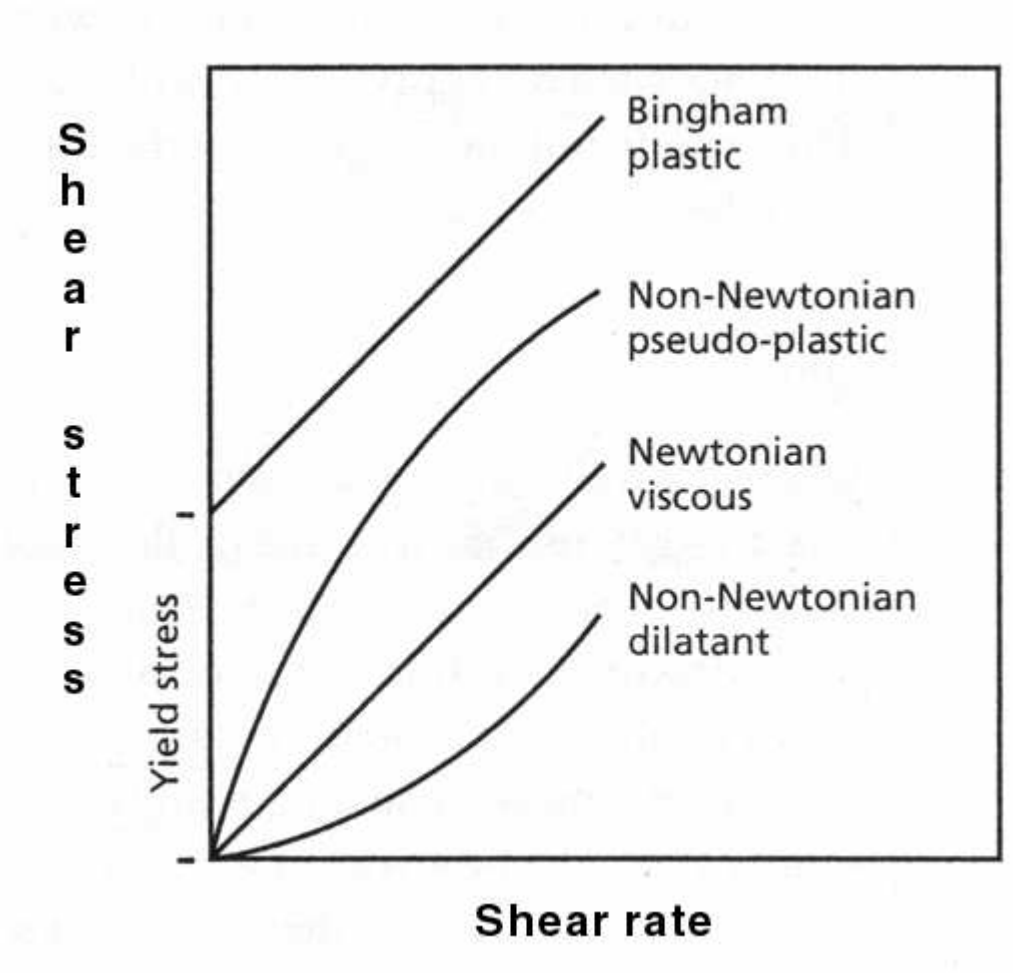

Figure 2.3 Shear stress plotted against shear rate for materials of different rheological behaviour (Leeder, 1999).

Based on the behaviour of substances under shear, several types of rheological response can be distinguished (Figure 2.3). In pseudoplastic (non-newtonian) materials the dynamic viscosity (μ) is high at low shear rates but decreases with increasing shear rate up to a constant value. Such substances are also known as shear-thinning, e.g. muddy fluids, showing a structure of interacting clay particles that increase the fluid's overall resistance to the flow. As the shear rate in a muddy fluid increases, this structure is gradually destroyed and then the shear-thinning behaviour is produced (Dyer, 1986). Dilatant (non-newtonian) fluids are those whose dynamic

viscosity (μ) increases with the shear rate. This type of rheological response is common in some polymer suspensions. Bingham plastic substances show a Newtonian behaviour, as the dynamic viscosity remains constant under increasing shear rates. However, an initial shear stress, termed as the 'yield stress', must be applied before strain occurs. The Bingham yield stress arises due to residual effect of particle interaction and is related to the magnitude of the attraction among the particles. Examples of natural flows showing plastic behaviour are lava and debris flows. In such flows, a finite yield strength allows morphological features like levees, flow snouts and flow wrinkles to be preserved during flow and after motion has stopped, while particle settling is likely to be hindered or even impossible.

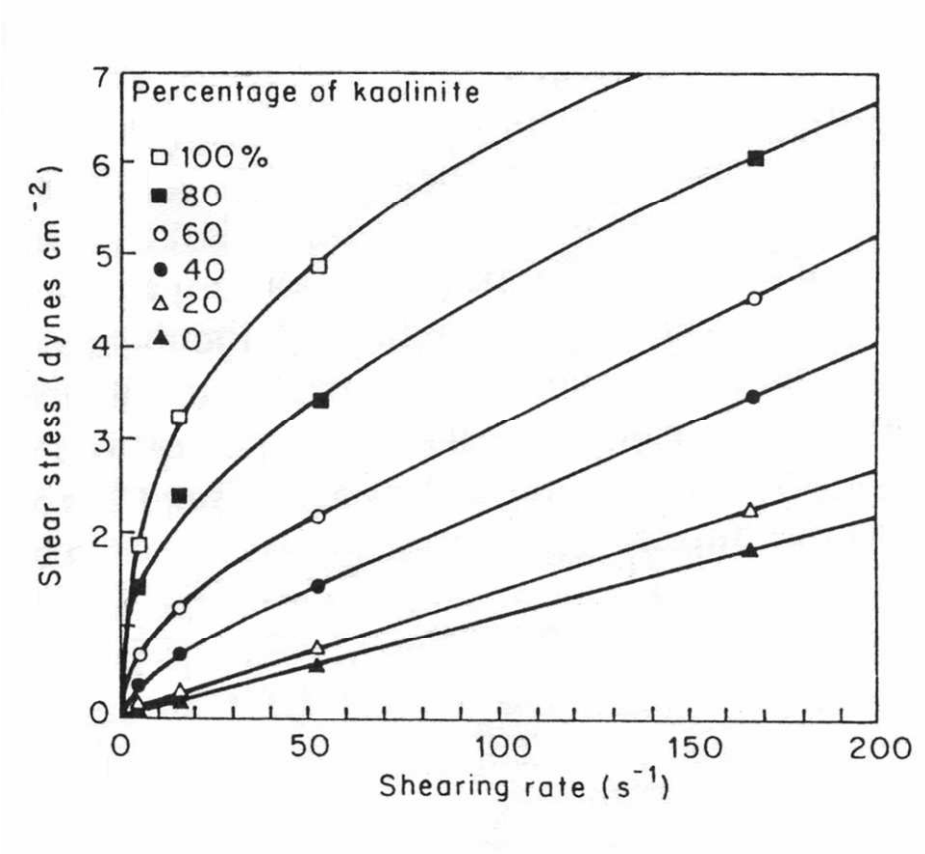

Figure 2.4 Rheological behaviour of quartz/kaolinite mixtures in suspension for varying percentages of kaolinite (Volumetric concentration is 0.2%) (James & Williams, 1982).

Some examples of geophysical flows, driven by various mechanisms and showing a Newtonian-flow type are the following: a) surface water flows in river and delta channels, driven by gravity b) gravity driven tidal flows c) ocean surface currents

driven by wind shear, pressure gradients and Coriolis force d) deep ocean currents driven by gravity acting on density contrasts, which are caused by salinity differences and differential heating or cooling. On the other hand, mass flows of sediment and water exhibit density contrasts due to the presence of suspended sediments, e.g. debris flows and turbidity currents. Such flows are also driven by gravity forces but show a flow type which varies from non-newtonian to newtonian (Leeder, 1999).

2.3 Newton's laws in Fluid Dynamics

Newton's laws of motion are very important in fluid dynamics, as they govern the motion of all fluids. According to the first law, known also as the 'principle of inertia', a constant mass of a fluid will remain still or continue to move along the same direction at a constant velocity, provided that none externally applied force is acting on this mass.

In the second Newton's law it is stated that the magnitude of an externally applied force equals to the rate of change of momentum that takes place along the direction of the force. Therefore, the magnitude of a force can be calculated according to the produced acceleration or deceleration. The momentum per unit volume of a fluid of a constant density is ρu, thus the rate of change of this momentum is:

$$F = \rho \, du / dt \qquad \text{Eq 2.4}$$

According to second law, the temporal and spatial variations of flow velocity result from pressure gradients, generated within the flow. Such pressure gradients are caused by forces, the magnitude of which can be estimated according to Newton's second law (Allen, 1985). These forces are those controlling the rate of sea-bed erosion and deposition, hence their accurate evaluation is fundamental in sediment transport investigations. Additionally, the Newton's second law (Eq 2.4) constitutes the physical background for the development of the Flow Deceleration method, described in chapter 4.

Finally, the third law states that the force exerted by one fluid/solid mass on another fluid/solid mass is equal and opposite to the force it experiences from the other mass. This law is applied to flows where velocity gradients are developed, e.g. within boundary layers. Then the shear stress exerted on the top surface of a thin fluid layer is opposed by an equal stress exerted below. Even in ideal flows, where frictional forces grown at solid boundaries are assumed to be negligible, Newton's third law applies and the fluid force is acted upon by an equal and opposite reactive force from the bed. However, in natural flows the movement of a fluid over a bed is strongly affected by frictional drag developed within a relatively narrow zone, the boundary layer (§2.4). In this zone the flow speed is decreased relative to the current speed away from the solid boundary.

2.4 The dynamics of the flow

Various aspects in fluid dynamics are approached by considering 'ideal' flows of inviscid fluids. Such 'ideal' fluids are characterized by zero viscosity ($\mu = 0$) and they don't show any resistance to the flow. Consequently, they don't develop frictional forces on their boundaries. However, this does not hold true in the case of natural flows of non-ideal fluids. Whenever a real fluid moves over a solid boundary, frictional drag forces are developed, decreasing the velocity within a narrow zone close to the boundary. The fluid molecules in immediate contact with the boundary, attach to it and form an adsorbed layer which is stationary relative to the free-stream flow. Obviously, the flow velocity decreases from its free value away from the boundary to almost zero at the boundary. Such zones of flow retardation are known as **boundary layers** (Figure 2.5). A boundary layer is formed every time a real fluid moves over a sediment-substrate or through a channel or around a fixed object or even when an object is moving relative to a stationary fluid mass (e.g. settling of particles). The flow velocity increases with the distance above the boundary, until it reaches its free-stream value. A boundary layer is characterized by the presence of velocity gradients and shear stresses, developed due to viscous and inertial forces.

If we consider a fluid moving over a flat plate with a uniform velocity u_{max} then a boundary layer will be formed, thickening downstream from the leading edge (Figure 2.5). Three sections can be distinguished. In the initial part the flow will remain laminar over some distance from the edge and the thickness (δ) of the boundary layer will increase with the square root of the distance x from the edge (Schlichting, 1951):

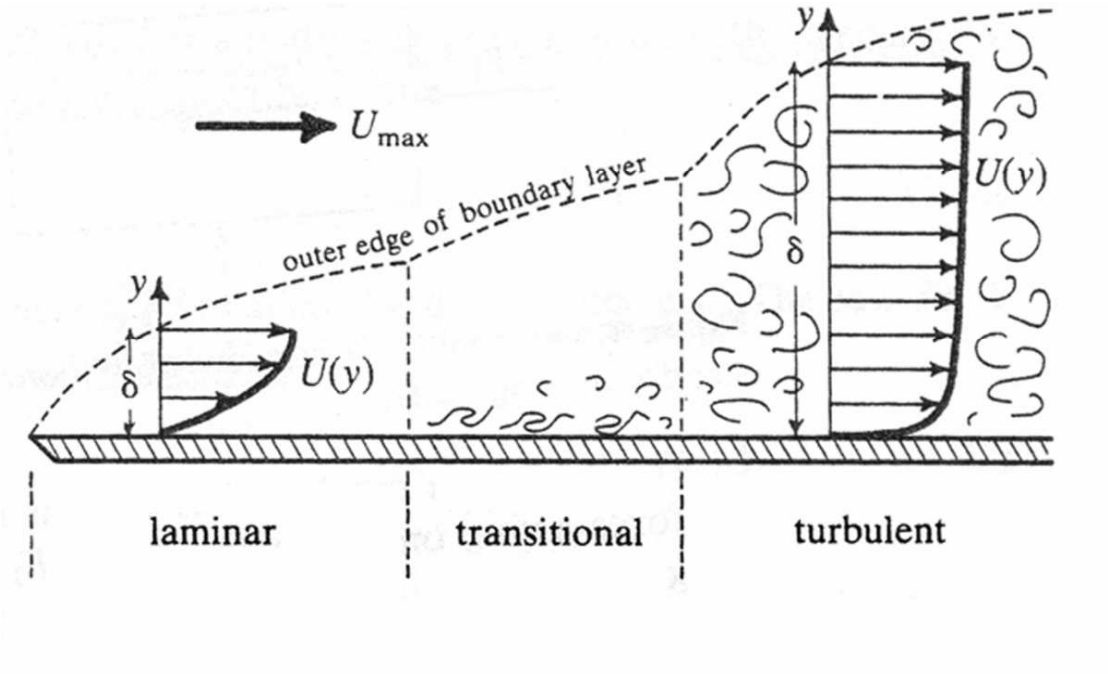

Figure 2.5 The boundary layer developed over a flat plate (Leeder, 1999).

$$\delta = 5\left(\frac{\mu x}{\rho \bar{u}_{max}}\right)^{1/2} \qquad \text{Eq 2.5}$$

where μ is the dynamic viscosity and ρ is the fluid density. Within the laminar boundary layer the time-averaged velocity at a fixed point will be exactly the same as the instantaneous velocity at that point. The velocity distribution is described by:

$$u = \frac{\tau}{\mu}(y - \frac{y^2}{2\delta}) \qquad \text{Eq 2.6}$$

where u is the flow speed at height y above the boundary, τ is the shear stress at the boundary, μ the viscosity and δ the boundary layer thickness (Leeder, 1999). Setting $y = \delta$ and $u = u_{max}$, where u_{max} is the flow velocity outside the boundary layer, Eq 2.6 yields:

$$\tau = \frac{2\mu u_{max}}{\delta} \qquad \text{Eq 2.7}$$

Eq 2.7 shows that the shear stresses associated with laminar boundary layers are very small. The thickness of the laminar boundary layer continues to increase with the distance along the plate so that at a certain distance the motion is not stable any more and starts to be turbulent. Then fluid eddies start to develop and the boundary layer becomes transitional. Finally, beyond some critical distance the inertial forces will dominate and the flow will become fully turbulent. The velocity distribution within the turbulent boundary layer is given by:

$$\frac{u}{u_{max}} = (\frac{y}{\delta})^n \qquad \text{Eq 2.8}$$

where u is the local time-averaged velocity. The exponent n varies from about 1/5 near transition to about 1/7 further downstream (Leeder, 1999).

The turbulent boundary layer formed over a smooth boundary can be divided in three regions (Figure 2.6). The **viscous sublayer** is a thin zone, lying immediately adjacent to the boundary where the flow velocity is low. The velocity gradient within the viscous sublayer is almost constant. The shear stress is controlled by dynamic viscosity μ and is given by Newton's viscous stress equation (Eq 2.2, $\tau = \mu \frac{du}{dy}$) or

$$u = \int \tau \frac{1}{\mu} dy = \frac{\tau y}{\mu} \qquad \text{Eq 2.9}$$

The thickness δ' of the viscous sublayer is experimentally defined (Sleath, 1984) as:

$$\delta' = 11.5\nu / u_*$$ Eq 2.10

The quantity u_*, is the **shear or friction velocity** and has the dimensions of velocity. It is defined as:

$$u_* = \sqrt{\tau / \rho}$$ Eq 2.11

where τ is the shear stress exerted on the boundary by the fluid and ρ is the fluid density. The shear velocity u_* is directly proportional to the rate of increase of fluid velocity with height, and it is therefore proportional to the slope of velocity distribution curve.

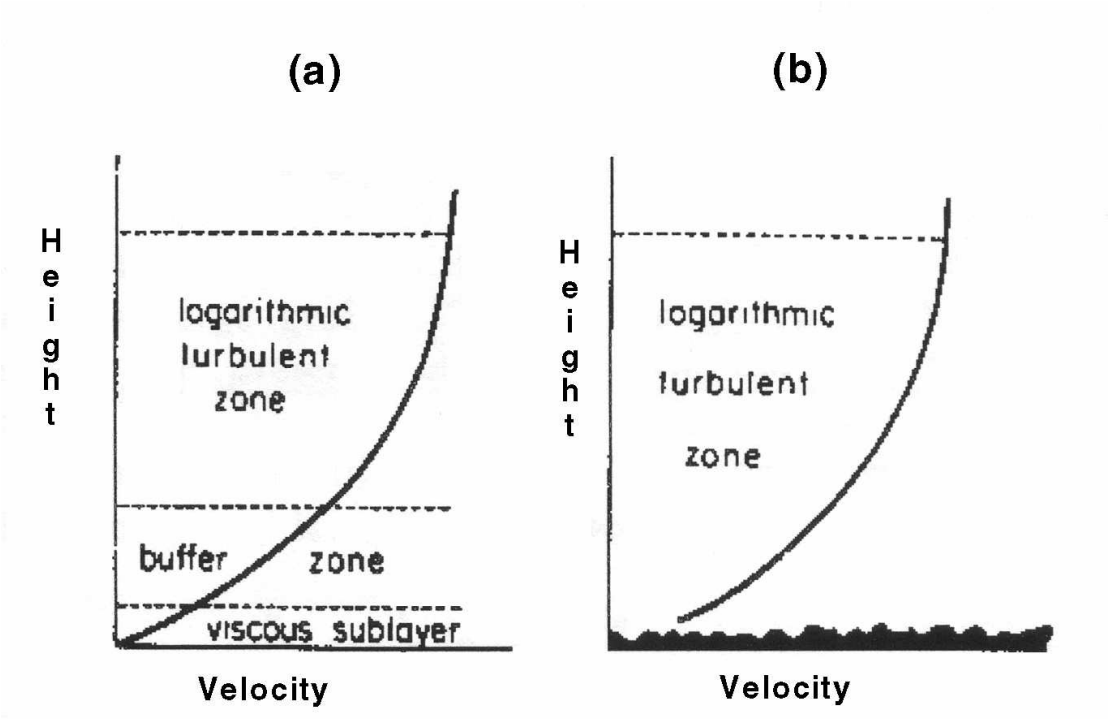

Figure 2.6 Turbulent boundary layers formed above smooth (a) and rough (b) boundaries (Komar, 1976).

Further out into the turbulent boundary layer and above the viscous sublayer the **logarithmic sublayer** is found, where the rate of du/dy decreases with height. Within the logarithmic sublayer the turbulent transfer of momentum dominates over

the viscous transfer. Based on the assumption that du/dy decreases with the distance from the boundary, we get: $\frac{du}{dy} \propto \frac{1}{y}$ or $u = k\int \frac{1}{y} dy$ or

$$u = k \log_e y + c \qquad \text{Eq 2.12}$$

where k and c are constants. A fuller form of the above equation is called the Prandtl's 'law of the wall' and provides the variation of streamwise velocity with height in turbulent flows (Coleman, 1981). The lower part of the logarithmic layer merges into the linear viscous sublayer via a narrow zone, which is known as the **buffer layer** (or **equilibrium layer**). In this zone the viscous and turbulent transfer of momentum are comparable. In Figure 2.6 the turbulent boundary layers developed over a smooth and a rough boundary are depicted. The presence of boundary roughness disrupts the viscous sublayer and the logarithmic zone extends to the boundary.

In Figure 2.7 the mean flow velocity measured across a smooth boundary, is plotted against height above the sea-bottom. The upper line, corresponding to the logarithmic sublayer, is a least-squares fit of a logarithmic form to flow velocities measured at 1 cm above bottom. The lower part of the plot represents a linear fit to flow velocities measured at heights below 0.6 cm and corresponds to the viscous sublayer.

The flow boundary roughness can be defined by comparing the thickness of the viscous sublayer of turbulent flows to the size of sediment grains or boundary irregularities. **Smooth** boundaries are those, whose roughness elements of sedimentary particles are completely enclosed within the viscous sublayer and consequently they develop only viscous forces. When the particles project through the sublayer, they favour the growth of eddies and the boundary is said to be **transitional** or **rough**, depending on the degree of penetration.

The turbulent eddies are able to transfer fluid momentum normal to the boundary within a turbulent boundary layer. This suggests that the viscosity of a turbulent fluid is some orders of magnitude higher than the true viscosity due to eddy viscosity. Therefore, the turbulent boundary layer exerts a much greater shear stress than a

laminar one. The turbulent viscosity is not a constant, so the shear stress has generally to be calculated empirically.

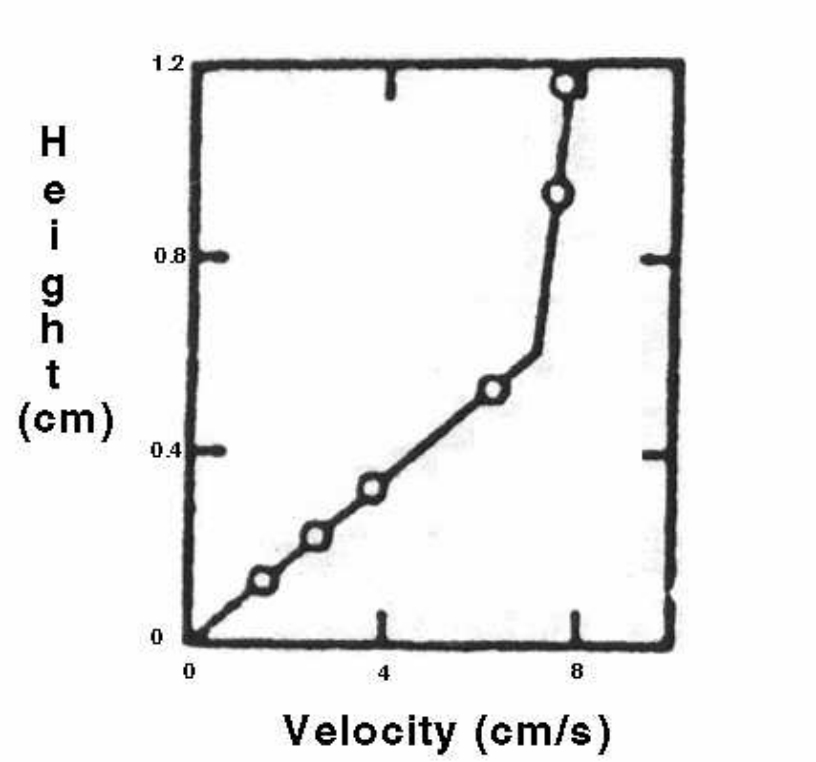

Figure 2.7 Mean flow velocity versus height above the sea-bed (Caldwell, 1979).

2.5 Reynolds number and flow regimes

Osborne Reynolds observed in 1883 that two distinct flow types can be distinguished: laminar or viscous flow at low flow velocities and turbulent flow at high flow velocities. Considering fluids of different viscosity flowing through pipes of various diameters, the change from laminar to turbulent flow was found to occur at a fixed value of a dimensionless parameter, known as the **Reynolds number (Re)**. It is:

$$\mathrm{Re} = \frac{ud}{\nu} \qquad \text{Eq 2.13}$$

where u is the mean flow velocity, d is the internal diameter of pipe and ν is the kinematic viscosity of the fluid. In the case of a river flow, the diameter d in Eq 2.13

is substituted by the hydraulic radius of the channel which equals the mean flow depth if the channel width is much greater than water depth.

The Reynolds number is a manifestation of the effect of viscous forces relative to inertial forces acting on a fluid. When Re is low, then viscous forces dominate and the flow is said to be **laminar**. A laminar flow is stable and the fluid particles move along definite straight trajectories. When Re is high, then inertial forces dominate and the flow is **turbulent**. A turbulent flow is characterised by irregularities or disturbances, which lead to the formation of eddies, diffusing across the flow as well as moving in the mean direction of the flow. In such a flow the fluid particles move along random fluctuating trajectories. The turbulent flow can be considered as a complex motion where random velocity fluctuations (due to the motion of eddies) are superimposed on the average motion of translation. The turbulent eddies can transfer momentum normal to the flow boundary at a rate much higher than the molecular transfer in laminar flows. In this case an additional resistance to the flow arises, expressed by the **eddy viscosity**, which is not constant for a given fluid and temperature. As an example, many water flows in rivers are turbulent. The change from laminar to turbulent flow conditions occurs progressively, over a range of values of Re. Within this range the flow is characterised as **transitional**. In open-channel flows, the transitional range of Re values is between 500 and 2000 (Leeder, 1999). For Reynolds numbers higher than 500, instabilities develop within the flow, which gradually becomes fully turbulent. The critical value of Re depends to some extent on the number of irregularities and obstacles, present on the channel bottom. For example, an open channel flow over a smooth bottom could remain laminar for $Re > 500$ and up to $Re = 2000$. However, in natural channels with a rough bottom the critical value of Re is low, as the bottom irregularities favour the growth of turbulent eddies and the transition to turbulent conditions. In natural flows the laminar conditions are very rarely observed, as turbulent flows dominate. The only exception is very close to a sufficiently smooth boundary, where the viscous sublayer can develop with viscous stresses dominating over turbulent stresses.

Furthermore, the grain Reynolds number (Re_*) is defined as:

$$\mathrm{Re}_* = \frac{u_* k_s}{\nu} \qquad \text{Eq 2.14}$$

where u_* is the shear velocity and k_s is the grain effective roughness height (Allen, 1985). Combination of Eq 2.10 with Eq 2.14 gives:

$$\mathrm{Re}_* = 11.5\frac{k_s}{\delta'} \qquad \text{Eq 2.15}$$

The grain Reynolds number (Re_*) is proportional to the ratio of the grain effective roughness height (k_s) to the thickness of the viscous sublayer (δ'). Thus, it provides a measure of grain protrusion through the viscous sublayer, which is further used in defining whether turbulent eddies are produced. When Re_* is less than 5, the bottom roughness has a negligible effect on the flow and the bottom is considered as smooth. For Re_* higher than 70, the viscous sublayer is completely disrupted and the bottom is considered to be rough. In such a case, viscosity appears to have a low effect on the mean flow. The change from smooth to rough boundary conditions occurs within the transition region $5 < \mathrm{Re}_* < 70$ (Schlichting, 1979).

2.6 Energy losses and friction factors

According to Newton's second law (see §2.3) when a fluid is moving over a solid boundary with a constant velocity then frictional forces arising from viscosity and turbulence, act on fluid elements in a direction opposing the fluid motion. Thus, in a steady flow of a non-ideal fluid there will be a continuous loss of energy due to friction and subsequently the total energy of the flow will decrease along a streamline because of energy dissipation.

In a moving fluid the energy dissipation is manifested by two ways: either by **'skin friction'** (expressed by stationary grain roughness) or '**form drag'**, which arises from the generation of eddies around bedforms. Additionally, energy dissipation is caused

whenever a fluid mass moves past a bend of the flow-channel or constricts or expands. Besides, due to sediment transport a mobile bed layer (bedload) is formed, causing further energy loss. All the previous forms of energy losses can be included in a synoptic friction coefficient for a particular flow. The friction factor f is dimensionless and is given by the ratio of shear stress τ, exerted by the flow on the surface of a solid boundary to the mean kinetic energy per unit volume, or:

$$\tau = f(\frac{1}{2}\rho u^2) \qquad \text{Eq 2.16}$$

Eq 2.16 is known as the **'quadratic stress law'**. The coefficient of proportionality f is called **drag coefficient** and expresses in a non-dimensional way the drag, which is exerted by the moving fluid to the solid stationary bed. Friction coefficients describe the total drag, including form and skin friction. Depending on how the proportionality factor is defined, the quadratic stress law appears in different forms. Regarding an object, which is moving within a stationary enclosing fluid, Eq 2.16 is written as:

$$\tau = c_D(\frac{1}{2}\rho u^2) \qquad \text{Eq 2.17}$$

where c_D is the drag coefficient. For channelized flows it is:

$$\tau = \frac{f}{4}(\frac{1}{2}\rho u^2) \qquad \text{Eq 2.18}$$

where the constant of proportionality is known as the Darcy-Weisbach friction coefficient.

A great variety of processes can affect the frictional dissipation of energy within a fluid flow and the subsequent friction factors. For example, friction coefficient f is strongly dependent on Reynolds number for laminar to transitional flows (Shames, 1962). For fully turbulent flows f is more or less independent of Reynolds number, however, it depends on the boundary roughness. In particular, f increases with increasing relative roughness, with relative roughness being the ratio of roughness

diameter to flow thickness. In the same way, the drag coefficient in a fully developed turbulent flow through a pipe depends on the wall roughness of the pipe (Nikuradse, 1950). Additionally, the bed drag coefficient can vary over a mobile sea bed (McCave, 1973) or due to bed-form development (Dyer, 1980) or in response to changes in the flow regime (Sternberg, 1968). The drag coefficient of a fixed bed is also known to vary, either with the direction of tidal current relative to bed forms (McCave, 1973) or due to the existence of waves, which interact nonlinearly with the steady flow within the wave boundary layer (Grant and Madsen, 1979; Green et al., 1990). Finally, the presence of saltating particles which act as a momentum sink, can differentiate the drag coefficient (Smith and McClean, 1977; Grant and Madsen, 1982), while the suspended particulate matter within a flow can cause a stable stratification of the boundary layer, thus considerably affect the observed values of drag coefficient (Huntley et al., 1994; Green and McCave, 1995).

The drag coefficient is considered a very important parameter, used in the evaluation of the shear stress induced on the sea bottom by the overlying flow. For example, in the quadratic stress law if the value of the drag coefficient at a fixed height above sea bed is accurately known, then the unknown shear stress can be estimated from a single measure of flow velocity at the considered height. This takes away the need for obtaining the complete velocity profile and then determining the shear stress using the law of the wall (Sternberg, 1968; Yalin, 1972). Sternberg (1968, 1972) calculated an average value for the drag coefficient for fully developed turbulent flows, through numerous measurements of velocity profiles in Puget Sound, Washington. He proposed:

$$C_{D100} = 3.1\times10^{-3} \qquad \text{Eq 2.19}$$

where C_{D100} = the drag coefficient at 100 cm above the sea bed. The use of the constant C_{D100} seemed very practical, as the bottom stress could be easily determined from a single measured value of flow velocity at 100 cm above the sea bottom. However, the obtained values of shear stress proved to be inaccurate under certain circumstances, as the use of Sternberg's constant drag coefficient showed two limitations. First, the large-scale bedforms (ripples, dunes, sand waves) are not taken

into account, although they provide higher resistance to the flow and so affect the value of C_{D100}. The second limitation is that the use of a mean constant C_{D100} assumes the absence of suspended sediment in the flow, which is not usually the case. Consequently, the generalised use of a constant value of drag coefficient, irrespective of flow strength, the presence of bedforms and suspended particulate matter could lead to erroneous shear stress estimations.

The friction coefficients are generally determined experimentally. In particular, the calculation of the bed drag coefficient in natural marine settings is difficult, as it is based on some conventionally used methods. The most common method is the velocity profile method, which requires velocity measurements on a vertical array within the boundary layer. Large sources of error are involved in this method, including noise in velocity measurements, inaccurate knowledge of the position of measurements relative to the bed, etc. Other conventional methods include the use of hot-film probes, which relate the heat dissipation directly to shear stress (Graham et al., 1992) and the measurement of Reynolds stresses near the boundary (Soulsby, 1983). This method is very sensitive to sensor misalignment and can give large errors of 156 % per degree of misalignment in wave-dominated environments (Soulsby and Humphrey, 1989). It is concluded that the routinely used methods of determining the bed drag coefficient show various problems when used in field applications and their use is based on assumptions, which should be carefully considered under certain circumstances.

2.7 The boundary shear stress - measurement techniques

In sediment transport investigations and particularly in predictions of movement initiation of sediment particles, a key parameter is the bottom shear stress (τ) exerted by the fluid which is moving over a sandy or cohesive substrate. Therefore, in such investigations the objective is the estimation of the fluid shear stress on the boundary and this can be achieved by several methods in the case of an assumed steady two-dimensional turbulent flow (in an open channel). The methods include the Velocity Profile method (Bowden, 1962; Sternberg, 1968; Yalin, 1972; Li & Gust, 2000) and the Quadratic Stress Law (Sternberg, 1968; McCave, 1973; Ludwick, 1975; Soulsby,

1983), which are considered as the most commonly used techniques. All of the conventionally used methods show some advantages but at the same time include sources of error and/or require measurement techniques which are not simple, hence they are not characterised by the ease of application.

In the velocity profile method, the mean flow speed is measured at a few levels within the water column. Assuming a logarithmic profile, the mean flow speed ($\bar{u}_z$) at a given distance (z) above the sea-bottom is related to the bottom shear stress by the Karman-Prandtl equation:

$$\bar{u}_z = \frac{u_*}{k} \ln\left(\frac{z}{z_o}\right) \qquad \text{Eq 2.20}$$

where u_* is the friction velocity $(\tau/\rho)^{1/2}$, k is von Karman's constant and z_o is the roughness length (generally increasing with the boundary roughness). The measured values of $\bar{u}_z$ are plotted against z on a semi-logarithmic scale and the slope of the velocity profile gives the boundary shear stress (τ). The application of this method is based on the assumption of a steady flow and a constant shear stress above the boundary. Consequently, a large scatter in the values of u_* and z_o can be obtained and this can be attributed to many reasons, including flow unsteadiness, noisy velocity measurements, inaccurate determination of the height of velocity measurements, varying bottom roughness. In addition, the drag form (if present) is not considered as well as the presence of suspended sediments, which change the value of k (Sternberg, 1972).

According to Quadratic Stress Law equation, the boundary shear stress is proportional to the fluid density and the square of the mean flow speed measured at a distance z from the boundary. Considering the bed drag coefficient C_{D_z} at height z as the coefficient of proportionality, the Quadratic Stress Law is given by:

$$\tau = C_{D_z} \rho \, \bar{u}_z^{\,2} \qquad \text{Eq 2.21}$$

Eq 2.21 relates the shear stress at the boundary to a single measured value of the flow velocity within the boundary layer. The main advantage of the method is the simplicity in its application. However, the use of the quadratic stress law is based on a logarithmic velocity distribution, which is not always the case. For example, it has been demonstrated that during various tidal flows, logarithmic velocity profiles occurred between 62% and 100% of the time (Sternberg, 1968). Consequently, a certain degree of uncertainty is introduced in the use of the quadratic stress law method when it is applied in shear stress estimations.

Furthermore, the boundary shear stress τ can be estimated using the 'eddy correlation method' (Soulsby, 1983), by measuring directly the Reynolds stresses in the constant stress layer of the flow:

$$\tau = -\rho \overline{u'v'} = const \qquad \text{Eq 2.22}$$

where u' is the longitudinal fluctuating component of velocity and υ' is the vertical fluctuating component of velocity. The overbar in Eq 2.22 indicates the mean value. This method is particularly sensitive to sensor misalignment and can give errors up to 156 percent per degree of misalignment under specific conditions (Soulsby and Humphrey, 1989). Although the method assumes the existence of a constant stress layer, it is known that the shear stress can also fluctuate with the distance from the boundary. In hydraulically smooth flows, the 'gradient method' is used for accurate determination of the bottom shear stress by mean flow measurements within the viscous sublayer:

$$u_* = (\nu \, d\bar{u}/dz)^{1/2} \qquad \text{Eq 2.23}$$

In flume experiments the 'energy slope method' is often used for shear stress estimation:

$$\overline{\tau} = \rho \, gRS \qquad \text{Eq 2.24}$$

where g is the gravity acceleration, R is the hydraulic radius of the flume, and S is the surface slope. Shear stress values calculated by Eq 2.22 and Eq 2.23 are local boundary stresses, while that obtained by Eq 2.24 is a bottom shear stress averaged over the entire flume. The latter value is not as accurate as the local stresses because it is affected by: the non uniform distribution of τ along the flume walls, the side-wall effects and the secondary currents (§ 3.3).

2.8 Sediment transport modes

The motion of the transported sediment particles normally takes place in three distinct modes: rolling and/or sliding motion, saltating motion and motion in suspension. It is known that when the value of the bed shear stress is just above the critical value for motion initiation, then the sediment particles are removed from their resting position and erosion starts to take place. The particles start rolling and/or sliding but they remain nearly always in contact with the bed. As the exerted bed shear stress increases, the sediment particles start making a leaping motion (saltation). The sediment grains moving along a bed by rolling, sliding and saltation constitute what is known as **bedload**. Finally, when the vertical component of the flow velocity becomes comparable to the particle settling velocity, then the particles are lifted to a level within the water column at which the upward turbulent forces can balance their submerged weight, so the sediment particles can go into suspension (Francis, 1973). Such moving particles form the **suspended load** and practically move with the same speed as the speed of the carrier flow. The fine uniformly dispersed particles are responsible for the turbidity of the flow. The suspended load also includes the **washload**, which is a broad term describing the clay-size particles brought into suspension more or less permanently.

Bedload and suspended load transport can occur at the same time within the same current, however the limit between these two modes of transport is not strictly defined. The relative percentage of transported sediment grains, moving in three different modes is shown in Figure 2.8 as a function of the transport stage. The latter is defined as the ratio u_* / u_{*_c} of the flow friction velocity to the critical friction

velocity, required for the initiation of particle motion. It is obvious that near the threshold the rolling motion dominates over saltation and suspension. However, at high values of the ratio u_* / u_{*_c} the proportion of rolling particles decreases very steeply, while the proportion of suspended particles increases.

Additionally, experimental work has shown that bedload transport could be observed both in laminar and turbulent flows (Bagnold, 1955). Regarding the forces acting on transported sediment grains, bedload can be defined as the portion of grains whose immersed weight is balanced by an upward intergranular force, arising due to grain shearing over a solid bed (Bagnold, 1966). This does not apply to the suspended load transport, occurring only in turbulent flows. In such flows the fine suspended particles are evenly distributed within the whole water column and the collisions among them are very rare, so intergranular forces supporting the suspended load cannot be developed. In this case, the suspended load is supported by forces developed due to fluid turbulence.

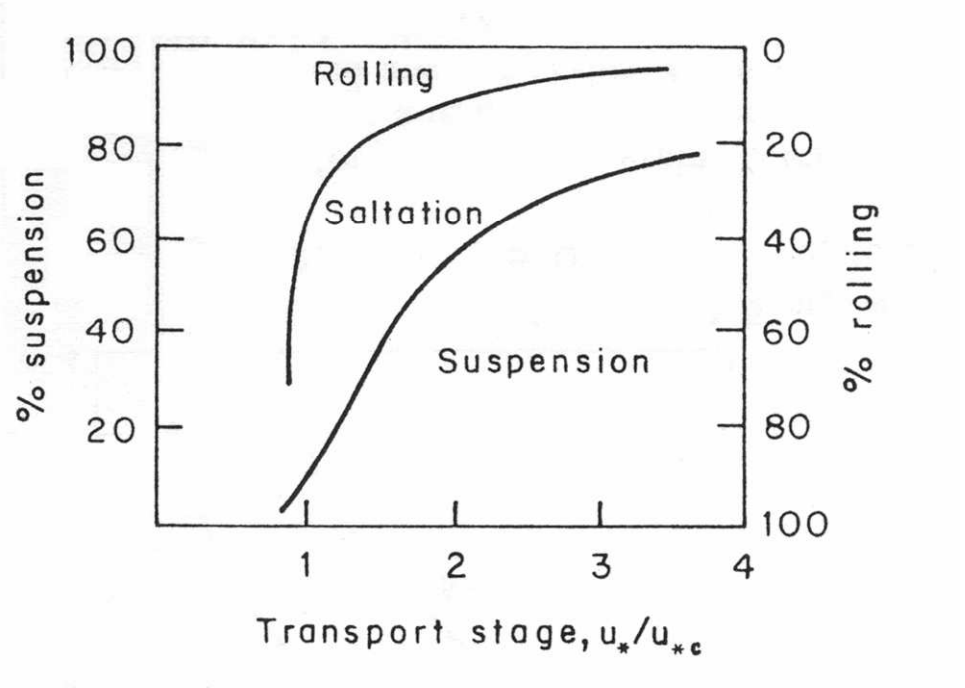

Figure 2.8 The proportions of rolling, saltating and suspended sediment particles against the transport stage (Abbott & Francis, 1977).

2.8.1 Cohesive sediment transport

The previous considerations were based on the assumption that the transported sediments were relatively coarse cohesionless grains, moving as separate particles. However, if clay minerals, clay mineral flocs and cohesive clay beds are involved, then the situation is different, because the clay solids in transport do not behave as separate individual particles but interact electrostatically, showing a certain degree of cohesion.

Clay size particles are platelike and carry a negative electric charge on their surfaces, caused by isomorphous substitution in their lattices. The presence of a saline fluid, e.g. seawater, causes the negative charges to be neutralized and subsequently the approaching clay particles do not repel any more, allowing London-van der Waals molecular forces to establish attraction between individual clay platelets Such attractive forces can counteract the electrostatic repulsive forces. In this case, the process of **flocculation** takes place, where larger aggregates of grains are formed from many individual platelets. On the contrary, in fresh water (e.g. in river water) the electrostatic repulsive forces normally dominate and the flocculation process is inhibited. Consequently, flocculation is more effective in saline water. The attractive London-van der Waals forces are known to be inversely proportional to the square of the distance between the clay platelets. Therefore, the formation of flocs depends on intergranular collisions, which bring the clay platelets in very close proximity. The concentration of suspended particles is also important, as in dense suspensions the probability of particles brought very close together is high. Temperature variations also affect the flocculation process. At high temperatures the thermal motion of ions is more intense and the repulsive forces become larger, so the formation of aggregations is prevented. Additionally, the presence of organic material on the particles encourages organic binding, which leads to larger and stronger flocculates (Whitehouse et al., 1960). The formation of aggregates is known to be a reversible phenomenon, which means that if sediment flocs are put in fresh water, then they will be subject to disaggregation processes, particularly enhanced by turbulent shearing (Jeffrey, 1982; van Leussen, 1997). An important problem involved in the study of flocculated mud aggregates is the difficulty of measuring the floc size from fluid samples, as the extraction of these (e.g. through pumping) could lead to disruption of

the flocs and disaggregation. In order to get over such problems, a number of in situ techniques have been developed (McCave, 1979; Eisma et al., 1997). For example, Owen (1971) has developed a tube for measuring the fall velocity under laboratory conditions closely resembling the natural state. Holographic techniques have also been used successfully in the open sea for in situ measurements of the flocs size and their fall velocity (Carder et al., 1982).

It is known that the flocculation process depends on clay particle concentration: increased concentration leads to increased number of interparticle collisions and therefore, to increased flocculation rate. As expected, the settling velocity of the grown aggregates will increase with increasing concentration. However, after the settling velocity obtains a peak value, a further increase in particle concentration causes a decrease in settling velocity due to the effect of 'hindered settling' phenomenon (Figure 2.9). This means that both the settling flocs and single particles, moving downwards within the dense suspension displace a certain fluid mass, which in turn moves upwards, preventing further settling. The flocculation rate also increases with increasing salinity and subsequently a given fall velocity of flocculates will be observed at a lower concentration if the ambient fluid is more saline (Owen 1970).

The reduced settling velocity of flocculates in dense suspensions due to 'hindered settling' has been described by Maude & Whitmore (1958). The proposed formula was:

$$w_s = w_o(1-C)^m \qquad \text{Eq 2.25}$$

where w_s is the fall velocity of a particle in a suspension of other falling particles, w_o is the fall velocity of a single particle in an otherwise particle-free fluid, C is the volume concentration of particles in the suspension, and m is a function of particle size and shape. For small particles m is equal to 4.65, while for large particles $m = 2.32$. From the above relation is evident that the fall velocity of a particle in a dense suspension will be smaller than that in an otherwise sediment-free fluid and strongly dependent on concentration.

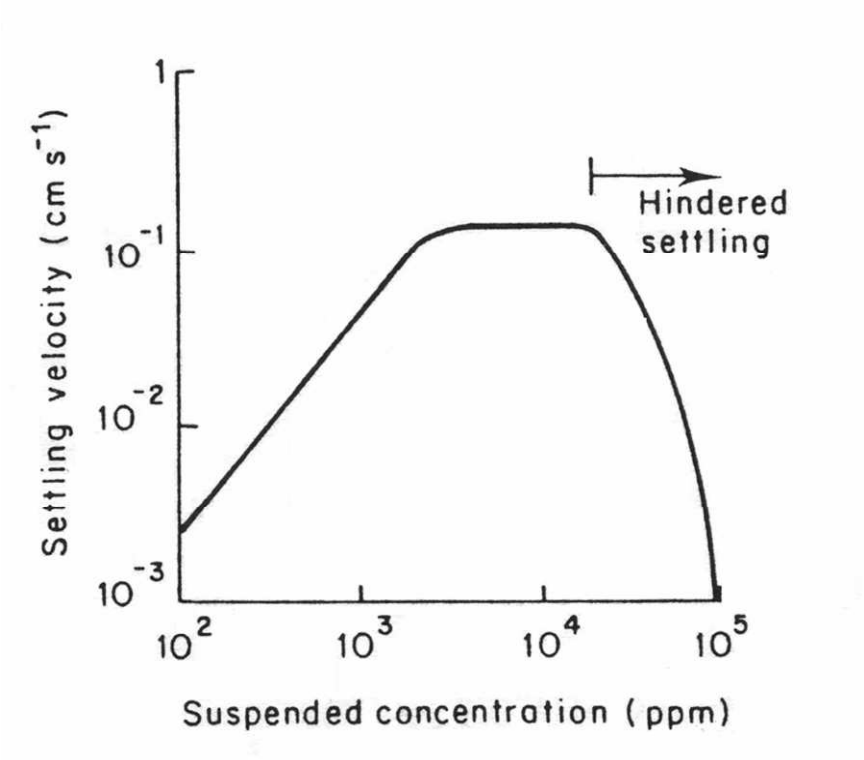

Figure 2.9 The settling velocity plotted against suspended sediment concentration for mud from the Severn Estuary (Odd, 1982).

In certain environments flocculation becomes a very important process, e.g. at estuary heads, where fresh water is mixed with seawater by turbulent eddies. The mixing of fresh and salt water causes estuarine circulation driven by density gradients. It has been observed that the combined effect of the flocculation process and hindered settling can lead to the development of distinct layers of high suspended sediment concentration in great proximity to the sea bottom (Figure 2.10).

This is particularly common in tidal-dominated estuaries (Kirby and Parker, 1983). In such environments silt- and sand-sized particles combine in larger aggregates, which then settle and form large areas of mobile and stationary mud suspensions (**fluid muds**) of very high densities. Mobile suspensions can potentially flow along the bottom without mixing considerably with the overlying flow because of the high density contrast. Additionally, they can move freely downslope as density currents under the influence of gravity. Stationary fluid muds show high densities (up to 200 g/l) and can be rapidly deposited at a thickness of 2-4 m (Dyer, 1986). They are separated by a sharp interface (lutocline) from the overlying suspension layer where

the sediment concentration is much lower. Such suspensions do not move horizontally, however, gradual settling could occur. Sediment cores obtained through stationary fluid muds reveal structureless muddy silts with occasional thin sandy laminae (Kirby and Parker, 1983), while sonar records show sharp upper surfaces of stationary suspensions.

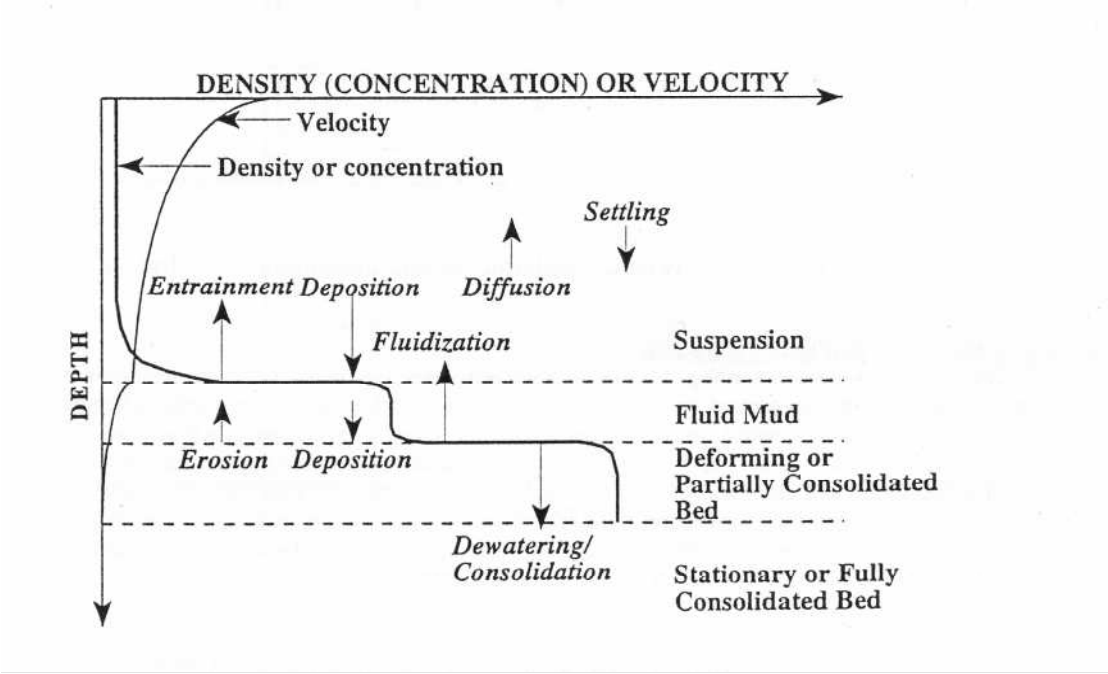

Figure 2.10 Concentration and velocity profiles with associated sediment fluxes. The velocity profile represents wave motion. (Mehta & Li, 1998)

The erosion of a muddy bed by a flow will generally occur when the bed shear stress exceeds the local critical shear resistance. However, the threshold conditions for entrainment of mud are not simply a function of grain size, but depend on various parameters, like clay mineralogy, chemical composition of fluid, state of fluid flow, organic content and previous depositional history. For example, consolidation of deposited muddy beds is very important, because it causes an increased cohesiveness, hence increased erosion resistance with depth. This results in high surface erodibility of muddy beds, which is followed by stability at a greater depth. Additionally, the presence of surface algal films and coatings on many marine deposited muds exhibits a binding effect, which decreases erodibility (Paterson, 1997).

3 Sediment-laden flows

In this chapter a general review on studies concerning sediment-laden flows is presented, including basic observations and experimental results. Emphasis is placed on experimental investigations, conducted with the use of artificial channels (laboratory flumes) and in particular the annular flumes. The subchapter 3.1 consists of some background information on suspension flows, including specific difficulties introduced by the presence of cohesive suspended solids within a flow. The subchapter 3.2 refers to the drag reduction phenomenon, exhibited by natural and laboratory turbid flows. In subchapter 3.3 a brief overview is given on the use of laboratory and in situ annular flumes by various researchers, who studied sediment-laden flows.

3.1 Complications introduced by the transported solid phase

Most of the natural flows are not homogenous because they carry a certain amount of suspended load. If the suspended material is cohesionless, then the flow can be considered as Newtonian. In this case, only Von Karman's constant k and kinematic viscosity ν are changed (Hunt, 1954). If the suspended sediments are cohesive, then Bingham-like behaviour occurs, with an increase in apparent bulk viscosity directly related to the amount of transported clay and shear rate (Wan, 1982). In other words, we have a two-phase system which behaves as a viscous non-Newtonian fluid (Wood et al., 1995; Metzner, 1961). The latter was proven experimentally by Gust (1976), who used a dilute seawater-clay suspension in a laboratory channel and found that the applicability of the universal 'law of the wall' (see §2.4) was not correct in this particular case.

It is known that the friction velocity (Eq 2.11) $u_* = (\tau/\rho)^{1/2}$ (τ = bottom stress, ρ = fluid density) is a fundamental parameter, used in the investigation of erosion and sedimentation processes of geophysical boundary layers. It can be estimated from mean streamwise velocity measurements in the logarithmic layer of the turbulent boundary layer. For hydraulically smooth flows of Newtonian fluids the friction velocity u_* is calculated by solving the equation:

$$\bar{u}/u_* = 1/k \ln(yu_*/\nu) + C_1 \qquad \text{Eq 3.1}$$

where $\bar{u}$ = local mean streamwise velocity, y = vertical coordinate, and ν = kinematic viscosity. Eq 3.1 is known as the 'Law of the Wall' and with k=0.4 and C_1=5.5 is valid for equilibrium boundary layers of fully developed turbulent Newtonian smooth flows. Within the range of validity, the values of k and C_1 slightly depend on Reynolds number (Tennekes and Lumley, 1971; Tennekes, 1973). Therefore, the values of the critical friction velocity u_{*crit} and erosion rates obtained under the assumption of a Newtonian flow structure should be reviewed in the case of sediment-laden flows. This means that the universal law of the wall is not valid for turbulent two-phase flows.

Gust (1976) in his previously mentioned experiment simulated a tidal flow under highly controlled laboratory conditions, using an artificial channel coated with mud and unfiltered seawater from the North Sea. He obtained mean streamwise velocity profiles for Reynolds numbers between 5400 and 27800 (i.e. non-eroding and eroding flow rates) in order to investigate the boundary layer structure of the seawater-clay suspension down into the viscous sublayer. Although the distributions of concentration showed no substantial increase towards the wall, he found that the thickness of the viscous sublayer (which was normally of the order of 1 mm) was increased by up to a factor of 5 compared with Newtonian flows under the same conditions. Additionally, the friction velocity u_* determined by the 'gradient method' (Eq 2.23) in the viscous sublayer was reduced up to 40% in suspension flows. Gust used mean velocity profiles to express the wall shear stress τ in terms of the friction

factor f, which is a function of Reynolds number Re and clay suspension parameters causing the reduction in the friction velocity u_*. It is:

$$f = 8\,(u_*/\overline{U})^2 \qquad \text{Eq 3.2}$$

where $\overline{U}$ is the mean channel flow velocity, and:

$$\mathrm{Re} = 4\overline{U}\,R/\nu \qquad \text{Eq 3.3}$$

where R is the mean hydraulic radius. In Figure 3.1 the data for the clay suspension show a downward shift from the clear water values, demonstrating the occurrence of the drag reduction phenomenon which is explained in §3.2.

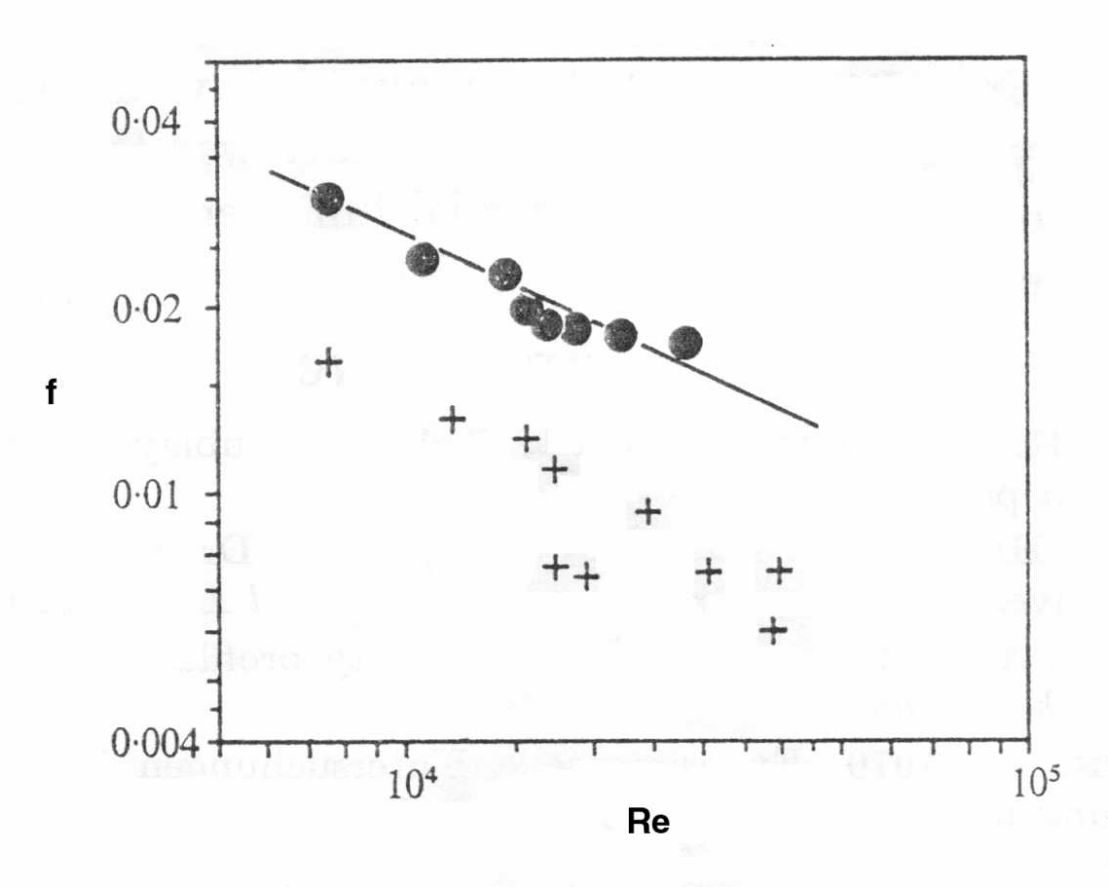

Figure 3.1 Friction coefficient f as a function of equivalent pipe Reynolds number Re for experimental smooth turbulent flows (●: clear water, + : clay suspension) (Gust, 1976).

3.2 The drag reduction phenomenon

Drag reduction is a hydrodynamic phenomenon, observed in turbulent flows when polymers or fibrous solids are added in small concentrations to a fluid. It is referred to the reduction of skin friction in a turbulent flow of a suspension or solution below that of the solvent alone.

In 1948 Toms pointed out that the resistance of clear water flow could be reduced if some polymers were added to the flow. The observed drag reduction phenomenon occurred because the polymer molecules show a long chain structure, so their presence suppresses the development of turbulence near the boundary. Flocs of some clay minerals suspended in water show a long chain structure as well, so they may induce drag reduction. Besides earlier, Fortier and Scobey (1926) had observed that for water flows transporting cohesive sediments the permissible channel velocities were higher than for clear water flows. As an explanation they suggested that the sedimented cohesive particles cemented the bottom material, which then became less subject to the erosive action of the flow. In other words, the drag reduction phenomenon which occurred in their experimental smooth and rough flows had been responsible for the decreased shear stress applied to the bottom or the increased critical friction velocity u^*_{crit} required for erosion. The drag reduction phenomenon caused by clay suspensions was later suggested by Zandi (1967) but his results were questioned by other researchers. Since then, suspension flows have further been studied and the drag reduction phenomenon has been clearly exhibited.

Regarding the generating mechanisms of drag reduction, the agglomeration of charged particles is proposed as a possible cause in clay suspension flows (Gust and Walger, 1976). According to Radin et al. (1973), viscoelastic solutions and fibrous suspensions can exhibit drag reduction. However, it has been proposed that all types of elastically deformable aggregates which can also be built up by bioaggregation,

will cause drag reduction in natural turbulent flows, or alternatively, those agglomerations which can change their shape under the effect of shear or vorticity in the turbulent flow can cause drag reduction. Other rheological properties like thixotropy or dilatancy of the suspensions could also change the rheological behaviour of turbulent flows and cause this phenomenon.

Experimental studies of sediment-laden flows have revealed that in such flows a thickened viscous sublayer or buffer layer is formed below the logarithmic layer (Virk, 1971). As a result, increased mean velocities in the logarithmic layer are needed in order to achieve the same critical (fluid-transmitted) friction velocities u_{*crit} for erosion of a subaqueous substrate than found with clear water flows. Additionally, many researchers have confirmed that the turbulence characteristics of particle-laden flows can be affected by the presence of dispersed particles if the concentrations of the dispersed phase are high enough. This 'turbulence modulation' effect is an extremely complex phenomenon that is not completely understood. Gore and Crowe (1989) have shown that turbulence levels can be enhanced for large particles in dispersion apparently due to the formation of turbulent wakes behind such particles. The effect of small particles, however, is usually to suppress the turbulence by extracting energy from the primary flow turbulence (Graham, 2000). Consequently, the general effect of small particles is to attenuate turbulence.

Based on the preceding information, it is concluded that the assumption of a Newtonian flow structure can not be valid for many sedimentological investigations in flume experiments and natural flows. As an example, it has been observed in experiments on the determination of the erosion rate of clay beds (Migniot, 1968; Terwindt et al., 1968; Partheniades and Paaswell, 1970), that the applied bed shear stress τ_0 exceeded the erosion threshold $\tau_{0,crit}$ without erosion being caused. This can be explained if the drag reduction phenomenon is considered, as under such conditions the flow contains freshly eroded suspended sediments. Once more the values of τ_0 have to be reviewed in case they are obtained via velocity measurements in the logarithmic layer. Regarding the deposition of cohesive sediments from suspension flows, the balance of sedimentation/erosion processes is modified in drag reducing flows, although the exact mechanism requires further investigation. It is

supported that the thickened wall layer, observed in drag reducing flows, causes upward migration of the zone of maximum turbulent shear stress. This produces a thicker zone where the disaggregation of clay flocs is less likely to occur. Consequently, within the thickened wall layer the resuspension rate of the deposited flocs is decreased, while the deposition rate is increased (McCave and Swift, 1976). Furthermore, Gust and Walger (1976) conducted both field and laboratory experiments and found that when drag reduction occurs in tidal flows with suspended cohesive sediments, then the friction velocity is reduced by possibly 20-40% as compared with sediment-free flows. This allows the preservation of freshly deposited mud over several tidal periods. In their flume experiments they used a mixture of illite, kaolinite and chlorite minerals with concentrations less than 380 mg/l. As the main generating mechanism for the observed turbulent drag reduction, they proposed the dynamic interaction between turbulent shear strain in the flow and deformation of aggregates.

Some aspects of the dynamics of turbidity currents and subaqueous slides might also be explained by the drag reduction phenomenon. In dilute turbidity currents drag reduction could cause lower bed friction factors, allowing higher flow speeds than those expected in clear water flows (Stow and Bowen, 1980; McCave, 1984). In such a case, previously estimated values of velocity and range may be underestimated. Besides, it is known that the mud/silt interlaminations and microripples present in the Bouma D/E divisions of turbidites are formed due to the processes of size segregation. Such processes are strongly linked to the turbulent characteristics of the thickened wall layer, which is observed in drag reducing flows (Hesse and Chough, 1980; Stow and Bowen, 1980). Besides, Best and Leeder (1993) performed qualitative experiments in order to further investigate the effects of drag reduction upon bedform development. In their first experimental run they developed a uniform flow over a sand bed, with a maximum flow velocity just above the threshold of movement. Then a suite of current ripples formed on the bed surface. In the second experimental run, the first experiment was repeated but this time a clay-suspension flow of 0.2 g/l was established over the sand bed. The developed current ripples showed significantly lower amplitudes and wavelengths than those formed in clear-water flow. It was proposed that drag reduction was responsible, as it didn't allow the true threshold of movement to be reached during the second run. Flow separation still occurred over

the current ripples, however, the reduced near bed velocities caused a decrease in near bed erosion at flow reattachment points. It is noteworthy that the current ripples generated on the sand bed show analogues to the forms (microripples), which are common in the deposits of dilute turbidites (Hesse and Chough, 1980).

It is generally accepted that several aspects of sediment transport, deposition and bedform development in natural marine environments are significantly affected by the drag reduction process. This is supported by many researchers, whose observations on natural and experimental turbid flows, are presented in the following brief overview. It is obvious that experimental study of these processes requires flow-measuring devices with adequate spatial and temporal resolution. It should be noted that more recent experimental data (e.g. data obtained with the use of LDV and ADV sensors) are considered to be accurate and reliable.

According to Dyer (1986) and Mehta & Dyer (1990) the suspension of fine-grained sediments can significantly change the boundary layer structure and bed shear stress, and this in turn affects the processes of cohesive sediment erosion. Best and Leeder (1993) demonstrated the drag reduction in turbulent sea-water flows by laboratory experiments using non-intrusive laser Doppler anemometry in clay suspensions of 2.2 g/l (maximum concentration). They observed that an increase in clay concentration caused progressively lower velocities near the wall due to a gradual thickening of the buffer region of the turbulent boundary layer. Besides, Graham (2000) confirmed the general effect of particles to attenuate turbulence, studying the influence of a dispersed phase on carrier flow turbulence. The carrier flow is assumed to be a simple homogeneous shear, in which the fluid Reynolds stress tensor is independent of spatial location, but in which there is a linear mean shear across the flow. He found extra dissipation terms in the Reynolds stress equations compared with those arising in isotropic turbulence. He also developed a simple model for predicting the reduction of turbulent kinetic energy in particle-laden turbulent shear flows, and compared the theoretical results with his experimental data.

Finally, Li and Gust (2000) observed the drag reduction in suspension flows of clay concentrations 4 and 8 g / l. In their approach velocity profiles and bed shear stresses, expressed as shear velocities, were measured using epoxy-coated hot-film sensors in

order to evaluate drag reduction and controlling factors. The shear velocity was directly measured in the viscous sublayer and was reduced by as much as 70% relative to the profile-derived shear velocity in the logarithmic layer. The magnitude of drag reduction was found to depend both on clay concentration and flow strength. For a fixed flow strength (represented by flow Reynolds number in flume experiments), drag reduction increased with increasing clay concentration, while for a given clay concentration drag reduction increased with decreasing flow strength. The data obtained from the flume experiments were used to derive the following empirical relationships, which can predict the magnitude of drag reduction and the reduced shear stress in mud suspensions for both laboratory and field cohesive sediment transport studies:

$$u_{*s}/u_{*\log} = -62.28(C/\rho_s) + 9.171\times10^{-6}\,\mathrm{Re} + 0.425 \qquad \text{Eq 3.4}$$

$$u_{*s} = -54.42(C/\rho_s) + 4.463\times10^{-5}\,\mathrm{Re} + 0.0398 \qquad \text{Eq 3.5}$$

where: u_{*s} = the directly measured skin-friction shear velocity, $u_{*\log}$ =the log-layer shear velocity derived from the velocity profile, C =clay concentration, ρ_s =kaolinite density, Re =Reynolds number. The two parameters, u_{*s} and $u_{*s}/u_{*\log}$, are predicted from clay concentration and flow strength measurements. In particular the predicted ratio $u_{*s}/u_{*\log}$ indicates how much the bed shear stress is reduced with respect to the apparent shear stress of the logarithmic layer, for a fixed flow strength and clay concentration.

The previous predicted values are in line with earlier findings by Amos et al. (1997), who measured in situ the stability of the fine-grained sediments on the foreshore and upper foreslope of the Fraser River delta, using a benthic flume -the Sea Carousel (Amos et al., 1992). The reduction in the bed shear stress (τ_0) and the corresponding friction velocity (v_*) due to suspended sediment concentration (C) are predicted by the equation:

$$v_*(C) = v_*(0) - [0.2267\log(C)\times0.157v_*(0)] \qquad \text{Eq 3.6}$$

where $v_*(C)$ =the reduced friction velocity due to sediment concentration C and $v_*(0)$ =the friction velocity for sediment-free conditions. In Figure 3.2 the predicted values of friction velocity v_* are plotted against the concentration C of the suspended solids. This plot illustrates the decrease in v_* due to C for various starting values of v_*, which correspond to clear-water conditions.

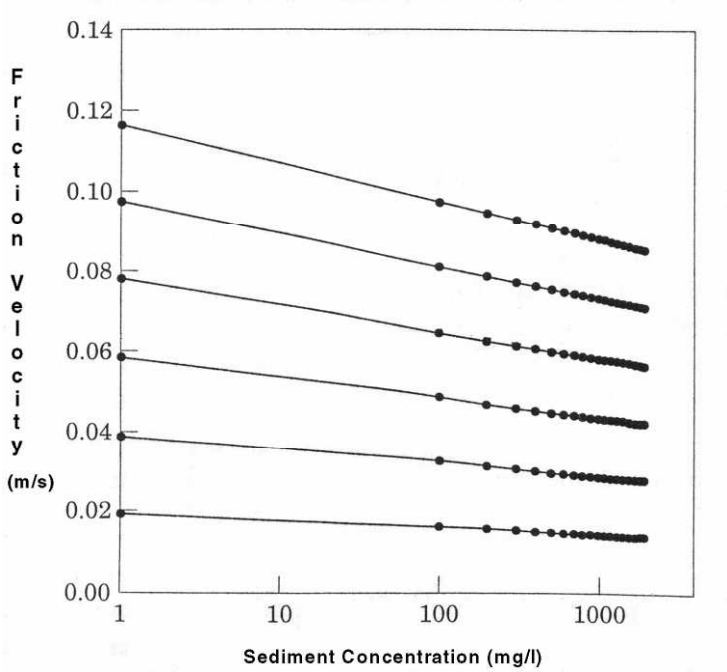

Figure 3.2 The reduction in friction velocity due to suspended sediment concentration, as defined by Eq 3.6 (Amos et al., 1997).

It is concluded that the drag reduction phenomenon is generally observed in sediment-laden flows, however there have been a few cases in which drag reduction has not been clearly verified. For example, Wang et al. (1998) conducted experiments with clay suspensions flowing over smooth and gravel-coated beds and showed that resistance of the flow may be considerably reduced if the flow boundary is rough. For flows of high clay concentrations over the gravel bed, the friction factor was found to be less than half of the clear-water flow at the same discharge and energy slope. They proposed that at low concentrations controversial results could be obtained concerning drag reduction because the flocs of some clay minerals can extend in one direction with a long chain structure, damping turbulence and causing drag reduction. However, some clay particles form spherical flocs and do not show a long chain structure. Such

kinds of flocs do not damp turbulence and do not cause drag reduction. At high concentrations all flocs in clay suspension connect together and form a three-dimensional net structure, which affects the resistance in two ways: first by damping turbulence (Figure 3.3) and reducing the resistance and second by increasing the viscous resistance. In turbulent flows over a gravel bed the turbulent shear dominates the resistance, so the three-dimensional clay structure suppresses the development of turbulent eddies and causes drag reduction. In turbulent flows over a smooth boundary both viscous stress and turbulent stress are high enough, so the effect of damping turbulence is counterbalanced by the effect of increasing viscous resistance. Therefore, drag reduction is not observed.

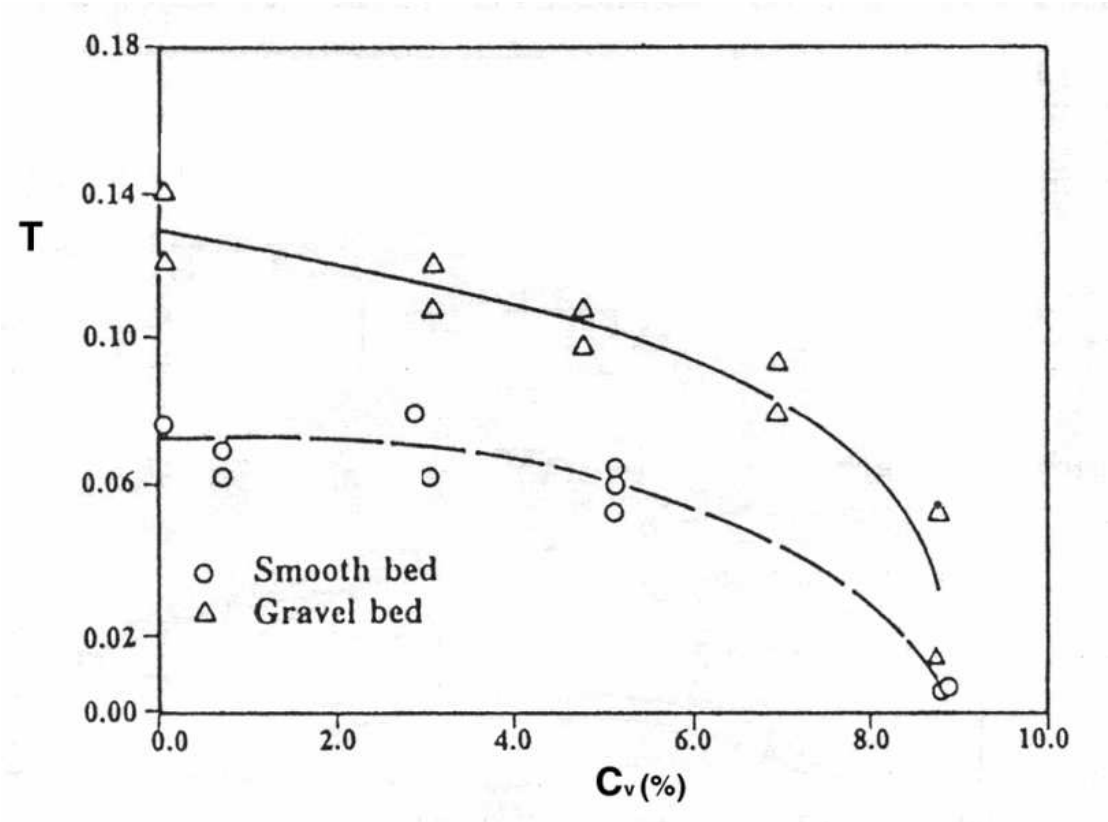

Figure 3.3 Average turbulence intensity T as a function of volume concentration C_v of clay suspensions (Data of Wang et al., 1998).

Additionally, Bogue and Metzner (1963) did not find drag reduction in turbulent pipe flows of clay suspensions, while Hou and Yang (1983) used clear water and clay suspensions between rotating and fixed smooth plates in order to study the fluid resistance on the relatively moving plates. They found that almost in all

measurements, clay suspensions showed higher resistance than clear water and drag reduction in this case was questionable.

3.3 The use of annular flumes in the study of sediment-laden flows

In experimental studies of cohesive sediment beds, artificial channels (the laboratory flumes) are commonly used in order to investigate the erosion characteristics of clay substrates and the transport of suspended sediments. Such studies require knowledge of the precise flow field and the bed shear stress distribution. It has been verified that the flume measurements allow a particularly detailed and well-conducted determination of these parameters under highly controlled laboratory conditions. In particular annular flumes have been widely used in recent years both in laboratory and in-situ measurements, as they overcome various problems encountered during the use of the more conventional straight-channel flumes.

The main disadvantage of straight flumes is that the suspended sediment has to be recirculated by pumps and recirculation loops, so its structure can be significantly changed (e.g. the structure of aggregates can be externally disturbed). In annular flumes such a problem does not exist, as the flow in them is driven by a rotating lid, which provides a shear force at the top of the water column (Maa, 2001). Besides, the flow length in annular channels is considered to be infinite, thus allowing a fully developed benthic boundary layer to be formed. However, the flow in annular flumes is not unidirectional and shows more complex characteristics: the shear force applied on the top boundary induces a primary flow in the tangential direction and a secondary circulation in the radial direction. The secondary flow is caused by the centrifugal force due to channel's curvature and the vertical gradient of the tangential velocity (Yang et al., 2000). As a consequence, the shear stress distribution across the bed is not uniform in the radial direction, showing a considerable increase from the inner wall to the outer wall and resulting in higher erosion in the outer edge of the flume. This makes the accurate determination of the flow and shear stress field necessary before the experimental results can be interpreted (Graham et al., 1992).

It is generally recognised that due to complex chemical and physical processes involved, the detailed mechanisms that control the cohesive sediment transport and erosion have not been absolutely clarified yet. However, the shear stress exerted on the interface of cohesive sediment and overlying fluid appears to play the most significant role on deposition and erosion of cohesive sediments (Partheniades, 1986), as a critical value of shear stress should be exceeded before erosion of the cohesive substrate can take place. It has been exhibited that annular flumes have been successfully used so far in critical shear stress evaluation, shedding light on the previous aspect. Graham et al. (1992) determined numerically and experimentally the flow field and the surface shear stress distribution, generated in the Hydraulics Research annular carousel (located in Wallingford). The numerical predictions were made by the computational fluid dynamics program HARWELL-FLOW 3D. The tangential velocity profiles were measured by laser doppler anemometry (LDA), while the bed and sidewall shear stresses were measured by hot-film probes. The comparison between the predicted and measured values showed a very good agreement in the case of velocity profiles and a good agreement in the case of shear stress.

Regarding the secondary flows induced in annular flumes, Maa (1990) used a numerical model in order to evaluate the secondary flow field for the annular sea-bed flume developed at Virginia Institute of Marine Science (the VIMS Sea Carousel). He found that the radial flow velocities were about 15% of the tangential velocities, being maximum near the top of the flume. The radial components of the bed shear stress were found to be about 15% of the tangential components as well (Figure 3.4). However, the radial velocities are much larger than the settling velocities of the suspended clay particles. This shows the advantage that the suspended sediment concentration will be fairly uniform in the entire flume and no stratification problem will occur. As a consequence, the annular flumes can be considered excellent tools for studying the erosion behaviour of cohesive substrates, however their reliability in studying deposition processes is still questioned. Besides, Maa (2001) has proposed that the secondary circulation in an annular flume can be significantly reduced, if the ratio W/R is low (less than 0.14) (R = radius of the flume = $(r_{in} + r_{out})/2$ and W =

channel width = $r_{out} - r_{in}$). In other words, in annular flumes with a suitably large R and small W, the bed shear stress distribution can be considered uniform.

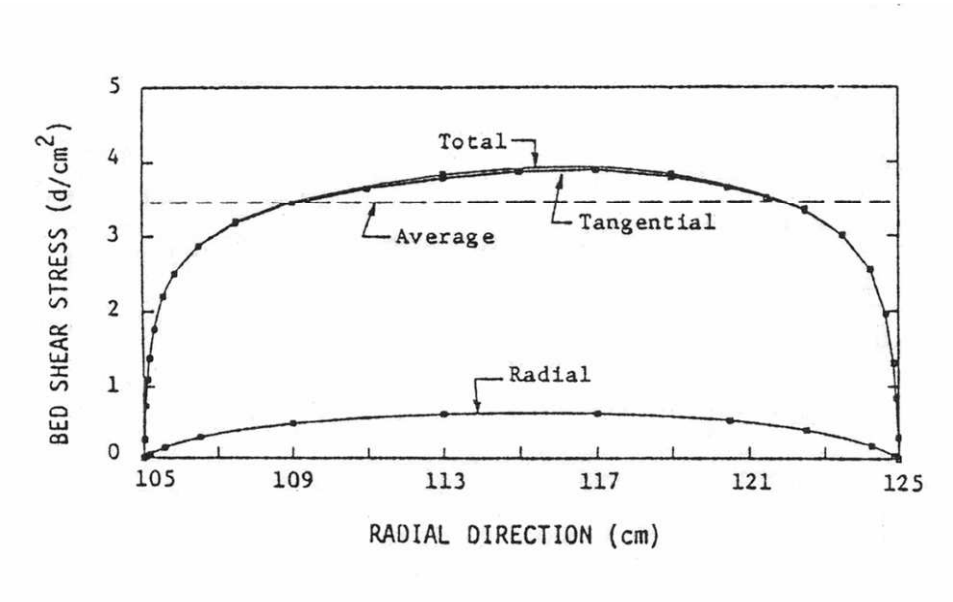

Figure 3.4 Bed shear stress profiles in VIMS annular flume for a constant speed of rotating ring (= 7 rpm) (Maa, 1990).

Sea-bed annular flumes operate in a similar way like other annular flumes, used in many other laboratories (Fukuda, 1978; Burt and Game, 1985; Amos et al., 1992; Maa et al., 1993). However, the sea-bed flumes have been specifically designed for field deployments. In particular, they can be operated on the floor of shallow water environments, so they have no bottom and are lowered from a boat to penetrate into the subaqueous substrates. As an example, a benthic annular flume designed for both laboratory and field applications, had been successfully used on intertidal mudflats to provide a useful means of quantifying material flux across the sediment-water interface in relation to changes in current velocity (Widdows et al., 1998). Earlier, another sea-bed flume had been used by Young and Southard (1978) in order to investigate the incipient motion of sandy sediments, while the SEADUCT had been deployed by Nowell et al. (1985) to define erosion rates. The VIMS Sea Carousel had been planned for use in field investigations of erosion and deposition rates (Maa, 1990). It proved to be a very reliable tool for critical bed shear stress measurements, used in the study of sediment resuspension off the North Carolina coast (Maa et al., 1995). The VIMS Sea Carousel is similar to the Sea Carousel, a benthic annular flume

developed and tested in Canada (Amos et al., 1992). The Sea Carousel has been extensively used in field investigations of the stability/erodibility of cohesive beds in a variety of natural marine settings (Amos et al., 1996; Amos et al., 1997; Amos et al., 1998; Amos et al., 2003). The erosion rates obtained from in situ deployments were based on the rate of change in the suspended sediment concentration, monitored within the flume. Three optical backscatter sensors (OBS) mounted in the flume wall, were used in concentration measurements. During a test deployment the time-averaged friction velocity ($\bar{v}_*$) was determined, using a flush-mounted hot-film probe (Amos et al., 1992). It was demonstrated that for mean azimouthal flow speed above 0.32 m/s, the friction velocity increased in the radial direction almost linearly (Figure 3.5) and in particular, the cross-channel gradient in friction velocity increased with the azimouthal flow velocity.

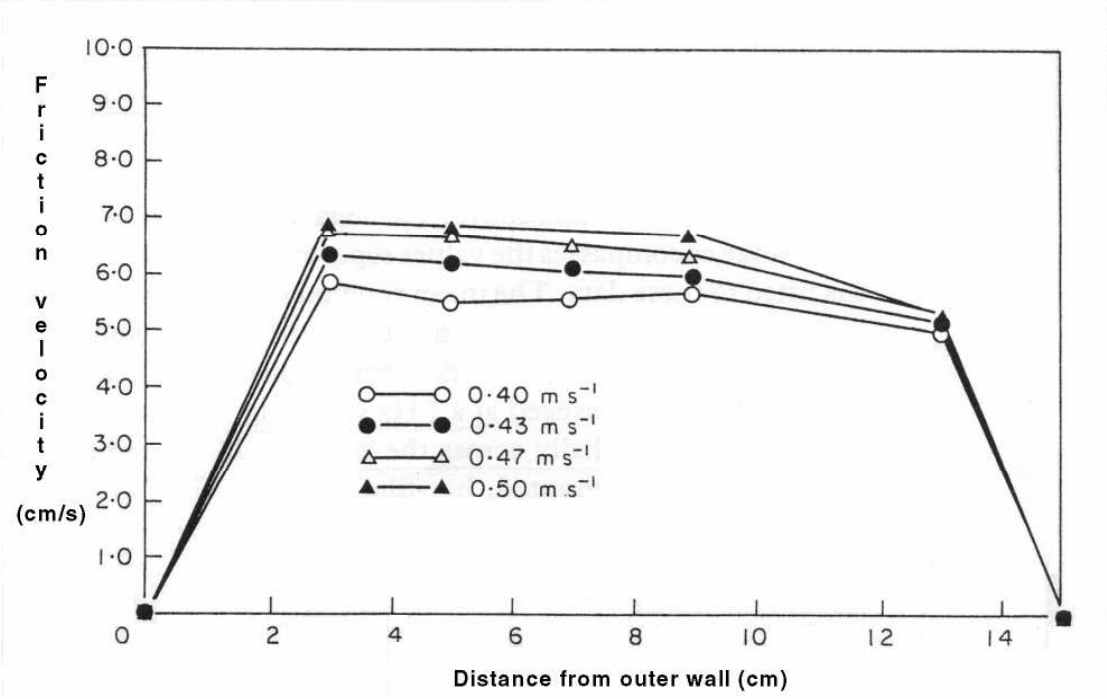

Figure 3.5 Total friction velocity distribution in radial direction in the Sea Carousel. Friction velocity was measured at four levels of azimouthal flow speed (Amos et al., 1992).

The laboratory analogue of the Sea Carousel is the Lab Carousel (§ 4.1), an annular channel designed for studies of sediment-laden flows under highly controlled laboratory conditions. Cloutier et al. (2003) studied the effect of suspended sediment concentration on the structure of a turbulent flow, developed in the Lab Carousel.

They showed that for clay concentrations over the range 50-4800 mg/l, the turbulent intensity and energy dissipation rate were influenced by concentrations higher than 200 mg/l, as both of these parameters decreased by nearly 30% of their clear water values. As the generating mechanism, it was proposed that the suspended clay solids hindered the development of turbulent eddies and modified the energy transfer from larger to smaller eddies. This can lead to a considerable decrease in the shear stress exerted on the bottom and consequently to lower erosion and resuspension rates.

The Lab Carousel was also used by Thompson et al. (2004), who developed and tested the Flow Deceleration method (§ 4.4). This method proved to be a very practical tool, used for reliable and fast estimations of the drag coefficient (C_D) in smooth and rough flows of a wide range of Flow Reynolds numbers (Re) within an annular flume. Considering a smooth boundary, the drag coefficient depends only on flow strength, expressed by Reynolds number (Re) (Nikuradse, 1950). Therefore, the drag coefficient is proportional to the rate of velocity change, exhibited by a constant mass of decelerating fluid within the Lab Carousel and is given by:

$$C_{D_z} = \frac{m}{A}\frac{dV}{dt}\frac{1}{\rho\overline{V_z}^2} \qquad \text{Eq 3.7}$$

where C_{D_z} = the drag coefficient at height z, m = fluid mass, A = the wetted area of the flume, ρ = fluid density, $\overline{V_z}$ = mean flow velocity at height z above bed. The values of drag coefficient calculated by Eq 3.7, assuming a smooth decelerating flow in the Lab Carousel, are in good agreement with earlier findings on smooth plates (Hughes and Brighton, 1967). In order to test the validity of the new method, Thompson et al. (2003) compared eight different methods of estimating the mean, fluid-transmitted bed shear stress within the Lab Carousel under smooth bed conditions. The used methods, except the Flow Deceleration method, included the Hot-Film probe and Turbulent Kinetic Energy (TKE) method. At low flow velocities there was a good convergence among the various methods, while at higher flow velocities the results of Flow Deceleration and Turbulent Kinetic Energy method were found to be similar. The latter was also confirmed under rough bed conditions, establishing further the validity of the method. It was demonstrated that the use of

Sternberg's smooth-bed constant drag coefficient ($C_{D100} = 3.1 \times 10^{-3}$) (Sternberg, 1968; Sternberg, 1972), measured at 1 m above bed, in the Quadratic Stress Law resulted in the highest overpredicted values of shear stress in relation to the Flow Deceleration method results. In addition, the data obtained by hot-film probes showed that the mean total bed shear stress values varied radially. In particular, the highest shear stresses were persistently observed in the middle of the annular channel, while the lowest values were found at the outer edge of the channel (Figure 3.6).

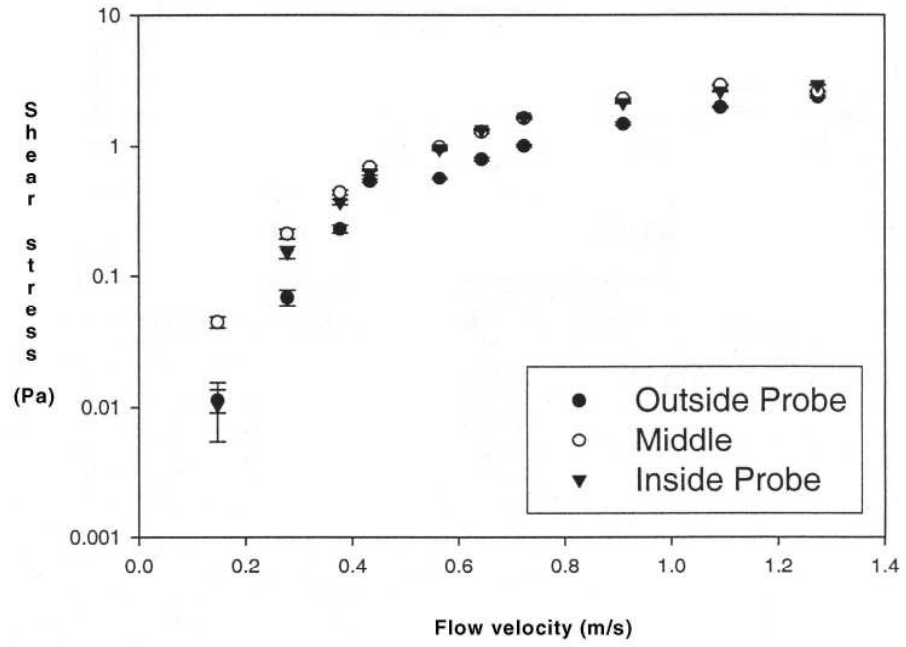

Figure 3.6 Mean total shear stress in the Lab Carousel, as measured by hot-film probes at three different points across the flume channel (Thompson et al., 2003).

This work aims to use the new method of Flow Deceleration in the Lab Carousel in an attempt to examine the effect of cohesive suspended matter on the bed drag coefficient and the bed shear stress within the boundary layer of smooth turbulent flows.

4 Experimental Procedure

In this chapter a short description of the laboratory flume used in the experiments and its mode of operation is presented, followed by the calibration curves of the various sensors fitted in the flume (§4.1, §4.2). In §4.3 a detailed description of the experimental procedure is given, while in §4.4 the Flow Deceleration method is explained. In §4.5 the Flow Deceleration method is applied in the estimation of the bed drag coefficient and bed shear stress within the Lab Carousel. Finally, in § 4.6 the effect of increasing clay concentration on the dynamic viscosity of the clay-water mixtures is evaluated.

4.1 Equipment

The laboratory simulations described in this thesis were performed in a laboratory annular flume, the Lab Carousel (Figure 4.1), which is the laboratory version of the Sea Carousel (Amos et al., 1997; Amos et al., 1992) (§ 3.3). The Lab Carousel is an annular flume, 2 m in diameter. The annular channel has a rectangular cross section, which is 0.15 m in width. These specifications allow a maximum water depth of 0.40 m. The base and walls of the channel are made of acrylic and have a flat smooth surface. The flow in the annular channel is driven by the rotation of a mobile lid, which is also made of acrylic and can float on the fluid surface. The rotating lid can be submerged within the fluid, which is then set into motion by eight small paddles, fitted equidistantly on the lid. The speed of rotation is controlled by an E-track® AC inverter motor controller. The motor is placed upon a hydraulic jack, which enables the user to lift the lid out of the water while it is still rotating at any time during the experiment.

The Lab Carousel is equipped with: i) A one-dimensional class IIIb Helium-Neon 10 mW Laser Doppler Velocimeter (LDV) ii) A single point Nortek® Acoustic Doppler Velocimeter (ADV) iii) A Marsh McBirney® Electro-magnetic Current Meter (EMCM) (model 512) iv) Three optical backscatter sensors (OBS's; Downing, 1983) v) A digital video camera. It is known that the Laser Doppler Velocimeter (LDV) is a reliable tool, used in non-intrusive measurements of turbulent flow in the laboratory (Nezu and Rodi, 1986; Agrawal and Belting, 1988). The system used in these experiments measured the tangential component of the flow velocity at a height of 0.15 m above the bed at the centre of the channel. The acquired data from LDV were logged to a PC at a rate of 20 Hz.

Figure 4.1 The Lab Carousel filled with clay suspension. The Laser Doppler Velocimeter and the digital camera are shown.

The acoustic Doppler velocimeter (ADV) is an acoustic instrument, capable of measuring three components of flow velocity at high sampling rates and with a small sampling volume (Lohrmann et al., 1994; Gratiot et al., 2000). It consists of a transmitter and three receivers, arranged equidistantly (at 120^{o}) on a circle around the transmitter (Figure 4.2). The backscattered signal recorded by the three receivers results from a common sampling volume, which is positioned at a distance of ~10 cm from the probe (Figure 4.2). The ADV sensor used in the Lab Carousel had been firmly attached to the flume wall (Figure 4.3), so that the head of the instrument was

approximately aligned along the centerline of the channel, while the measurements were obtained at a height of about 0.01 m above the flume bottom. For a sampling volume size equal to 9 mm the flow was sampled at a rate of 25 Hz and the data were logged to a PC.

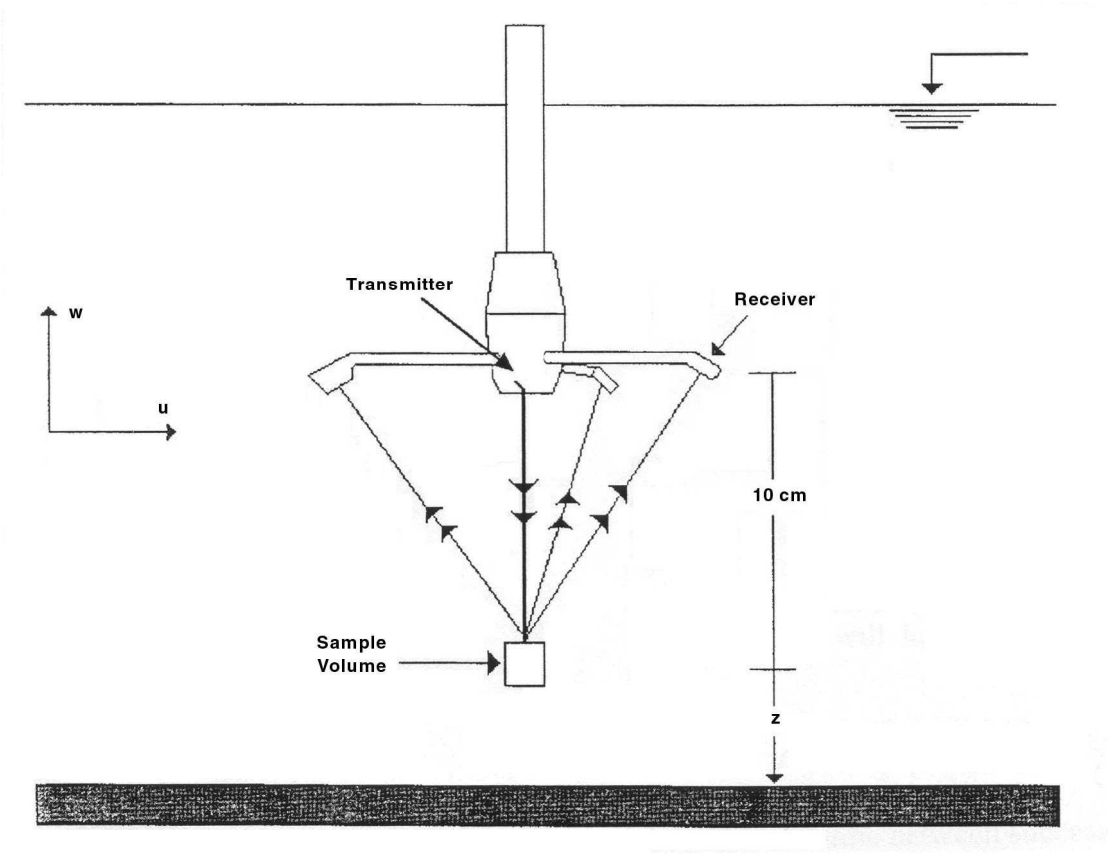

Figure 4.2 Operation of ADV sensor

The Electromagnetic Current meters (EMCM) are sensors very commonly used in turbulent velocity measurements (Sternberg, 1991; de Witt and Kranenburg, 1996). However, they show some disadvantages, such as zero-drift problems (zero point tends to shift over time) and flow disturbance due to their relatively large size. They also have a low spatial resolution (Soulsby, 1980). In the Lab Carousel the electromagnetic current meter (Figure 4.4) measured the flow speed in both the tangential and radial direction at a height of 0.15 m above the base in the middle of the channel. The sampling rate was 2 Hz and the data were logged from the EMCM to a Campbell Scientific CR10 data logger. The three optical backscatter sensors (OBS) were mounted in the flume wall and monitored the temporal variations of the

suspended sediment concentration at heights of 0.03, 0.10 and 0.20 m above the flume bed.

The flow velocity field and the structure of the boundary layer within the Lab Carousel over a range of flow speeds have been determined from velocimetric measurements of various researchers, using a laser Doppler velocimeter (LDV) (Fung, 1995; Thompson et al., 2003). Their results confirmed the existence of a bottom boundary layer of a thickness up to 0.02 m, developed under various smooth flow conditions (Figure 4.5). It was also confirmed that the tangential component of flow velocity varies along the radial direction in the Lab Carousel, indicating the presence of secondary circulation (§ 3.3).

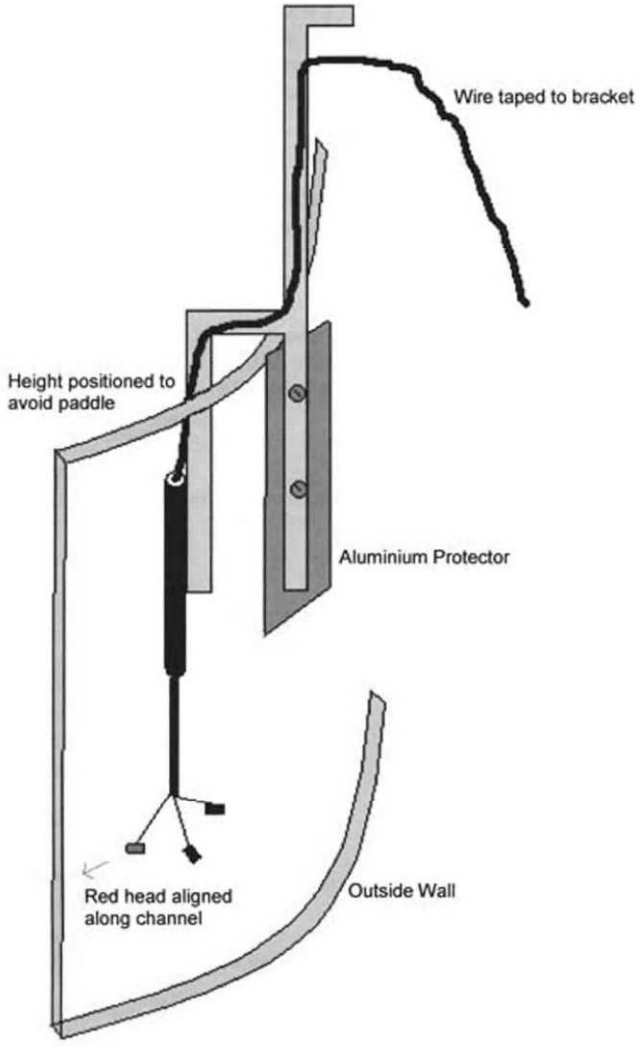

Figure 4.3 The ADV setup within the Lab Carousel

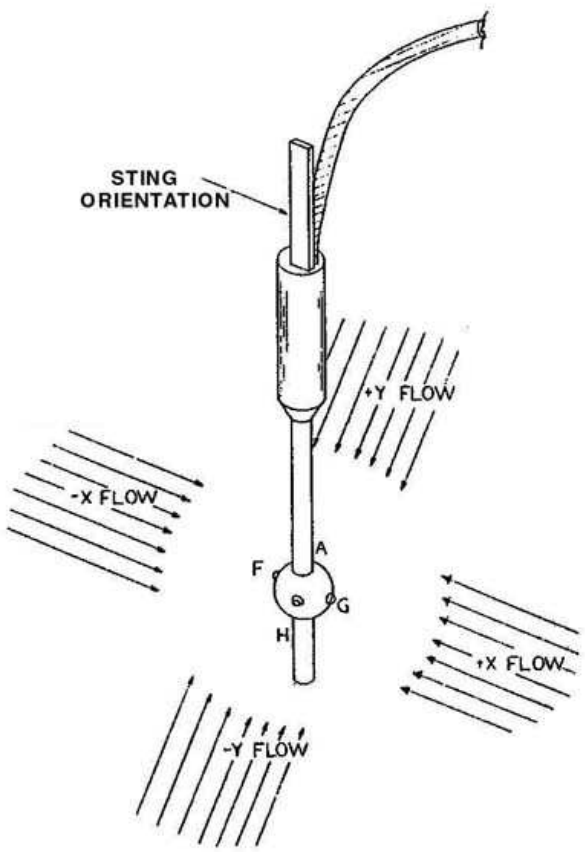

Figure 4.4 The Marsh McBirney® EMCM sensor

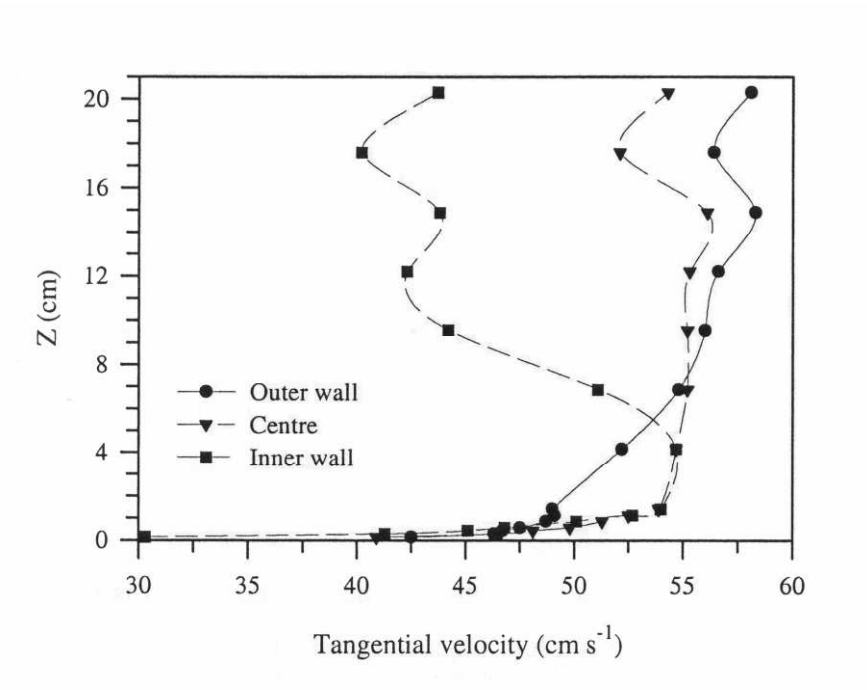

Figure 4.5 Profiles showing the variation of tangential velocity with height above bottom in the Lab Carousel (Cloutier et al., 2003)

4.2 Calibration

The various sensors (LDV, ADV, and EMCM) were calibrated using a digital video camera. The Lab Carousel was filled with fresh water up to a depth of 40 cm and allowed to adjust to room temperature. Then neutrally buoyant Goodyear pliolite® particles were added to the water. Previously, the particles had been sieved to a size range of 710 μm-1.4 mm and soaked in a soap solution, in order to remove air trapped on the surface of particles. Then a clear water flow was created in the flume for gradually increased motor inputs, starting from 10 Hz up to 70 Hz with a step of 10 Hz. The motion of white particles was monitored against a black grid for one minute using a digital video camera, which was focused on the center of the channel to eliminate wall effects on the recorded speeds. The height of focusing was the same as the height of the sensors above the flume base. Consequently, the particle speed at each particular level could be obtained from the video recordings. At the same time, the flow speed was measured continuously with each sensor for five minutes. The resulting calibration curves of the LDV, ADV and EMCM are illustrated in the figures 4.6, 4.7 and 4.8 respectively, while figures 4.9, 4.10 and 4.11 show the calibration of the three OBS sensors. Additionally, figure 4.12 shows the relationship between the lid rotational speed and the azimuthal flow speed.

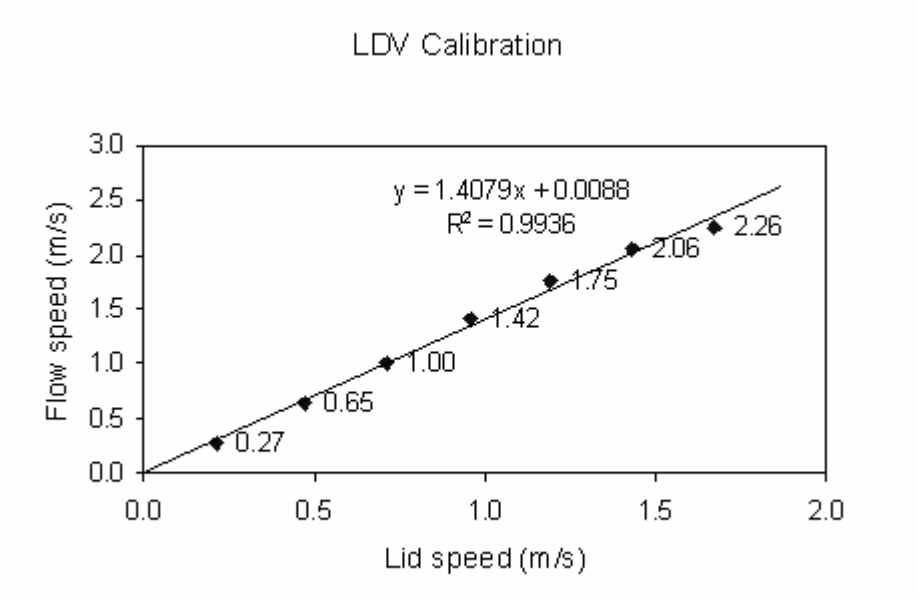

Figure 4.6 The calibration of the LDV sensor

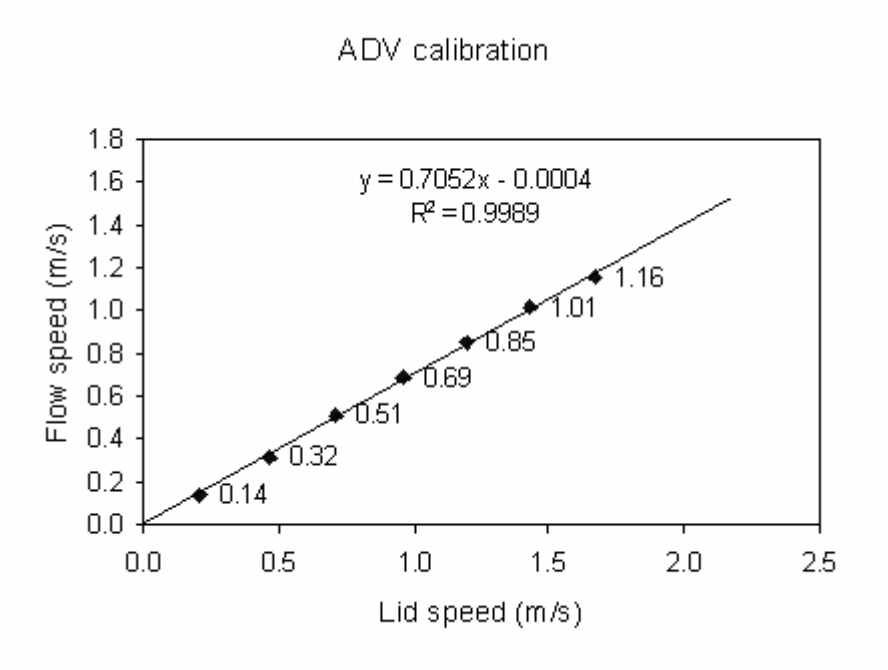

Figure 4.7 Calibration curve for the ADV

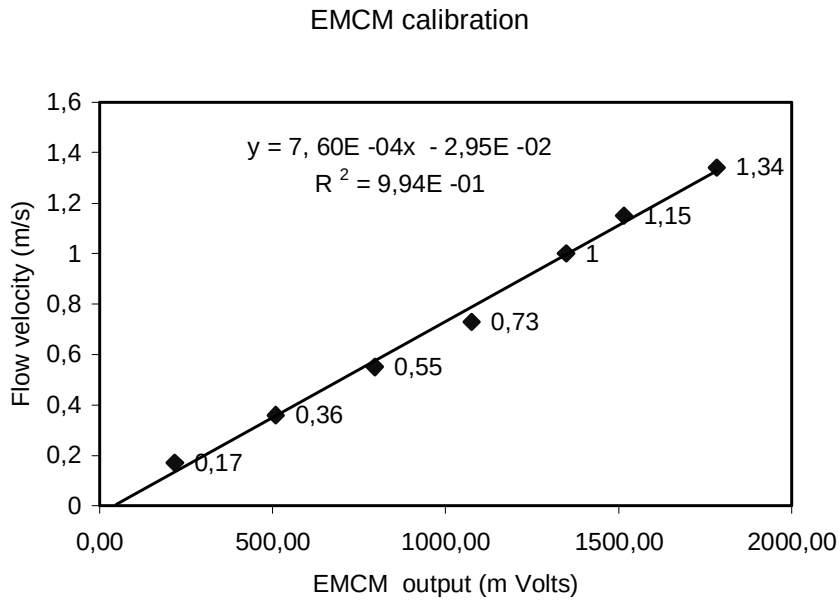

Figure 4.8 Calibration curve for the EMCM

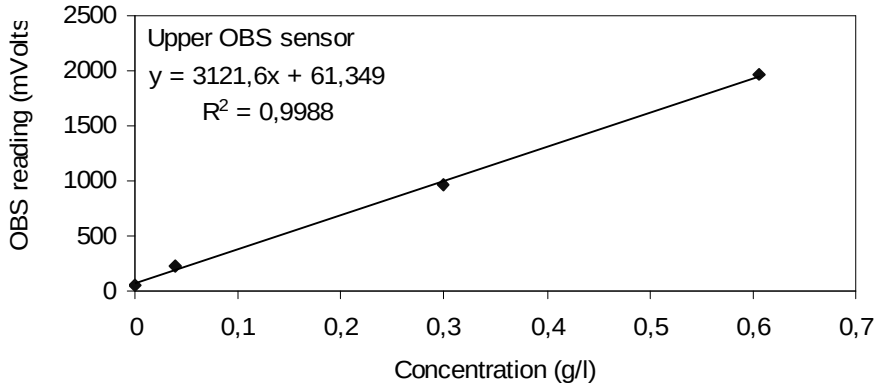

Figure 4.9 Calibration of the top most OBS sensor

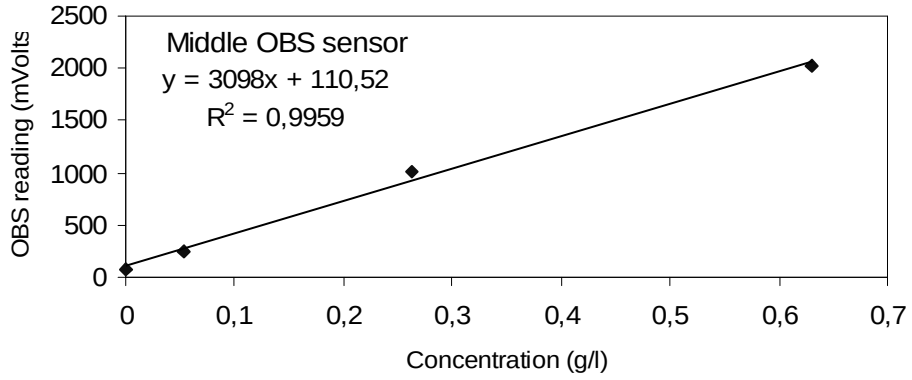

Figure 4.10 Calibration of the middle OBS sensor

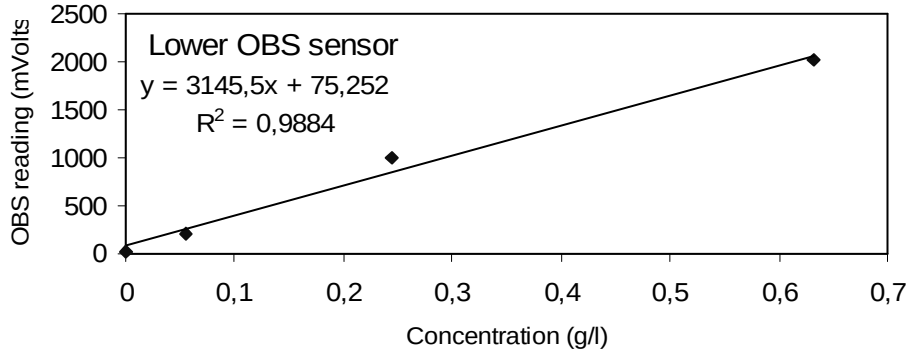

Figure 4.11 Calibration of the lower OBS sensor

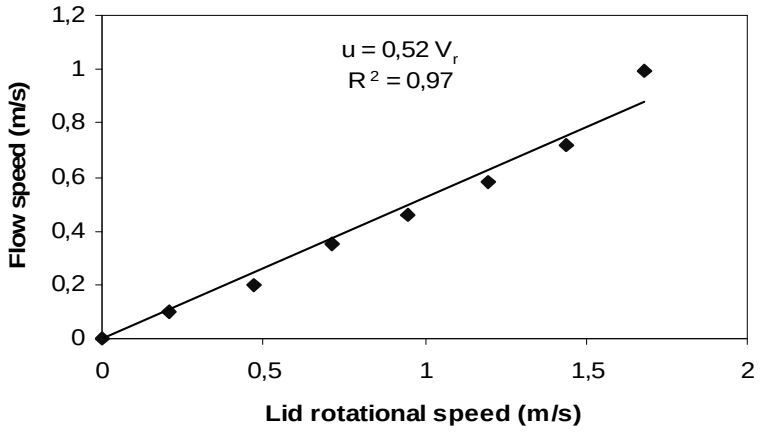

Figure 4.12 The Lab Carousel calibration curve. For each lid rotation speed, the azimuthal speed of a clear water flow was measured at the centre of the flume channel at a height of 0.15 m above bed.

4.3 Schedule of experiments

Two series of flow deceleration measurements were carried out in the Lab Carousel. For both, the maximum flow velocity was 1m/s, and the temperature of the fluid in the flume was 14^{o} C. In the first experimental series clear water has been used in order to provide controls. For clear water runs within the Lab Carousel, a well developed boundary layer with a thickness of ~ 0.02 m had been previously confirmed for a range of smooth flows by velocimetric measurements, obtained with the Laser Doppler Velocimeter (Thompson et al., 2003). In the second series of experiments, clay suspensions were used with different concentrations of the suspended material: 0.1 g/l, 0.5 g/l, 1 g/l, 3 g/l, 5 g/l, 10 g/l, 20g/l, 40 g/l and 60 g/l. For each concentration the whole procedure was repeated three times.

Commercially available potter clay (Briar Wheels, Alpha White Earthenware) was used in the preparation of the considered water-clay mixtures to a total amount of 27 kg. The water content of the clay was 21.6% and its particle density was 2.65 g/cm^3. The XRD analysis of a potter clay sample showed that it consisted mainly of kaolinite. It didn't contain organic matter, while quartz and illite were detected in negligible amounts. The mean size of the particles was 0.006 mm. For each

concentration a suitable amount of clay material (Table 4.1) was dissolved in freshwater up to a total fluid volume of 0.349 kg^3, in order to achieve a flow depth of 0.4 m within the Lab Carousel.

Concentration (g/l)	**Clay mass (kg)**	**Fluid density (kg/m^3)**
0.1	0.04452	1000.062
0.5	0.2226	1000.31
1	0.4452	1000.62
3	1.3355	1001.86
5	2.2258	1003.1
10	4.4515	1006.2
20	8.9031	1012.4
40	17.8061	1024.8
60	26.7092	1037.2

Table 4.1 Clay concentration and fluid density

During each experiment the data were initially recorded under still water conditions for five minutes to evaluate the offset of the sensors, and then the flow speed was gradually increased up to 1 m/s. This constant velocity of the flow was maintained for at least five minutes, so that a complete adjustment of the water column could be achieved with a subsequent fully developed bottom boundary layer. Then, three fluid

samples of volume 100 ml were collected, using the three sampling ports fitted on the wall of the flume at heights similar to those of the OBS sensors. The samples were filtered and the filtrate was oven dried at 40^{o} C for 24 hours. After weighing the dry sediment, the exact concentrations were determined and they were used in the calibration of the OBS sensors. After the samples were taken, the lid was lifted out of the flow using the hydraulic jack and the subsequent deceleration of the suspension was recorded by the ADV, and EMCM over the next 30 minutes. The LDV could not measure effectively for flow velocities higher than ~0.35 m/s, so it was not used in the second series of deceleration experiments. For concentrations of the suspension higher than 1 g/l the OBS sensors became saturated and therefore no useful records could be obtained from these sensors.

4.4 The Flow Deceleration Method

The method of flow deceleration (§ 3.3) has been previously used in reliable and fast estimations of the bed drag coefficient (C_D) for smooth and rough turbulent flows in the Lab Carousel (Thompson et al., 2003; 2004). The method is based on Newton's second law (§ 2.3) according to which the drag force, exerted by a solid boundary to a decelerating given mass of an inviscid fluid, is proportional to the deceleration of the fluid mass. Therefore, the estimation of the drag coefficient can be based on the inversion of this proportionality. It is proven that with the flow deceleration method, we can efficiently estimate the drag coefficient over a wide range of Reynolds numbers.

The drag force (F_D), which is exerted on a fluid mass by a rigid boundary and summed over a given time, causes a change in the momentum of the fluid mass. This change in fluid momentum represents the transfer of momentum from the fluid normal to the bed, taking place across the boundary layer. The fluid momentum transfer per unit area per unit time is expressed as a deceleration of the given fluid mass, which in turn results in the growth of a velocity gradient. Consequently, the drag force (F_D) and hence, the shear stress (τ) are proportional to the rate of velocity change in the decelerating fluid mass. In such a case, the drag coefficient (C_D) is the

factor of proportionality between the shear stress (τ) and the flow velocity (u). Thus, using mathematical formulation it is:

$$F_D = m\frac{du}{dt} = \tau A \qquad \text{Eq 4.1}$$

It is also:

$$\tau = C_{D(z)}\rho \bar{u}_{(z)}^2 \qquad \text{Eq 4.2}$$

Eq 4.2 is based on the assumption that the experimental flows are within the turbulent regime, where the variation of drag coefficient at a specific height above bed is not significant (Soulsby, 1983). The combination of (Eq 4.1) and (Eq 4.2) results in:

$$C_{D(z)} = \frac{m}{A}\frac{du}{dt}\frac{1}{\rho \bar{u}_{(z)}^2} \qquad \text{Eq 4.3}$$

where $C_{D(z)}$ is the drag coefficient at height z, m is the fluid mass, A is the wetted area or wetted perimeter per unit length (in fact the area of interaction), (ρ) is the fluid density and $\bar{u}_{(z)}$ is the mean flow speed at height z, averaged over a 1 second time interval. The drag coefficient can be calculated from Eq 4.3 if the change in velocity with time is estimated from the mean flow speed over a 10 seconds interval. It is assumed that the rate of deceleration is constant throughout the flow velocity measurements. This assumption is confirmed by observation of the decelerating fluid mass. The method shows the advantage of ease of application, as it permits an accurate estimate of C_D, simply from data obtained entirely from point-velocity measurements. This means that with the flow deceleration method it is not necessary to obtain velocity profiles, which introduce certain complications in the measuring procedure.

4.5 Estimation of drag coefficient and shear stress

The aim of the laboratory measurements undertaken in this work is the estimation of the bed drag coefficient and bed shear stress on the flat smooth bed of the Lab Carousel using the method of Flow Deceleration. The drag coefficient given by Eq 4.3 is the total value of the drag coefficient, representing the total drag force exerted by the flume walls and base. Thus, the wetted area A in Eq 4.3 is equal to the total wetted area of the flume ($=5.521\,\mathrm{m}^3$). Considering clear water flows, the fluid density ρ in Eq 4.3 is equal to the density of fresh water (ρ=1000 kg/m^3), while $m = 349.7\,\mathrm{kg}$, which is the mass of water in the flume for a flow depth of 0.4 m. In the suspension flows $m = m_m$, where m_m is the total mass of the clay-water mixture, calculated as the sum of the water mass plus the mass of the clay added to the suspension, thus:

$$m_m = 349.7 + m_{\mathrm{clay}} \qquad \text{Eq 4.4}$$

In the same way the density in Eq 4.3 is the bulk density of the clay-water mixture (Table 4.1), calculated as:

$$\rho = 1 + 0.00062C \qquad \text{Eq 4.5}$$

where C is the suspended clay concentration.

The bed component $F_{D(bed)}$ of the total drag force is given by:

$$F_{D(bed)} = F_{D(total)} - F_{D(wall)} \qquad \text{Eq 4.6}$$

where $F_{D(wall)}$ is the wall component of frictional drag. It is also:

$$F_{D(bed)} = C_{D(z)_{(bed)}} \rho u^2 A_{(bed)} = m\frac{du}{dt} \qquad \text{Eq 4.7}$$

where $A_{(bed)} = 0.872\, m^3$. As it was mentioned in §4.1, the base and walls of the Lab Carousel are made of the same material (acrylic) and have a flat smooth surface, so we can assume that $C_{D(z)} = C_{D(z)_{(total)}}$ (Thompson et al., 2004). Therefore, the value of the bed drag coefficient can be calculated from Eq 4.3 for each concentration of the suspended sediment, while the bed shear stress τ is derived from Eq 4.2. It is obvious that if the value of the bed drag coefficient is known, then the bed shear stress can be calculated from simple point-velocity measurements.

4.6 Viscosity calculation

It is known that the dynamic viscosity coefficient of a fluid is influenced by the presence of sediment particles in suspension. The viscosity of a water-sediment mixture exhibits a significant deviation from that of clear water for concentrations of suspended particles higher than about 50 kg/m^3 (Van Rijn, 1993). In Figure 4.13 the relationship between the relative dynamic viscosity coefficient n_m / n (where n_m = dynamic viscosity of the fluid-sediment mixture, n = dynamic viscosity of clear fluid) and the suspended sediment concentration is illustrated for natural muds.

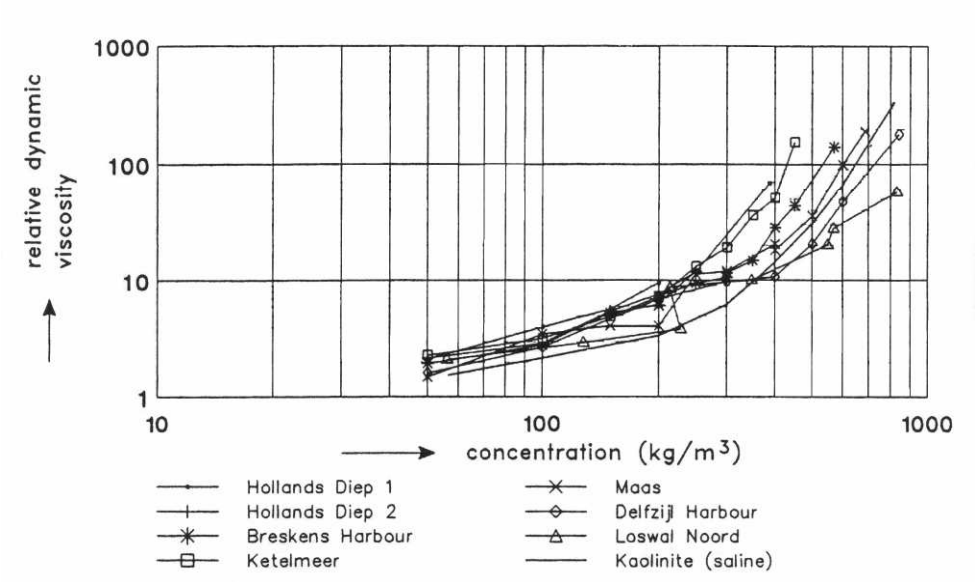

Figure 4.13 Dynamic viscosity coefficient plotted against suspended sediment concentration for natural muds in The Netherlands (Winterwerp et al., 1991)

Einstein (1906) studied the effect of elastic, spherical particle movements on the viscosity of dilute suspensions with $C_V < 0.1$. The volumetric sediment concentration C_V is calculated as:

$$C_V = \frac{1}{\rho_s} C \qquad \text{Eq 4.8}$$

where C is the mass concentration and ρ_s is the density of sediment particles, taken equal to 2.65 g/cm^3. An increase in dynamic viscosity with increasing concentration (Figure 4.14) was observed, according to the formula:

$$n_m = n(1 + 2.5C_V) \qquad \text{Eq 4.9}$$

Bagnold (1954) conducted experiments with higher volume concentrations of suspended sediment in the range of C_V =0.1- 0.6 and also found an increase of the dynamic viscosity, expressed as:

$$n_m = n(1+\lambda)(1+0.5\lambda) \qquad \text{Eq 4.10}$$

where λ is a dimensionless concentration parameter with $\lambda = [(0.74/C_V)^{1/3} - 1]^{-1}$.

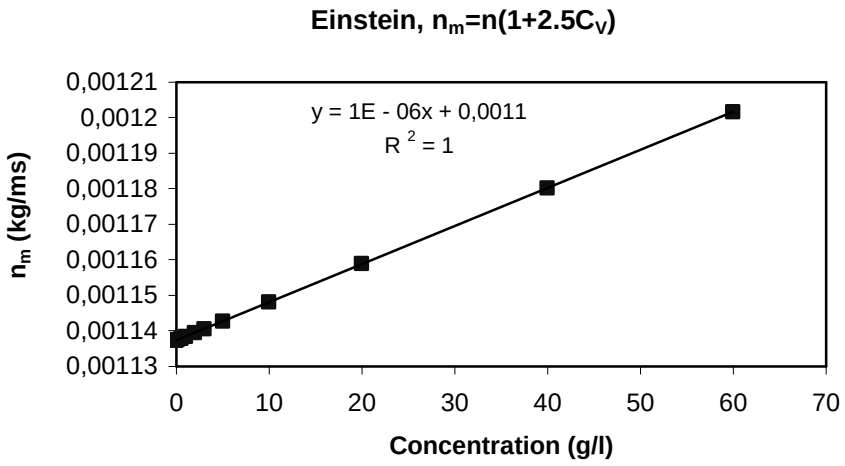

Figure 4.14 Dynamic viscosity (n_m) versus concentration for the clay-water mixtures used in the experiments (n is the dynamic viscosity of the water at 14°C)

Lee (1969) suggested the empirical relationship:

$$n_m = n(1-C_V)^a \qquad \text{Eq 4.11}$$

in which $a = -(2.5+1.9C_V + 7.7C_V{}^2)$.

Graf (1971) observed that in a two dimensional channel flow with sediment in suspension the downward flux of sediment due to settling was balanced by an upward flux due to turbulent lifting of material. In this case the suspension was considered to be stable, so that the dynamic viscosity of the sediment-water mixture could be approximated by:

$$n_m = n(1+2.5C_V + 6.25C_V{}^2 + 15.62C_V{}^3 + \ldots) \qquad \text{Eq 4.12}$$

where n_m is the dynamic viscosity of the sediment-water mixture, n is the dynamic viscosity of clear water, and C_V is the volumetric sediment concentration. Therefore, the dynamic viscosity of a sediment-water mixture in a channel flow can be predicted from Eq 4.12, using only terms up to the third order. According to Graf the effect of the suspended particles concentration on the dynamic viscosity of the clay-water mixtures used in the present experiments, is depicted in Figure 4.15.

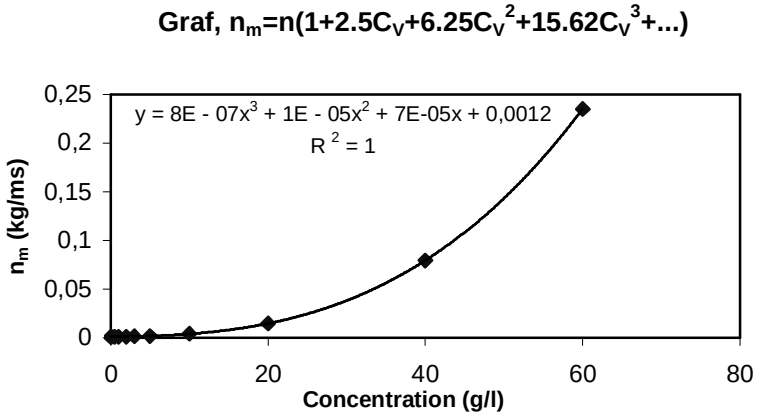

Figure 4.15 Dynamic viscosity of clay-water mixtures as a function of clay concentration

In the present study, the relationship proposed by Graf (1971) has been used in the determination of dynamic viscosity for the various concentrations of clay-water mixtures (Table 4.2). In this way the effect of increasing viscosity on the values of drag coefficient and bed shear stress obtained by the flow deceleration method, could be evaluated.

Concentration (g/l)	**Volumetric Concentration (%)**	**n_m (kg/ms) (Graf, 1971)**	**n_m (kg/ms) (Einstein, 1906)**
0	0	0.001137	0.0011373
0.1	0.003773443	0.00114783	0.001148029
0.5	0.018864365	0.00119327	0.001190936
1	0.037721614	0.00125529	0.001244552
3	0.113079533	0.00157498	0.001458813
5	0.188323917	0.00204296	0.001672752
10	0.37593985	0.00415356	0.002206191
20	0.74906367	0.01471795	0.003267075
40	1.486988848	0.07947017	0.005365181
60	2.21402214	0.23501133	0.007432318

Table 4.2 The values of Mass concentration, Volume percent and Dynamic viscosity of the clay suspensions used in the experiments. For clear water the value of dynamic viscosity at 14^o C has been used.

5 Results

The velocimetric data obtained as described in § 4.3 were further processed using Visual Basic for Applications. The results presented in this chapter, concern clear water runs and suspension flows of water-kaolinite mixtures.

5.1 Clear water flows

Two examples of decelerating clear-water flows are shown in Figure 5.1 and 5.2, recorded by the ADV and EMCM sensors respectively. In both cases the velocity data were averaged over one second. Figure 5.3 shows the bed drag coefficient (C_D) plotted against flow velocity in the Lab Carousel. The data were recorded by the ADV and averaged over 20 seconds for clarity. The drag coefficient is shown to decrease rapidly with increasing velocity in a quadratic fashion up to a value of about 0.1 and then tends asymptotically to a constant value of about 0.01. The same pattern is observed between drag coefficient (C_D) and Reynolds number (Re) (Figure 5.4), confirming the fact that the drag coefficient is not constant but a function of the Reynolds number. The mean C_D value for the maximum flow velocity was calculated as 0.002. Figure 5.5 shows a quadratic increase in shear stress with increasing flow velocity, described by the relationship $\tau = 0.89u^2 + 2.41u + 0.09$, $R^2 = 0.97$. The results shown in the figures 5.3, 5.4 and 5.5 confirm previous observations by Thompson et al., (2004). Data obtained with EMCM gave similar results (Figure 5.6 and Figure 5.7) and a mean C_D value for the maximum flow velocity of 0.006 was derived. The data shown are averaged over 20 seconds. It should be stressed that the drag coefficient estimations from EMCM recordings have been based on flow velocities measured at a height of 0.15 m above the flume base.

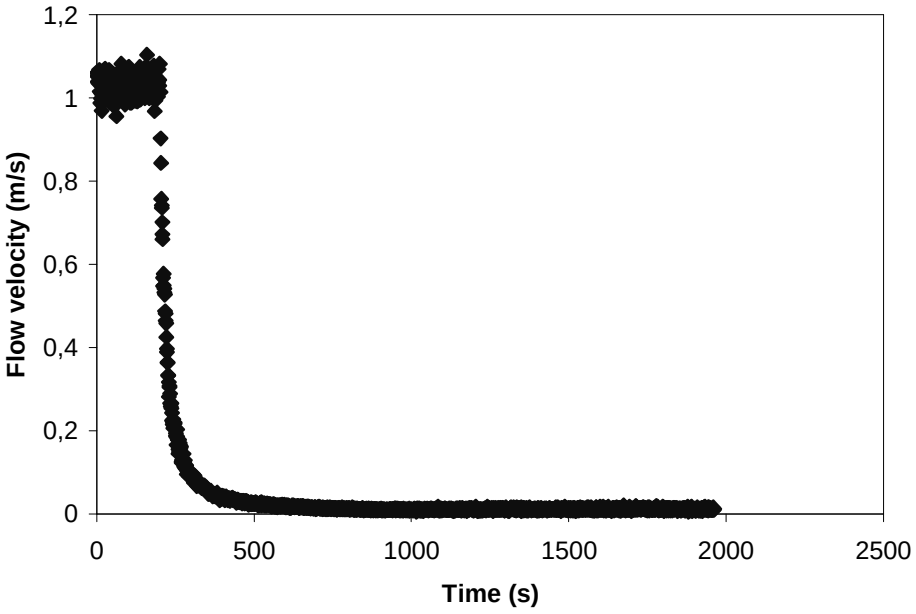

Figure 5.1 A typical deceleration time series recorded by the ADV at a height of 0.01 m above the flume bed. The data averaging has occurred over 1 second.

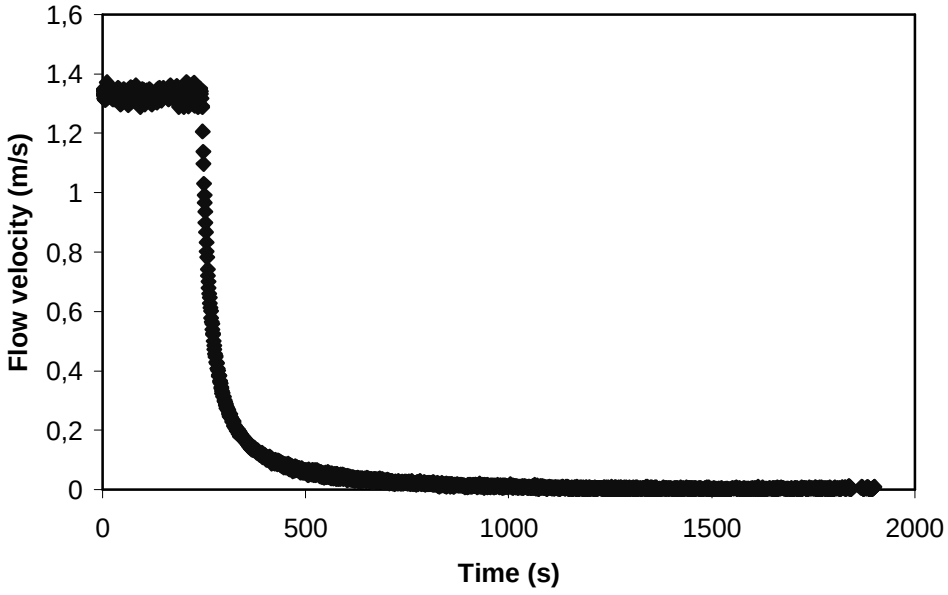

Figure 5.2 An example of decelerating flow recorded by the EMCM at 0.15 m above the flume bed. The data have been averaged over 1 second.

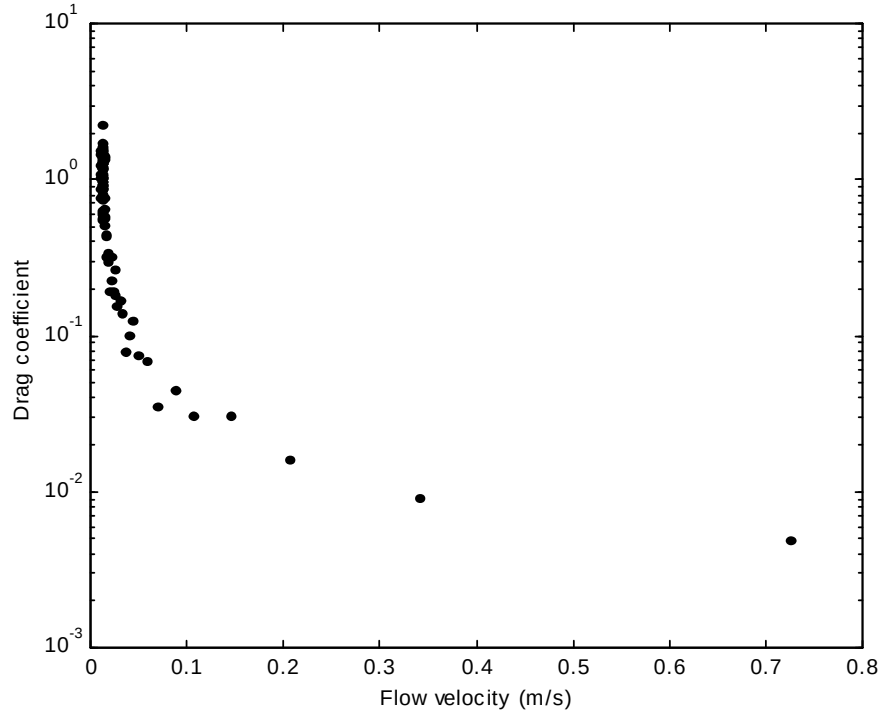

Figure 5.3 The bed drag coefficient versus flow velocity as recorded by the ADV at 0.01 m above bed. The data have been averaged over 20 seconds for clarity.

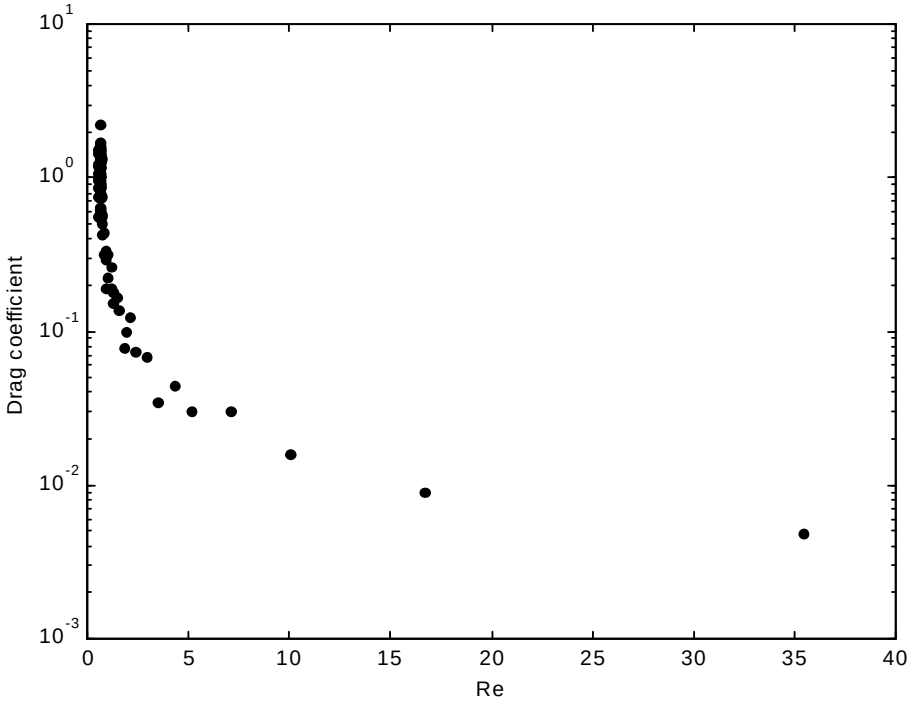

Figure 5.4 The bed drag coefficient versus Reynolds number. The ADV data have been recorded at 0.01 m above bed and averaged over 20 seconds.

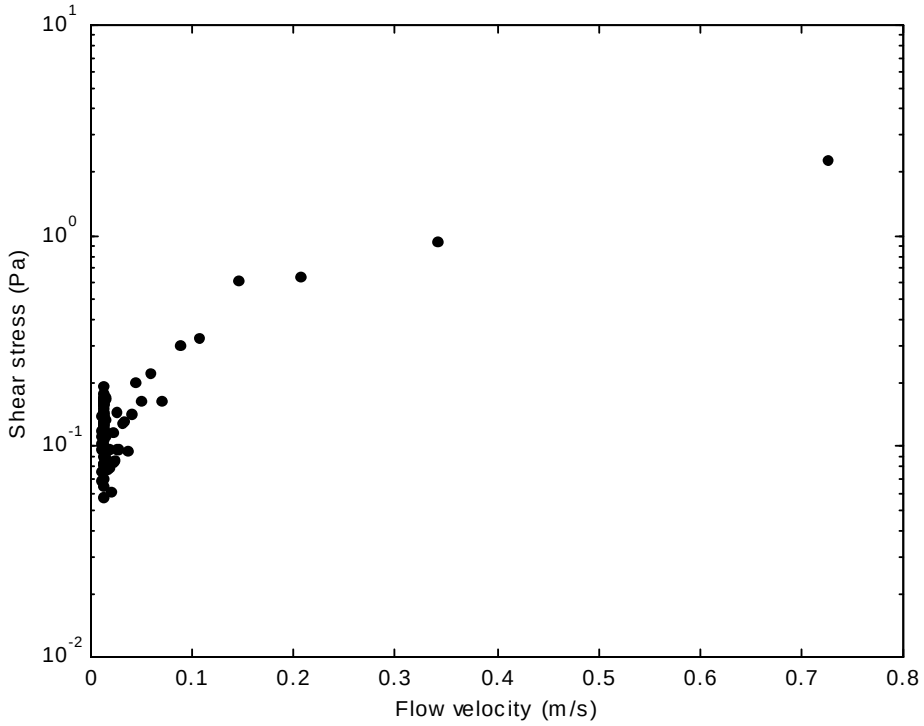

Figure 5.5 The bed shear stress versus flow velocity (ADV data)

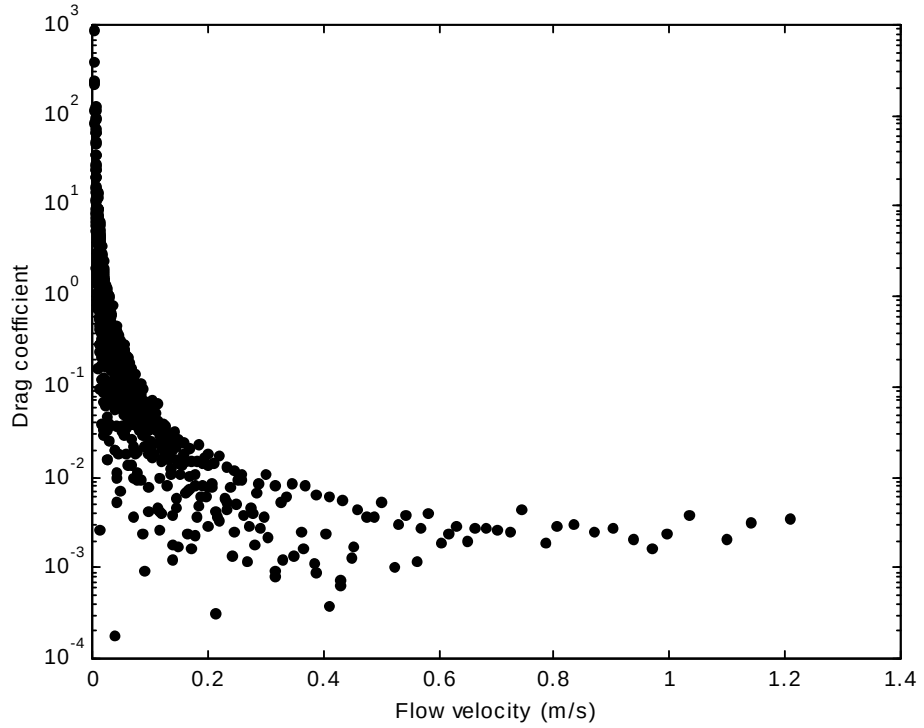

Figure 5.6 The bed drag coefficient versus flow velocity (EMCM data recorded at 0.15 m above the flume bed)

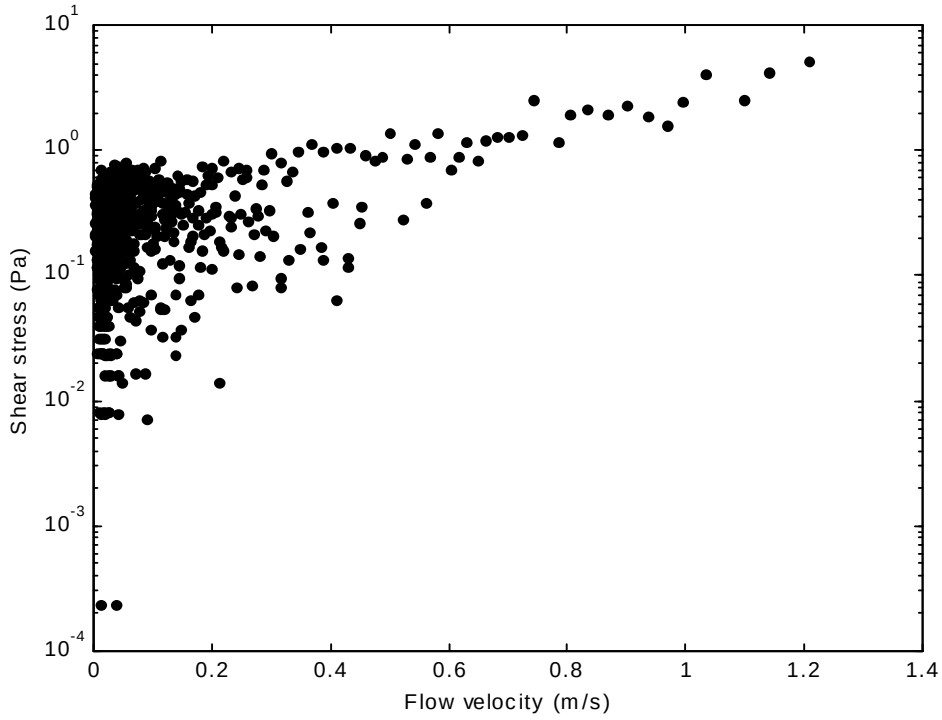

Figure 5.7 The bed shear stress versus flow velocity (EMCM data recorded at 0.15 m above the flume base)

5.2 Turbid flows

A variety of turbid flows were simulated in the Lab Carousel using clay material suspended in fresh water at nine different concentrations: 0.1 g/l, 0.5 g/l, 1 g/l, 3 g/l, 5 g/l, 10 g/l, 20 g/l, 40 g/l, and 60 g/l. The clay-water mixtures were accelerated up to ~1 m/s and then left to decelerate up to a final velocity less than 0.01 m/s. During each measurement the flow velocity of the decelerating fluid was recorded by the ADV and EMCM sensors at a height of approximately 0.01 m and 0.15 m above the flume base respectively. The sampling rate was 25 Hz for the ADV and 2 Hz for the EMCM. From these records the mean value of the bed drag coefficient was calculated for four different velocity ranges: 0.8 m/s, 0.5 m/s, 0.3 m/s, and 0.1 m/s. The data obtained by the Acoustic Doppler velocimeter have been considered as the most reliable, and hence the most appropriate for the particular purposes of this investigation. This is due to the measurement height, which is within the flow

boundary layer in the case of ADV. Furthermore, the ADV has a higher sampling rate. Therefore, the drag coefficient and shear stress estimations for the sediment-laden flows in the Lab Carousel have been exclusively based on velocity measurements obtained by the ADV. Table 5.1 shows the drag coefficient values under the four different velocity ranges. It is clearly exhibited that there is an increase in C_D at lower flow velocities and an overall decrease of C_D values with increasing concentration. The maximum decrease is also shown in Table 5.1 and suggests that significant drag reduction has occurred, the highest (51%) being observed within the range of 0.8 m/s (Figure 5.8).

Concentration (g/l)	**0.8 m/s**	**0.5 m/s**	**0.3 m/s**	**0.1 m/s**
0	0.004983	0.007544	0.012978	0.039609
0.1	0.004591	0.007914	0.014304	0.036547
0.5	0.004768	0.007934	0.012101	0.035081
1	0.004877	0.008979	0.013114	0.03846
3	0.005289	0.007854	0.011509	0.036689
5	0.003893	0.008164	0.012835	0.036341
10	0.003557	0.007247	0.009271	0.03211
20	0.00311	0.006823	0.0091	0.030339
40	0.003152	0.006274	0.008031	0.023615
60	0.00244	0.005605	0.007335	0.021079
Maximum decrease (%)	**51.0**	**25.7**	**43.5**	**46.8**

Table 5.1 The mean bed drag coefficient under various velocity ranges (ADV data)

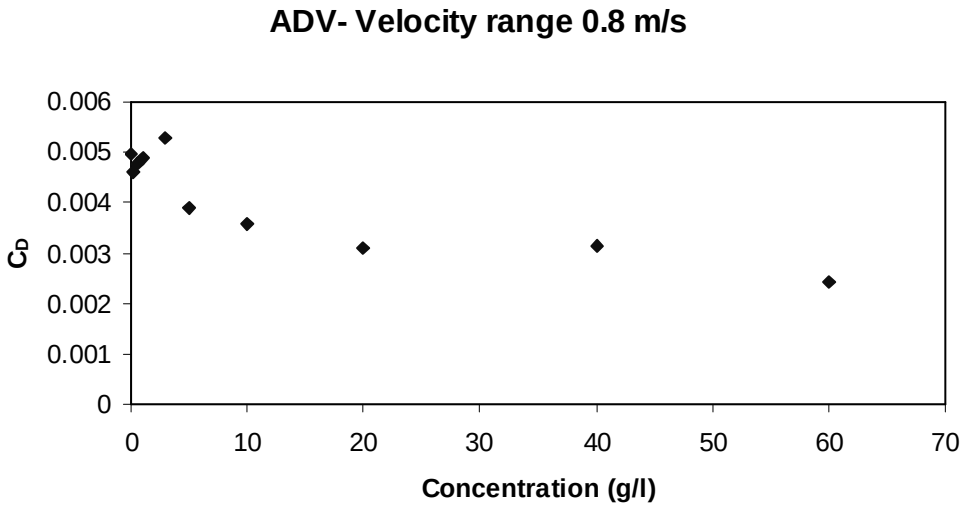

Figure 5.8 The bed drag coefficient versus concentration for a velocity range of 0.8 m/s

The same procedure was repeated for all of the four velocity ranges but this time the increase in the total mass of the suspensions with increasing concentration was taken into account. Therefore, the drag coefficient values were normalised according to the relationship:

$$C_{D(norm)} = C_D * \frac{m_{total}}{m_{water}} \qquad \text{Eq 5.1}$$

where $m_{water} = 349kg$ (= the mass of water in the Lab Carousel for a flow depth of 0.40 m), and $m_{total} = m_{clay} + m_{water}$. The normalised values of drag coefficient showed the same pattern of a general decrease at higher concentrations (Figure 5.9), although the maximum reduction (%) was slightly lower (Table 5.2).

Finally, the bed drag coefficient was normalised by the relationship:

$$C'_{D(norm)} = C_D * \frac{n_m}{n} \qquad \text{Eq 5.2}$$

In this way the effect of the increased viscosity was removed. Decreased values of drag coefficient were still observed at high concentrations compared to clear water flow, however the occurred drag reduction was smaller (Table 5.2).

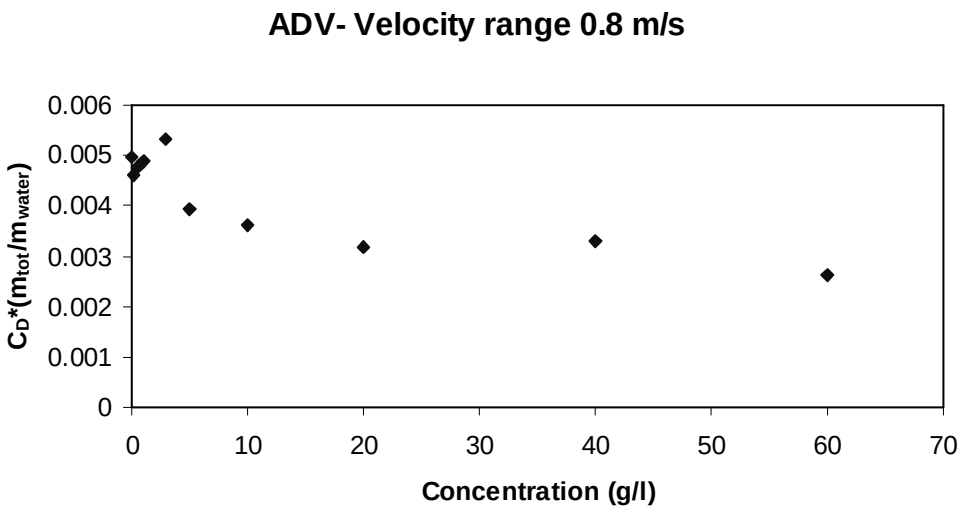

Figure 5.9 Mass-normalised drag coefficient versus concentration (Velocity range=0.8 m/s)

Velocity range (m/s)	**0.8**	**0.5**	**0.3**	**0.1**
$\mathbf{C_D}$	51.0	25.7	43.5	46.8
$\mathbf{C_D * m_{total}/m_{water}}$	47.3	20.0	39.2	42.7
$\mathbf{C_D * (n_m/n)}$	49.2	22.9	41.3	44.8

Table 5.2 Maximum decrease (%) of drag coefficient for various velocity ranges

Furthermore, in figures 5.8 and 5.9 two ranges of drag coefficient values can be distinguished: one corresponding at lower concentrations (0-3 g/l) and a second one corresponding at higher concentrations (5-60 g/l). In the first range the drag coefficient appears more or less constant, suggesting a Newtonian behaviour of the

dilute suspension flows. For the high concentration suspensions the drag coefficient decreases with increasing concentration in a linear way, indicating a distinct range where drag reduction occurs. The distinction is more obvious on a semi-logarithmic plot of C_D against concentration (Figure 5.10).

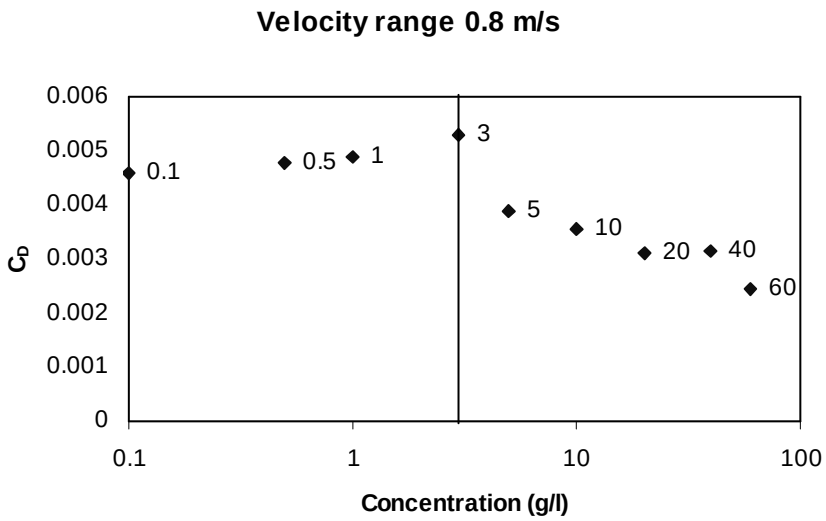

Figure 5.10 Drag coefficient versus concentration for a velocity range of 0.8 m/s. The line separates the two areas of dilute suspension flows of a constant c_D and drag-reducing flows.

The decrease (%) in C_D values for various velocity ranges is shown in Figure 5.11 and Table 5.3. The decrease was found to increase with increasing clay concentration, although it didn't show a distinct trend with respect to the flow velocity.

A similar behaviour was exhibited by the shear stress, which increased with increasing flow velocity and decreased with increasing concentration of clay suspensions (Figure 5.12, Table 5.4). These observations are valid for the normalised values of shear stress as well, where the effect of the increase in mass and viscosity are removed (Figure 5.13, Figure 5.14, Table 5.5). For the higher concentration flows, the observed reduction (%) in shear stress increases with increasing clay concentration, while the general trend is for a decrease at low flow velocities (Table 5.6, Figure 5.15).

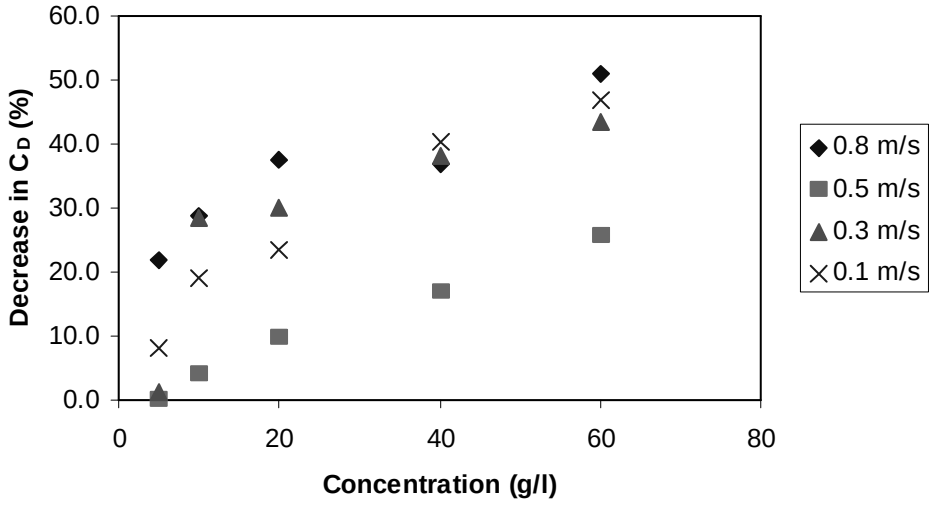

Figure 5.11 The effect of clay concentration and flow velocity on the decrease of drag coefficient

Concentration (g/l)	0.8 m/s	0.5 m/s	0.3 m/s	0.1 m/s
5	21.9	-8.2	1.1	8.3
10	28.6	3.9	28.6	18.9
20	37.6	9.6	29.9	23.4
40	36.7	16.8	38.1	40.4
60	51.0	25.7	43.5	46.8

Table 5.3 Reduction (%) in drag coefficient for various flow velocities in high clay concentration suspensions

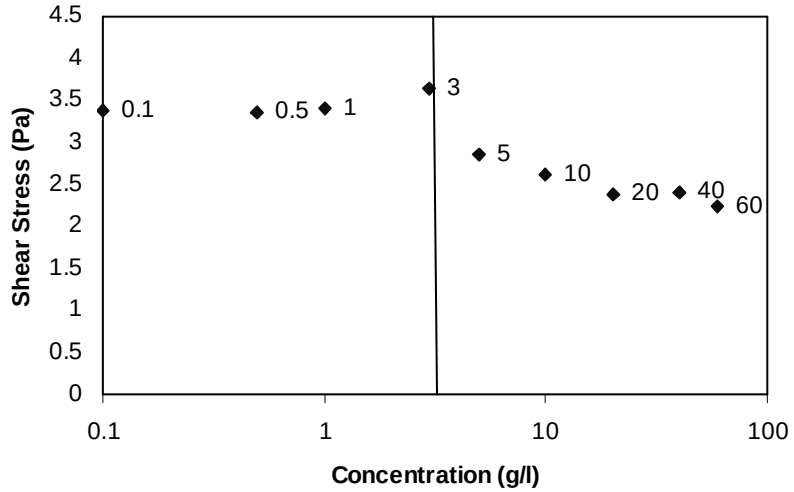

Figure 5.12 Bed shear stress versus concentration for dilute suspension flows and drag-reducing flows (velocity range = 0.8 m/s)

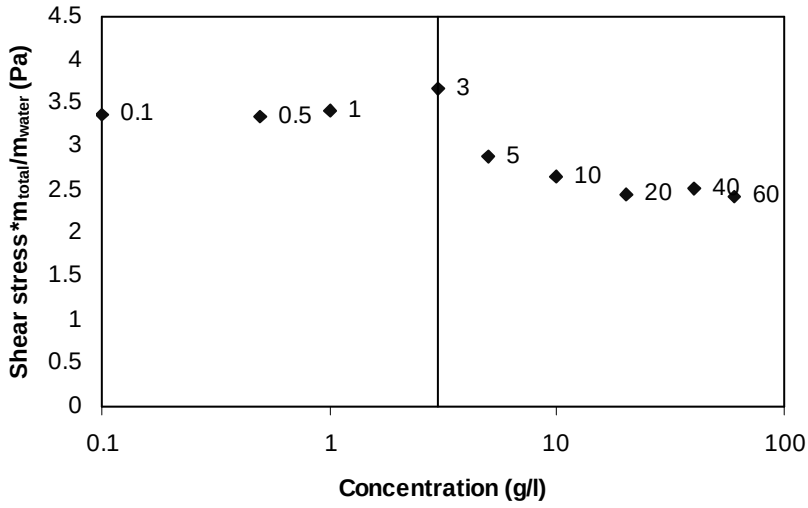

Figure 5.13 Mass-normalised shear stress versus concentration (velocity range = 0.8 m/s)

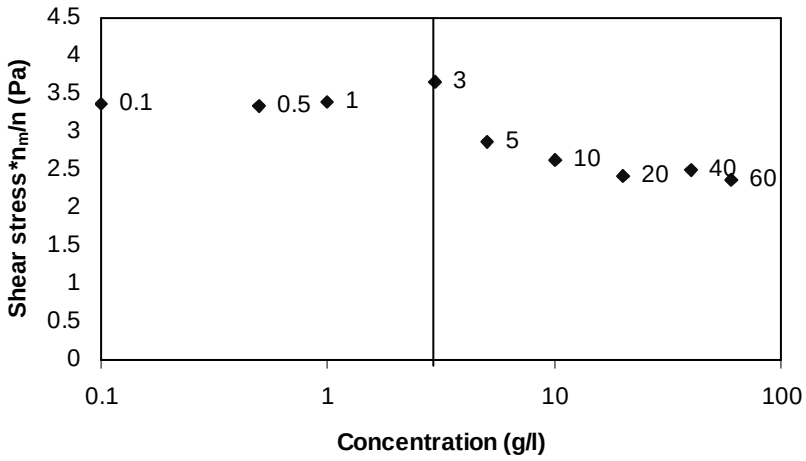

Figure 5.14 Viscosity-normalised shear stress versus concentration (velocity range = 0.8 m/s)

Concentration (g/l)	**0.8 m/s**	**0.5 m/s**	**0.3 m/s**	**0.1 m/s**
0	3.85737	1.920406	0.830979	0.395015
0.1	3.371136	1.774336	0.86809	0.308307
0.5	3.353654	1.925812	0.854066	0.272073
1	3.400544	2.108657	0.733637	0.376071
3	3.648037	1.652226	0.859978	0.370845
5	2.855003	1.826071	0.994936	0.36541
10	2.615835	1.620728	0.691349	0.316658
20	2.374434	1.74421	0.748644	0.323129
40	2.399525	1.558216	0.660009	0.292177
60	2.243233	1.212585	0.544612	0.355817

Table 5.4 The mean bed shear stress under various concentrations and flow velocities

Flow velocity	0.8 m/s	0.5 m/s	0.3 m/s	0.1 m/s
τ	41.8	36.9	34.5	9.9
$\tau^*(m_{tot}/m_{water})$	37.4	32.0	29.4	3.0
$\tau^*(n_m/n)$	38.6	33.3	30.8	4.8

Table 5.5 Maximum decrease (%) in shear stress for various velocity ranges

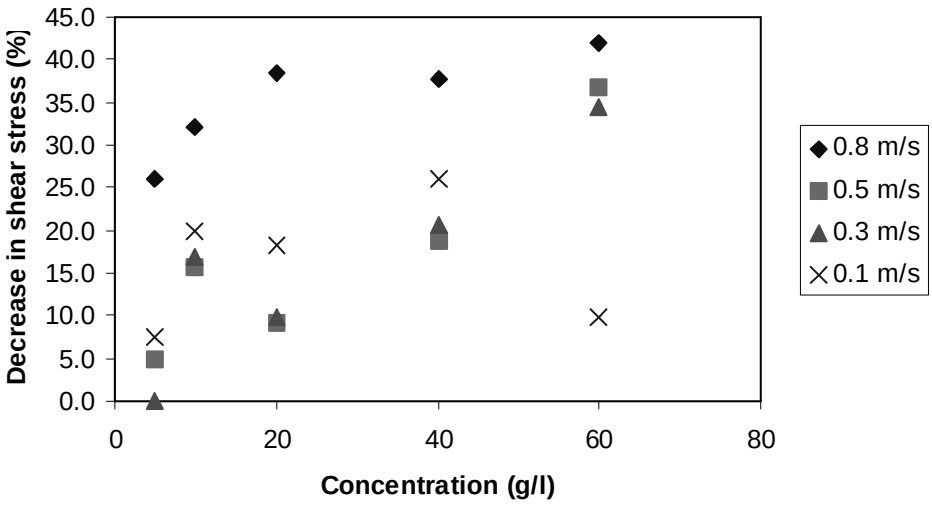

Figure 5.15 The effect of clay concentration and flow velocity on the decrease of shear stress

Concentration (g/l)	0.8 m/s	0.5 m/s	0.3 m/s	0.1 m/s
5	26.0	4.9	0.0	7.5
10	32.2	15.6	16.8	19.8
20	38.4	9.2	9.9	18.2
40	37.8	18.9	20.6	26.0
60	41.8	36.9	34.5	9.9

Table 5.6 Reduction (%) in bed shear stress under various flow velocities in high clay concentration suspensions

6 Discussion

It has been widely recognised that the presence of fine-grained sediments in suspension flows can significantly modify the structure of the boundary layer and therefore affect the frictional drag (Dyer, 1986; Mehta & Dyer, 1990; Komatina and Jovanovic, 1997). It was proved that the bed shear stress derived from either velocity profile measurements or the quadratic stress law, based on a single velocity measurement at a fixed height would be overestimated in clay suspension flows if turbidity levels are not considered (Gust, 1976; Gust & Walger, 1976). This has been explained by the existence of the drag reduction phenomenon, which results in the decrease in shear stress in the viscous sublayer relative to the apparent shear stress in the logarithmic layer. The results presented in chapter 5 are found to be in line with earlier findings (Gust, 1976; Best & Leeder, 1993; Li & Gust, 2000, Amos et al., 2003), and they confirm the occurrence of drag reduction in flows with concentration of clay suspended matter up to 60 g/l. The reduction in bed drag coefficient and shear stress under four different flow rates is listed in Table 5.3 and Table 5.6 respectively. The maximum decrease (~ 50%) in drag coefficient over the range 0-60 g/l was observed for clay concentration equal to 60 g/l under a flow velocity range of 0.8 m/s. In a similar way, the maximum decrease in shear stress was ~ 40% for 60 g/l and flow speed of about 0.8 m/s. Figure 5.11 and Figure 5.15 show that higher reductions occur systematically at higher concentrations, supporting previous observations by Li & Gust (2000). From both figures (5.11 and 5.15) it is concluded that the effect of flow strength on the decrease in drag coefficient and shear stress values doesn't show a distinct trend.

In Figure 5.9 the normalized (for mass increase) bed drag coefficient is shown to decrease at high clay concentrations but to a smaller extent than that observed if the effect of the increased mass of the suspension is not considered. Table 5.2 shows that

the maximum reduction (%) in drag coefficient, determined for the maximum suspended clay concentration of 60 g/l relative to the clear water flow is slightly lower, if we consider the normalized values of drag coefficient. In other words, if the effect of the increased mass and higher viscosity of the suspension is removed by normalization, then drag reduction is still observed but to a lower extent.

In Figure 5.13 and 5.14, where the normalised shear stress (for increased mass and increased viscosity respectively) is plotted against concentration, the same shaped relationship is observed, as in the case of the drag coefficient (Figure 5.10). However, for a given flow velocity range the reduction (%) in shear stress is lower if the normalized values are considered (Table 5.5). The effect of the increased viscosity of the suspension on the reduction of both drag coefficient and shear stress, appears to be slightly lower than the effect of the increased mass of fluid-sediment mixture (Table 5.2 and Table 5.5).

In earlier experimental investigations, various types of clay minerals have been used in the preparation of the suspensions, such as mixtures of illite and montmorillonite (Gust, 1976), mixtures of kaolinite and illite (Best and Leeder, 1993), or pure kaolinite (Li and Gust, 2000), as in the present experiments. The results from all these experimental studies agree because drag reduction has been demonstrated in all cases. This implies that the type of suspended clay minerals, does not play an important role in the drag reduction phenomenon and this is also supported by the current experimental work.

Regarding the mechanisms of the reduction in drag, it is known that for a given flow velocity range, a sufficient increase in suspended sediment concentration results in an increase in turbulence suppression near the solid boundaries, which in turn leads to a decrease in the bed shear stress. This effect was measured by Cloutier et al. (2003) for suspension flows in the Lab Carousel (§ 3.3). Therefore, the turbulence damping in the Lab Carousel could be responsible for the shear stress reduction, which has been observed in the measurements. Besides, Gust (1976) measured velocity profiles in suspensions of clay concentration 150-380 mg/l and found that the viscous sublayer increased by a factor of 2-5 under the particular experimental conditions. In the present experiments in the Lab Carousel the ‘thickening’ of the viscous sublayer

could also account for the drag coefficient suppression, although the thickness enhancement was not determined by velocity profiling.

6.1 Summary and conclusions

Experimental results regarding flow resistance in smooth turbulent sediment-laden flows are presented. The range of suspended clay concentration in the experimental flows was between 0-60 g/l. The friction factor (or drag coefficient) in a sediment-laden flow is compared to a friction factor in an equivalent clear-water flow. The drag coefficient in all experimental runs was determined by the Flow Deceleration method in the Lab Carousel. The following conclusions are made: the water-clay mixtures exhibit the drag reduction phenomenon if the concentration of the suspended clay solids is appropriately high. For the analysed kaolinite clay suspensions, the decrease in drag coefficient is evident at concentrations over about 3 g/l, which is in accordance with findings reported in literature for other types of solid-liquid mixtures. The observed reduction in drag coefficient and shear stress can be attributed to turbulence suppression due to mechanical causes within the Lab Carousel.

Additionally, it was confirmed that the method of flow deceleration is a practical tool, used in fast estimations of the drag coefficient and associated shear stress. Its main advantage comprises of the ease of application, as a simple measurement of point-velocity is required at the considered height within the water column.

The study of turbulent flows and their ability to transport sediment and develop bedforms is based on experimental work where clear water has routinely been used (Van Tassell, 1981; Grant et al., 1984; Komar, 1985; Pantin & Leeder, 1987). As a result, there is a lack of data concerning seawater flows transporting clay solids in suspension (Dyer, 1989). Therefore, three possible ways in which the present work could be developed, are recognised. First, a more extensive series of laboratory simulations is needed, to investigate the effect of higher clay concentrations on the drag coefficient and shear stress values. In particular, the work described in this thesis has been further extended to concentrations up to 200 g/l (Thompson et al., 2006), so that the effect of the increased viscous resistance on the reduction of the bed drag

coefficient could be examined. The second recommendation is for an additional series of experiments with clay suspended in seawater, as there is a lack of data concerning sediment-laden seawater flows. The third option is the introduction of hydrodynamic roughness within the experimental turbid flows.

To the above future improvements one could add the investigation of motion of suspended sediment mixtures, consisting of cohesive and non-cohesive particles. This problem has not received particular attention so far, although mixed sediments are very common in coastal and estuarine environments. It has been widely observed that muddy sand-beds may contain only a small amount of clay minerals. However, they exhibit a non-newtonian response under threshold conditions. In an extended future laboratory investigation, a combination of clay material with fine-grained sand could be used, the fine-grained sand consisting of grains of different grades from very fine to medium.

Appendix A

An evaluation of bed shear stress under turbid flows

C. E. L. Thompson,[1] C. L. Amos,[1] M. Angelaki,[1] T. E. R. Jones,[2] and C. E. Binks[1]

Received 8 September 2005; revised 9 January 2006; accepted 23 January 2006; published 22 April 2006.

[1] This paper investigates the effect of various turbidity levels on the drag coefficient and bed shear stress in decelerating flows over a smooth bed. Turbid flows were simulated in a laboratory annular flume (Lab Carousel) using clay suspensions of different known mass concentrations. Flow velocity measurements were taken in the turbulent boundary layer and the values of bed drag coefficient and shear stress were calculated using the method of flow deceleration. Results showed that the bed drag coefficient responds significantly to an increase in the suspended sediment concentration (up to 20 g\L) showing a decrease of up to 50% in drag due to turbulence suppression. However, subsequent increases in mass concentration resulted in an increase in the drag coefficient reaching the clear water value at approximately 200 g\L because of the influence of viscosity. Thus the application of the law of the wall in flows of high concentrations of suspended cohesive sediments up to 200 g\L results in overestimation of the bed shear stress.

Citation: Thompson, C. E. L., C. L. Amos, M. Angelaki, T. E. R. Jones, and C. E. Binks (2006), An evaluation of bed shear stress under turbid flows, *J. Geophys. Res.*, *111*, C04008, doi:10.1029/2005JC003287.

1. Introduction

[2] Entrainment and the transportation of cohesive material in suspension occurs by tidal currents in estuaries and tidal flats, by storm surges and tidal currents on the continental shelf, and by turbidity and thermohaline currents in marine basins. Entrainment is the rule rather than the exception, yet effects of SPM on flow character and shear within these settings is ambiguous. Traditionally studies on the ability of flows to transport sediment have focused on experimental work in clear water [*Grant et al.*, 1984; *Komar*, 1985; *Pantin and Leeder*, 1987]. Thus the determination of the correct value of friction factor in the presence of suspended sediments has remained unresolved [*Khullar et al.*, 2002].

[3] Material entering into suspension in a moving fluid may cause changes to the flow characteristics that affect the resistance to the flow [*Khullar et al.*, 2002]. *Li and Gust* [2000] measured directly shear velocity in the viscous sublayer of a steady, unidirectional flow: they showed it was reduced by up to 70% relative to the clear water profile–derived shear velocity using law of the wall, and hence greater drag reduction resulted by increasing concentrations of clay in suspension. However, studies carried out by other researchers have shown that friction factors of rigid boundary channels increase with increasing SPM [*Yano and Daido*, 1964; *Taggart et al.*, 1972; *Ippen*, 1973; *Lyn*, 1991].

[4] The effect of suspended sediment on flow resistance can be evaluated by calculating the drag coefficient ($C_{D(z)}$, where $C_{D(z)} = \left(\frac{\overline{U_z}}{u_*}\right)^2$), a parameter used to transform flow velocity (measured at height z in the flow) to friction velocity or bed shear stress. However, it is erroneous to assume a constant value of $C_{D(x)}$, irrespective of flow strength, structure, turbidity level, and bed roughness [*Sternberg*, 1972].

[5] Many experiments in the past cover a range of concentrations ~2–3 g/L [*Amos et al.*, 1992; *Best and Leeder*, 1993; *Gust and Walger*, 1976; *Li and Gust*, 2000]. The purpose of this work is to extend the results on the effects of concentration of fine suspended sediment on the bed drag coefficient and shear stress into the fluid mud range (up to 200 g\L) in the light of previous work.

[6] The experimental work was carried out in a laboratory annular flume – the Lab Carousel, and consisted of measurements of the flow of clay suspensions at various known concentrations over a smooth flat bed. An annular flume was used as flow turbulence, flow structure and drag may be considered radially symmetrical (Couette), hence simplifying measurement. A full discussion of the problems associated with annular flumes and the justification for using one for bed drag coefficient calculations is given by *Thompson et al.* [2004].

2. Mechanism of Drag Reduction

[7] If suspended material is cohesionless, the flow is Newtonian and only von Karman's constant k and kinematic viscosity ν are altered by the suspension [*Hunt*, 1954]. The latter effect was demonstrated experimentally by *Gust* [1976], who found that the universal law of the wall was not

[1]School of Ocean and Earth Science, National Oceanography Centre, Southampton, UK.
[2]School of Mathematics and Statistics, Plymouth University, Plymouth, UK.

0148-0227/06/2005JC003287$09.00

applicable to dilute seawater-clay suspensions in a laboratory channel. The friction velocity $u_* = (\tau_0/\rho)^{1/2}$ where τ_0 is the bed shear stress and ρ is fluid density, [*van Rijn*, 1993; *Soulsby*, 1983] is computed from mean streamwise velocity measurements in the logarithmic layer of the turbulent benthic boundary layer. The friction velocity (u_*) of hydraulically smooth Newtonian fluids is calculated by solving:

$$\bar{u}_z/u_* = 1/k \ln(z\bar{u}/\nu) + C_1 \quad (1)$$

where u = local mean streamwise velocity, z = vertical distance, and ν = kinematic viscosity. In equation (1): von Karman's constant, k has been found experimentally to be 0.38–0.41 and C_1 is an empirical coefficient found empirically to be 5.5 for clear water. The law of the wall is only valid for equilibrium benthic boundary layers under fully developed turbulent smooth Newtonian flows. However, *Gust* [1976] states that C_1 changes once sediment is suspended in the water column. The significance of drag reduction to the phenomena of sediment transport has been examined extensively for the case of the formation and behavior of fluid muds [*Mehta and Dyer*, 1990]. However, the mechanics of clay behavior in the development of fluid muds and the consequent effect on the phenomenon of sediment transport is less well known. For example, *Fortier and Scobey* [1926] found that the permissible (artificial) channel velocities to exhibit scour were higher in turbid water than for clear water. They suggested, erroneously, that the deposited cohesive particles cemented the bottom material, and in so doing became less subject to the erosive action of the flow. In fact drag reduction, which occurred in their experimental smooth and rough flows, decreased the bed shear stress to subthreshold values. This is evident in the work of *Gust and Walger* [1976], who conducted flume and field experiments in which clay suspensions in seawater caused drag reduction (20–40%) leading to an overestimation in bed shear stress from the law of the wall: they used mixtures of illite, kaolinite and chlorite at (relatively low) concentrations less than 380 mg\L. They proposed that the observed turbulent drag reduction at such low concentrations is caused by dynamic interaction between turbulent shear strain in the flow and energy required to deform suspended aggregates.

[8] *Best and Leeder* [1993] confirmed drag reduction in turbulent seawater flows through laboratory experiments using a nonintrusive laser Doppler anemometer to measure flows in clay suspensions of up to 2.2 g\L. They found that increasing the concentration of clay caused progressively lower velocities near the wall because of a gradual thickening of the buffer region of the turbulent boundary layer. Several aspects of sediment transport, deposition and bed form development in natural marine environments are thus considered to be significantly affected by drag reduction.

[9] Flocs of some clay minerals may extend into a long-chain structure similar to polymer molecules [*Wang et al.*, 1998]. This long-chain structure damps turbulence leading to drag reduction. It has been demonstrated that these long chains thicken the viscous sublayer or buffer layer below the logarithmic layer [*Virk*, 1971], so greater mean velocities in the logarithmic layer are needed to maintain the equivalent critical (fluid-transmitted) friction velocities u_{*crit} for erosion of a subaqueous substrate than is the case for clear water flows. *Wang et al.* [1998] found that flocs in a high-concentration clay suspension connect together and form a three-dimensional skeleton structure. This has a certain strength that resists the shear stresses across the structure. This skeleton was found to suppress turbulence, but also resulted in higher viscous shear than clear water flows.

[10] It has been proposed that all types of elastically deformable aggregates, which can form from bioaggregation, will cause drag reduction in natural turbulent flows. Other rheological properties like thixotropy or dilatancy of suspensions could also change the behavior of turbulent flows and cause this phenomenon [*Gust and Walger*, 1976].

3. Measurements of Stress Reduction in Annular Flumes

[11] *Amos et al.* [1992] developed, tested and calibrated a benthic annular flume, the Sea Carousel, and found that for a constant mean velocity, the shear velocity (measured using a hot film probe) dropped 5–10% when the mud concentration was increased from 0 to 280 mg\L. A relationship was thus proposed between drag reduction and clay concentration that was applied to estimates of bed shear stress in eroding flows within the Sea Carousel while being used on the Fraser River delta [*Amos et al.*, 1997]. This stress reduction algorithm is in agreement with *Li and Gust* [2000], who studied turbid flows in a straight laboratory flume.

[12] The effect of suspended sediment concentration on flow turbulence in a laboratory annular flume, the Lab Carousel, was investigated by *Cloutier et al.* [2002]. Three components of a constant mean flow (of 0.57 m/s) were recorded at 25 Hz using a 3-D Acoustic Doppler Velocimeter (ADV). It was shown that turbulence intensity and energy dissipation rate of the flow decreased by nearly 30% of the clear water values over the range 0.2–4.8 g\L. The observed reduction of turbulence was found to cause a significant reduction in bed shear stress and consequently a diminution of the erosion and resuspension processes.

[13] The laboratory experiments undertaken within this project, deal with the determination of the drag coefficient of fluid muds at concentrations up to 200 g\L using the method of flow deceleration in an annular flume [*Thompson et al.*, 2004]. The purpose of this study is to extend measurements into the region considered dominated by 'fluid mud' (viscous) behavior.

4. Methods

[14] The Lab Carousel (Figure 1), the laboratory equivalent of the Sea Carousel [*Amos et al.*, 1997, 1992], was used in this study. This annular flume is constructed of smooth acrylic and is 2 m in diameter; it has a workable channel width of 0.15 m and a maximum water depth of 0.40 m. A current is generated within the channel by means of a rotating lid, fitted with 8 paddles. The speed of rotation is controlled by an E-track® AC inverter motor controller. The motor is placed upon an hydraulic jack, so the lid can be lifted out of the water while it is still rotating; the flow subsequently decelerates because of the influence of drag over the wetted area. The flume is equipped with two current measurement devices: (1) a one-dimensional class IIIb, Helium-Neon, 10 mW Laser Doppler Velocimeter

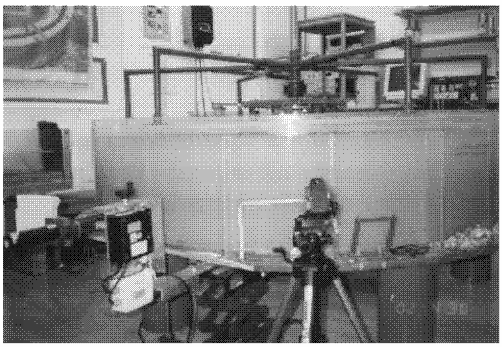

Figure 1. The Lab Carousel: the LDV and the digital camera are shown.

(LDV) that measures the tangential component of the flow velocity at 20 Hz at the channel centre at a height of 0.15 m above the bed and (2) a single point ADV that measures three components of flow (tangential (x), radial (y) and vertical (z)) at a rate of 25 Hz, and a height of ~0.01 m above the flume bed.

[15] It is known that the ADV sensor introduces drag to the flow. However, this drag is measurable, and the effect was determined using the LDV by comparing clear water deceleration rates with and without the intrusive sensors. The flow character and structure of the boundary layer within the Lab Carousel have been studied by *Fung* [1995] under varying flow speeds in clear water and over a smooth (acrylic) bed. *Thompson et al.* [2004] have made an accurate determination of the bed drag coefficient using the flow deceleration method for clear water conditions using the Lab Carousel, and the wall effects on flow have been defined. The drag coefficients for a variety of bed types have been determined in clear water and the effect of the drag of naturally rough beds on the mean bed shear stress has been defined.

[16] *Graham et al.* [1992] measured the radial distribution of bed shear stress in a laboratory annular flume using hot film probes. A very close agreement was found between these sensors and stresses determined from measured velocity profiles using laser Doppler anemometry.

5. Calibration

[17] The assessment of stress reduction is predicated on accurate measurements of flow velocity. Calibration of the velocity sensors was checked by measuring trajectories of particles suspended in the flow, recorded using a digital video camera. The calibration was undertaken with fresh water at room temperature (~18°C), in the Lab Carousel which was filled to a depth of 0.40 m. Prepared neutrally buoyant Goodyear pliolite® particles were added to the water. The white pliolite particles were filmed against a black gridded background for a range of seven current velocities, up to a lid rotational speed of 1.7 m s^{-1}. The camera was focused on the centre of the channel to eliminate those particles influenced by wall effects. The particles were filmed at a height of 0.15 m above the smooth bed to correspond with the height of the LDV sensor. The relationship between lid speed and mean tangential flow velocity is shown in Figure 2.

[18] The optical backscatter sensors were calibrated by taking three 100 mL water samples from the suspension, one for each OBS height. The samples were filtered and dried at 40°C for 24 hours. After weighing, the suspended sediment concentration was determined gravimetrically.

6. Experimental Procedure

[19] The method of flow deceleration was adopted as the standard for estimating the total drag within the flume (wall, bed and internal). The method is based on Newton's second law, in which the deceleration of a flow is proportional to the drag force in a balanced system of constant fluid (sediment) mass. This relationship, if inverted, can be used in the estimation of the bed drag coefficient. It is an integrated method in so far as it is a manifestation of total frictional drag. The flow deceleration method can be used to estimate efficiently and quickly the drag coefficient over a wide range of Reynolds numbers. Two series of flow deceleration measurements were carried out in Lab Carousel: the maximum flow velocity for both was ~1 m/s. The first experimental series used clear, fresh water as controls and standards. A well developed boundary layer ~0.02 m thick was measured for a range of flows over the smooth bed using the LDV [*Thompson et al.*, 2004], and the estimates of drag (C_{D10}) converged with the often quoted value of 3×10^{-3} [*Sternberg*, 1972]. The second series of experiments used fresh water inorganic clay suspensions with concentrations: 0.1, 0.5, 1, 3, 5, 10, 20, 40, 50, 60, 80, 110, 140, 170 and 200 g\L. The procedure was replicated three times for each concentration. Tables 1 and 2 summarize the expected fluid properties of the experiments. Note the fluids tested ranged from "free settling behavior", through to "mobile fluid muds"; the upper limit corresponds to the lower limit of stationary fluid muds which possess yield strength by definition.

[20] X-Ray Diffraction (XRD) analysis showed the clay to be composed mainly of kaolinite, which has a density of 2600 kg m^{-3}. The clay (Table 1) was mixed in 349.7 litres of freshwater to yield a flow depth in the Lab Carousel. of 0.40 m The settling rate of kaolinite clays in fresh water was found by *Srinivas and Mehta* [1989] to be 2×10^{-6}m s^{-1} in

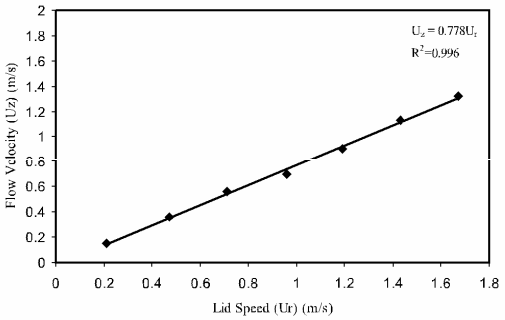

Figure 2. The clear water calibration of the Lab Carousel tangential flow velocity.

Table 1. Clay Concentration and Fluid Density of the Slurries Used to Evaluate Stress Reduction

Concentration, g/L	Total Suspended Clay Mass—Dry, kg	Fluid Density, kg/m^3	Sediment Slurry Behavior
0.1	0.045	1000	Free Settling
0.5	0.23	1000	Free Settling
1	0.45	1001	Floc Settling
3	1.3455	1002	Floc Settling
5	2.22	1003	Floc Settling
10	4.45	1006	Hindered Settling
20	8.90	1012	Hindered Settling
40	17.81	1025	Hindered Settling
50	19.33	1031	Hindered Settling
60	26.71	1037	Hindered Settling
80	28.41	1050	Fluid Mud (mobile)
110	39.79	1068	Fluid Mud (mobile)
140	48.86	1087	Fluid Mud (mobile)
170	59.82	1106	Fluid Mud (stationary)
200	67.71	1125	Fluid Mud (stationary)

the region of hindered settling, under an applied current of 0.05–0.1 m s^{-1}. Sediment settling during flow deceleration is thus considered minimal.

[21] Data were recorded under still water conditions for five minutes to evaluate the electronic offsets of the sensors and to define zero drift (if any). Then the flow velocity was accelerated to a speed of 1 m/s. The flow was maintained at a constant velocity for at least five minutes to ensure complete equalization of the water column (i.e., constant mean flow and steady state) and to eliminate any bubbles that may have formed on the flume walls. The lid was lifted rapidly out of the flow by a hydraulic jack while spinning and the subsequent deceleration of the suspension was recorded by the ADV over the subsequent 30 min. The LDV could not accurately measure flow velocities higher than ~0.35 m/s, so it was used only as confirmation of results at lower flows.

7. Flow Deceleration Method

[22] The method of flow deceleration [*Thompson et al.*, 2004] relates the deceleration of an inviscid fluid of constant and known mass (m) to the drag force (F_D) over rigid wetted boundaries summed over a given time ($\int_0^{\tau} F_D = m \frac{du}{dt}$). In other words, for a constant fluid mass, the flow deceleration gives a measure of the transfer of momentum from the fluid to the rigid boundary across the boundary layer through eddy (inertial) and molecular (viscous) activity. The loss of momentum per unit area (A) per unit time (t) gives a measure of the bed shear stress (τ).

$$F_D = m\frac{du}{dt} = \tau A \tag{2}$$

Table 2. Slurry Behavior for Fresh and Saline Conditions at 10°C

Concentration, g/L	Fresh Fluid Density, kg/m^3	State	Saline (30_{PSU}) Fluid Density, kg/m^3
0	1000	Free Settling	1020
0.3	1001	Floc Settling	1021
10	1006	Hindered Settling	1026
81	1050	Fluid Mud (mobile)	1070
161	1100	Fluid Mud (stationary)	1119
484	1300	Settled Mud	1318

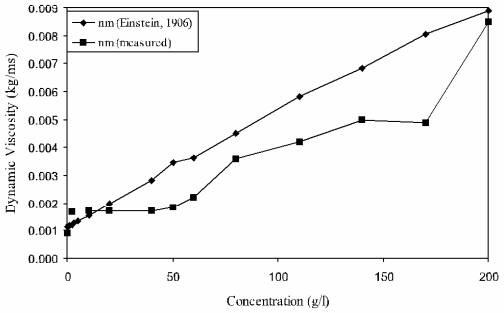

Figure 3. Predicted dynamic viscosity versus the concentration of clay suspensions over the concentration range evaluated in this study.

The Quadratic Stress Law states that:

$$\tau = C_{D(z)}\rho\bar{u}^2 \tag{3}$$

Combining equations (2) and (3) yields a general solution for the drag coefficient where all other variables are measured:

$$C_{D(z)} = \frac{m}{A}\frac{du_z}{dt}\frac{1}{\rho}\frac{1}{\bar{u}_z^2} \tag{4}$$

$\bar{u}$ is the mean time-averaged flow velocity (evaluated over a 1 second time interval) and A is the wetted area or wetted perimeter per unit length (the area of interaction). The drag coefficient is estimated from equation (4) where the change in velocity with time is calculated from the time-averaged flow velocity over a 10 second interval.

8. Estimation of the Drag Coefficient and Bed Shear Stress

[23] For a flat smooth bed the total drag coefficient evaluated for a flow velocity measured at height (z),

Table 3. Mass Concentration, Volume Concentration, and Dynamic Viscosity n_m of Clay Suspensions Used in Experiments[a]

Concentration, g/L	Volumetric Concentration, %	η_m,[b] kg/ms	η_m, kg/ms Measured
0	0	0.00114	0.0009
0.1	0.00377	0.00114	
0.5	0.0189	0.00116	
1	0.0377	0.00118	
2	0.0754	0.00122	0.001691
3	0.113	0.00127	
5	0.188	0.00135	
10	0.376	0.00156	0.001730
20	0.749	0.00199	0.001715
40	1.49	0.00283	0.001732
50	2.05	0.00347	0.00185
60	2.21	0.00365	0.002229
80	2.98	0.00453	0.0036
110	4.12	0.00583	0.0042
140	5.02	0.00684	0.0050
170	6.08	0.00804	0.0049
200	6.82	0.00889	0.00849

[a]For clear water the value of dynamic viscosity at 14°C (0.00114 kg/ms) has been used as a reference.
[b]From *Einstein* [1906].

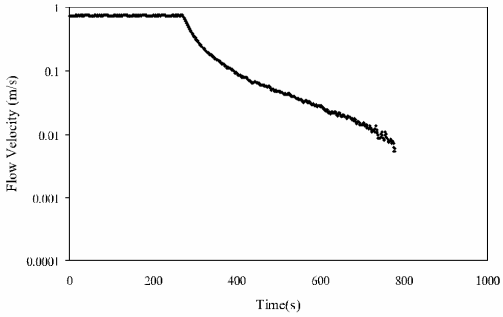

Figure 4. A clear water deceleration time series recorded by the ADV in Lab Carousel.

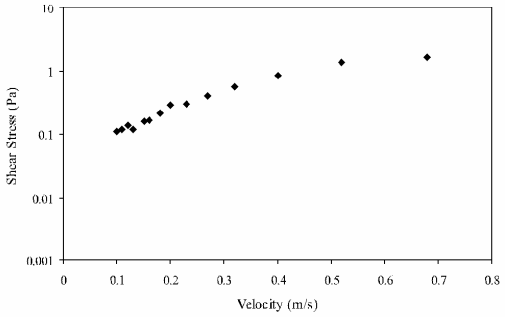

Figure 6. The clear water bed shear stress versus flow velocity for the time series illustrated in Figure 4.

including bed and wall effects $C_{D(z)(total)}$ is given by equation (5). Thus we have:

$$C_{Dz(total)} = \frac{m}{A_{(total)}} \frac{du_z}{dt} \frac{1}{\rho \bar{u}_{tz}^2} \quad (5)$$

where: $A_{(total)}$ is the total wetted area of the flume (5.521 m^2), and $\bar{u}_{tz}$ is the depth-averaged tangential flow velocity. For clear water runs, m = 349.7 kg and ρ = 1000 kg/m^3 at 10°C. For turbid flows, the total mass of the clay-water mixture is calculated as the sum of the water mass (m_w) plus the dry mass of the clay (m_{clay}) in suspension ($m_t = m_w + m_{clay}$,).

[24] The density term (ρ_t) in equation (5) is the bulk density of the clay-water mixture (see Table 1).
Thus the total drag force is:

$$F_{D(total)} = C_{D(z)(total)} \rho_t \bar{u}_z^2 A_{(total)} \quad (6)$$

and it can be considered as the sum of a wall component and a bed component of frictional drag. Thus

$$F_{D(toal)} = F_{D(wall)} + F_{D(bed)}$$

which yields:

$$F_{D(bed)} = F_{D(total)} - F_{D(wall)} \quad (7)$$

where

$$F_{D(bed)} = C_{D(z)(bed)} \rho u_z^2 A_{(bed)} \quad (8)$$

and

$$F_{D(wall)} = C_{D(z)(wall)} \rho u_z^2 A_{(wall)} \quad (9)$$

where $A_{(bed)}$ = 0.872 m^3 and $A_{(wall)}$ = 4.646 m^3. As the bed and walls are composed of the same materials, we assume that: $C_{D(z)} = C_{d(z)(total)}$ [*Thompson et al.*, 2004].For each concentration, the value of $C_{D(z)}$ (for a current measured at z = 0.15 m) is calculated from equation (5) and the bed shear stress τ_o is derived from the formula:

$$\tau_0 = C_{D(z)(bed)} \rho_t U_z^2 \quad (10)$$

[25] The manifestation of drag through deceleration of flow in our flume is influenced by (1) changes in mass, (2) changes in viscosity, (3) changes in roughness, and (4) changes in the hydraulic radius. It is unclear in the literature at present which of these effects dominate the transfer of momentum to the bed for a given level of turbidity and relative bed roughness.

9. Viscosity of Flows

[26] The viscosity of a fluid-sediment mixture (η_m) exhibits a significant deviation from that of clear water for

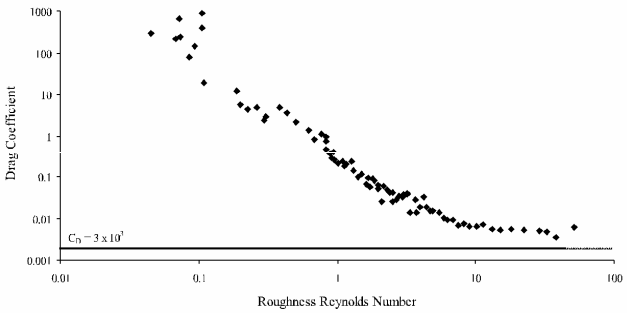

Figure 5. The clear water bed drag coefficient versus the roughness Reynolds number for the time series illustrated in Figure 4.

Table 4. Mean Bed Drag Coefficient Under Various Velocity Ranges Evaluated in the Turbulent Rough Region of Flow

$C_{dx(bed)}$ (Rough)	Drag Reduction,%
0.004983	0
0.004591	7.9
0.004768	4.3
0.004877	2.13
0.005289	−6.14
0.003893	21.9
0.003557	28.6
0.00311	37.6
0.003152	36.7
0.0032	35.8
0.00244	51.0
0.0033	33.8
0.0030	39.8
0.0031	37.8
0.0040	19.7
0.0044	11.7

concentrations higher than about 50 g\L [*van Rijn*, 1993], yet drag reduction takes place well below this level [*Li and Gust*, 2000].

[27] *Einstein* [1906] studied the effect of elastic, spherical particle movements on the viscosity of dilute suspensions with $C_V < 0.1$ (where C_V is the volumetric sediment concentration = volume of sediment/volume of water). He found an increase in dynamic viscosity with increasing concentration (Figure 3) according to the formula:

$$\eta_m = \eta(1 + 2.5C_v) \tag{11}$$

[28] The viscosity of the range of concentrations of the mud samples were measured using an AR1000 TA Instruments Rheometer. A concentric cylinder geometry was used to produce the data and the gap between the cylinders (1500 micrometres) was chosen to limit the effect of the gap on the measurements. The samples were subjected to preshear so that equilibrium data was obtained for all the concentrations considered. Instabilities caused by the formation of Taylor Vortices may be a source of error. Care was taken so that all the measurements were taken at shear rates below the critical Taylor number [*Taylor*, 1923]. The results can be seen in Table 3 and Figure 3. Thus the effect of increasing viscosity on the values of drag coefficient and bed shear stress obtained by Flow Deceleration may be evaluated.

[29] The measurements of viscosity generally parallel those of *Einstein* [1906]. Our results show a progressive divergence with concentration, to about 20% less than those predicted by Einstein. This is likely due to the nature and size of the material in suspension.

10. Results

10.1. Clear Water Flows

[30] An example of decelerating flow recorded by the ADV in the Lab Carousel at h = 0.01 m is shown in Figure 4. The data (logged at 25 Hz) have been averaged over one second to reduce scatter. Figure 5 shows the estimated drag coefficient ($C_{Dz(bed)}$) plotted against the roughness Reynolds number (Re_*, where the roughness length is 0.00045m for acrylic). The evaluation of $C_{D(bed)}$ from this time series decreases with increasing Re in a quadratic fashion to a value of about 0.1 and then tends asymptotically to a constant value of about 0.005. The mean $C_{D0.15}$ value for the turbulent rough flow regime was calculated as 0.005. Figure 6 shows an increase in shear stress with increasing flow velocity, described by the relationship, $\tau = 3.00\ u^2$, $R^2 = 0.88$. The results shown in Figures 5 and 6 support previous observations by *Thompson et al.* [2004].

10.2. Turbid Flows

[31] Fifteen different concentrations of turbid flows were simulated in the Lab Carousel by mixing clay suspensions in fresh water to: 0.1, 0.5, 1, 3, 5, 10, 20, 40, 50, 60, 80, 110, 140, 170 and 200 g/L. The clay-water mixture was accelerated in the Lab Carousel to ~0.8 m/s and then left to decelerate to still water conditions. The flow velocity of the decelerating fluid was recorded by the ADV sensor at a height of ~0.01 m above the flume bed at 25 Hz. The mean value of the bed drag coefficient from these records was calculated as a function of flow velocity (Table 4) for the turbulent rough regime. The investigation of drag reduction is restricted to the drag coefficients in the turbulent regime where C_D may be considered as constant. Within this region, it can be assumed that the eddy diffusivity processes exceed those of shear diffusion [*Leighton and Acrivos*, 1987], which can lead to changes in viscous effects in

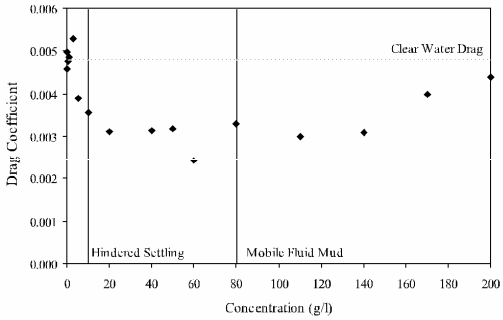

Figure 7. The bed drag coefficient versus concentration evaluated in the rough turbulent region.

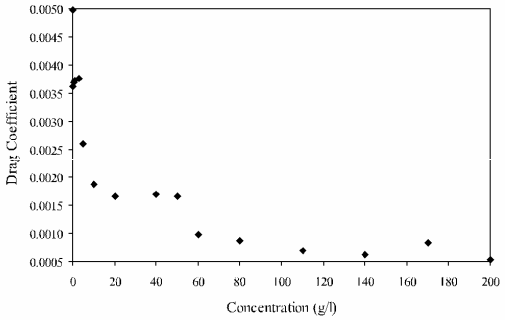

Figure 8. Bed drag coefficient normalized for both mass and viscosity, versus mass concentration.

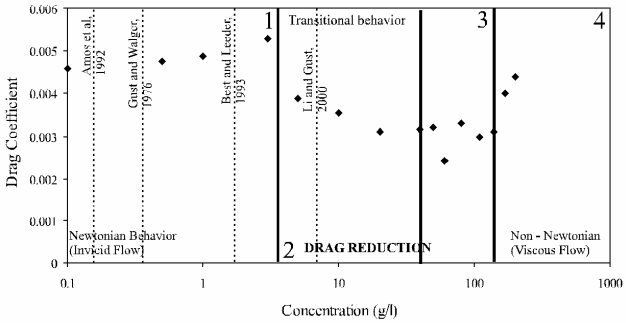

Figure 9. Drag coefficient versus concentration. The solid lines separate the different areas of behavior; the dotted lines show the maximum concentrations reported in the literature.

Couette flow type devices. There is an overall decrease of $C_{D(x)(bed)}$ values with increasing concentration up to approximately 200 g\L, at which point the drag coefficient increases to close to clear water values. The maximum reduction in drag coefficient of 51% suggests that significant drag reduction occurred because of the presence of suspended sediment (Figure 7).

[32] Flow deceleration is linearly related to the change in mass (m, and thus internal momentum) due to changes in concentration (see equation (2)). The increase in fluid/sediment mass of the suspensions has been evaluated and the effects normalised by application of equation (12). The turbidity-reduced C_D values were thus normalised according to the relationship:

$$C_{D(z)(bed)(norm)} = C_{D(z)(bed)}\left(\frac{m_{total}}{m_{water}}\right) \quad (12)$$

where m_{water} = 452 kg is the mass of water in the Lab Carousel and $m_{total} = m_{water} + m_{clay}$.

[33] The normalised values of C_D increase with increasing concentration. The bed drag coefficient was also normalised for changes in fluid viscosity by the relationship:

$$C'_{D(z)(bed)(norm)} = C_{D(z)(bed)}\left(\frac{\eta}{\eta_m}\right) \quad (13)$$

The drag coefficients are lower at high concentrations than in clear water, signifying higher drag reduction (Figure 8).

[34] The maximum drag reduction before the application of equations (12) and (13) appears to fall into four distinct ranges: (1) 0–3 g\L, (2) 5–20, (3) 20–140, and (4) >140g\L (Figure 9). In the first range, C_D appears constant indicating a Newtonian behavior of the dilute suspensions. For range 2 the drag coefficient decreases linearly with increasing concentration – the region of drag reduction. In range 3, the drag is relatively constant and minimum, and in range 4 an increase of the drag to near clear water values and greater occurs. The drag coefficient shows an increasing reduction in drag with increasing concentration after being normalised by both mass and viscosity. The normalised shear stress for velocities of ~0.8 m/s shows the same reduction with increasing concentration (Figure 10). Comparing the normalised and nonnormalised versions of the data allows us to isolate the effects caused by mass and viscosity changes due to increased suspended loads.

11. Discussion

[35] It has been proposed that the presence of fine-grained suspended sediment in flows can significantly change the structure of the boundary layer [*Dyer*, 1986; *Mehta and Dyer*, 1990] increasing the thickness of the viscous sublayer by a factor of 2 to 5 [*Gust*, 1976] Therefore the bed shear stress derived from either velocity profile measurements or the Quadratic Stress Law, based on a single velocity measurement at a fixed height would be overestimated in turbid flows if turbidity effects were not considered [*Gust*, 1976; *Gust and Walger*, 1976]. This has been explained by the existence of drag reduction, which results in the decrease of shear stress in the viscous sublayer relative to the apparent shear stress in the logarithmic layer [*Gust*, 1976; *Best and Leeder*, 1993; *Li and Gust*, 2000]. However, some researchers have found that an increase in friction factors occurs with increased suspended load concentrations [*Yano and Daido*, 1964; *Taggart et al.*, 1972; *Ippen*, 1973; *Lyn*, 1991]. It is this discrepancy which this investigation examines.

[36] The data presented in this paper confirm the occurrence of drag reduction in flows with concentrations of clay in suspension up to 200 g\L. The reduction in bed drag coefficient is shown in Figure 7 and peaks at over 50% of

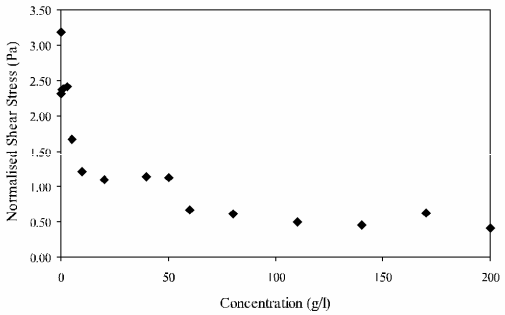

Figure 10. Normalized shear stress versus concentration for a velocity ~0.8 m/s.

the clear water drag values. However, above this concentration, drag enhancement occurs. The effect of drag reduction, while still present, appears to be reduced with increasing suspended sediment concentration, recovering to almost clear water values at maximum concentrations.

[37] Past investigators who discovered only a continuing reduction in drag values with increasing sediment concentrations were working with relatively low sediment concentrations. *Gust and Walger* [1976] used a maximum concentration of only 380 mg\L, and *Best and Leeder* [1993] used a maximum concentration of 2.2 g\L. The present study uses a range of concentrations of up to 200 g\L, which encompasses both phenomena of drag reduction at relatively low suspended concentrations and a drag enhancement at concentrations above 140 g\L.

[38] When the data are normalized to remove the inertial effect of the mass of sediment in suspension and the effect of changing viscosity (measured using a viscometer) on flow deceleration, the drag reduction at concentrations above 140 g\L appears to become more pronounced (Figure 10). This is due to the differences between the way the fluid acts within the viscometer (where it is forced into Laminar flow), and within the flume, where turbulence is free to occur. The large drag reduction over and above the effect of viscosity (which is illustrated when viscosity is accounted for by normalization) shows that at high concentrations there is still a reduction in drag, likely to be caused by turbulence damping, which works in opposition to the effect of increasing viscosity which leads to the appearance of drag enhancement.

[39] The findings of this investigation agree with the findings of *Wang et al.* [1998], who found that above a certain concentration, viscous effects become greater than the drag reduction mechanism masking the drag reduction mechanism.

12. Concluding Remarks

[40] Bed drag coefficient has been shown to respond significantly to an increase in the suspended sediment concentration: (1) a suspended sediment load up to 20 g\L subject to unidirectional channel flow exhibits a reduction of the bed drag coefficient up to 50% when compared to clear water values, (2) at higher concentrations (up to 200 g\L) the effect of drag reduction is masked by an increase in viscous resistance which returns the values of the drag coefficient to close to those of clear water (this is because, as suspended sediment concentrations increase, viscous effects begin to outweigh the drag reduction mechanisms), and (3) when the effect of this viscous resistance is removed by normalization, a reduction of drag by turbulence damping is evident.

[41] **Acknowledgment.** This paper was produced as part of the Centre for Coastal Processes, Engineering and Management (CCPEM) contribution to the EU-funded EuroStrataform project (EVK3-2001-00079) and was supported in part by a CORILA grant (Linea 3.15) to the second author.

References

Amos, C. L., J. Grant, G. R. Daborn, and K. Black (1992), Sea Carousel—A benthic, annular flume, *Estuarine Coastal Shelf Sci.*, *34*, 557–577.

Amos, C. L., T. Feeney, T. F. Sutherland, and J. L. Luternauer (1997), The stability of fine-grained sediments from the Fraser River delta, *Estuarine Coastal Shelf Sci*, *45*, 507–524.

Best, J. L., and M. R. Leeder (1993), Drag reduction in turbulent muddy seawater flows and some sedimentary consequences, *Sedimentology*, *40*, 1129–1137.

Cloutier, D., C. L. Amos, P. R. Hill, and K. Lee (2002), Oil erosion in an annular flume by seawater of varying turbidities: A critical bed shear stress approach, *Spill Sci. Technol. Bull.*, *8*, 83–93.

Dyer, K. R. (1986), *Coastal and Estuarine Sediment Dynamics*, 342 pp., John Wiley, Hoboken, N. J.

Einstein, A. (1906), Calculation of the viscosity-coefficient of a liquid in which a large number of small spheres are suspended in irregular distribution, *Ann. Phys.*, *19*, 286–306.

Fortier, S., and F. C. Scobey (1926), Permissible canal velocities, *Trans. Am. Soc. Chem. Eng.*, *89*, 940–956.

Fung, A. (1995), Accurate calibration measurements of flow in Lab Carousel under varying lid rotations, contract 23420–5–M083/01–HAL, *Geol. Surv. of Can.*, Halifax, N. S., Canada.

Graham, D. I., P. W. James, T. E. R. Jones, J. M. Davies, and E. A. Delo (1992), Measurement and prediction of surface shear-stress in annular flume, *J. Hydraul. Eng.*, *118*, 1270–1286.

Grant, W. D., A. J. Williams, and S. M. Glenn (1984), Bottom estimates and their prediction on northern California continental shelf during CODE-1: The importance of wave-current interaction, *J. Phys. Oceanogr.*, *14*, 506–527.

Gust, G. (1976), Observations on turbulent-drag reduction in a dilute suspension of clay in sea-water, *J. Fluid Mech.*, *75*, 29–47.

Gust, G., and E. Walger (1976), The influence of suspended cohesive sediments on boundary-layer structure and erosive activity of turbulent sea-water flow, *Mar. Geol.*, *22*, 189–206.

Hunt, J. N. (1954), Turbulent transport of suspended sediment in open channel, *Proc. R. Soc. London, Ser. A*, *224*, 322–335.

Ippen, A. T. (1973), Transport of suspended sediment, paper presented at International Seminar on Hydraulics of Alluvial Streams, Int. Assoc. Hydraul. Res., New Delhi, India.

Khullar, N. K., U. C. Kothyari, and K. G. Ranga Raju (2002), The effect of suspended sediment on flow resistance, paper presented at 5th International Conference on Hydro-Science and Engineering, Warsaw Univ. of Technol., Warsaw, Poland.

Komar, P. D. (1985), The hydraulic interpretation of turbidites from their grain sizes and sedimentary structures, *Sedimentology*, *32*, 395–407.

Leighton, D., and A. Acrivos (1987), The shear-induced migration of particles in concentrated suspensions, *J. Fluid Mech.*, *181*, 415–439.

Li, M. Z., and G. Gust (2000), Boundary layer dynamics and drag reduction in flows of high cohesive sediment suspensions, *Sedimentology*, *47*, 71–86.

Lyn, D. A. (1991), Resistance in flat-bed sediment-laden flows, *J. Hydrau. Eng.*, *117*, 94–114.

Mehta, A. J., and K. R. Dyer (1990), Cohesive sediment transport in estuarine and coastal waters, in *The Sea*, vol. 9, edited by B. Le Mehaute, and D. M. Hanes, pp. 815–839, John Wiley, Hoboken, N.J.

Pantin, H. M., and M. R. Leeder (1987), Reverse flow in turbidity currents: The role of internal solitons, *Sedimentology*, *34*, 1143–1155.

Soulsby, R. L. (1983), The bottom boundary layer of shelf seas, in *Physical Oceanography of Coastal and Shelf Seas*, edited by B. Johns, pp. 189–266, Elsevier, New York.

Srinivas, R., and A. J. Mehta (1989), Observations on estuarine fluid mud entrainment, *Int. J. Sediment Res.*, *15*, 15–22.

Sternberg, R. W. (1972), Predicting initial motion and bedload transport of sediment particles in the shallow marine environment, in *Shelf Sediment Transport*, edited by D. J. P. Swift, D. B. Duane, and O. H. Pilkey, pp. 61–82, Van Nostrand Reinhold, Hoboken, N. J.

Taggart, W. C., C. A. Yermoli, S. Montes, and A. T. Ippen (1972), Effects of fine sediments on flow phenomenon, *U.S. Geol. Surv. Water Supply Pap., 1498G*.

Taylor, G. I. (1923), Stability of a viscous liquid contained between two rotating cylinders, *Philos. Trans. R. Soc., Ser. A*, *223*, 289–343.

Thompson, C. E. L., C. L. Amos, M. Lecouturier, and T. E. R. Jones (2004), Flow deceleration as a method of determining drag coefficient over roughened flat beds, *J. Geophys. Res.*, *109*, C03001, doi:10.1029/2001JC001262.

van Rijn, L. C. (1993), *Principles of Sediment Transport in Rivers, Estuaries and Coastal Seas*, 715 pp., Aqua, Amsterdam, Netherlands.

Virk, P. S. (1971), Drag reduction in rough pipes, *J. Fluid Mech.*, *45*, 225–246.

Wang, Z. Y., P. Larsen, F. Nestmann, and A. Dittrich (1998), Resistance and drag reduction of flows of clay suspensions, *J. Hydraulic Engineering*, *124*, 41–49.

Yano, K., and A. Daido (1964), Fundamental study on mud flow (i) to (ii), *Bull Disaster Prev. Inst.*, *14*, 69–83.

C. L. Amos, M. Angelaki, C. E. Binks, and C. E. L. Thompson, School of Ocean and Earth Science, National Oceanography Centre, Southampton SO14 3ZH, UK. (celt1@noc.soton.ac.uk)

T. E. R. Jones, School of Mathematics and Statistics, Plymouth University, 2 Kirkby Place, Drake Circus, Plymouth PL4 8AA, UK.

References

Abbot, J.E. and Francis, J.R.D., (1977). Saltation and suspension trajectories of solid grains in water streams. *Phil. Trans. R. Soc. Lond.*, **A 284**, 225-54.

Agrawal, Y.C., and Belting, C.J., (1988). Laser velocimetry for benthic sediment transport. *Deep-Sea Res.*, **35**, 1047-1067.

Akan, A.O., (2001). Tractive force channel design aid. *Can. J. Civ. Eng.*, **28**(5), 865-867.

Allen, J.R.L., (1977). *Physical processes of sedimentation*. London: 248 pp.

Allen, J.R.L., (1985). *Principles of Physical Sedimentology*. George Allen &Unwin Ltd., United Kingdom.

Amos, C.L. and Greenberg, D.A., (1980). The simulation of suspended particulate matter in the Minas Basin, Bay of Fundy - a region of potential tidal power development. In: *Proceedings of Canadian Coastal Conference*, 2-20.

Amos C.L., Grant J., Daborn G.R., and Black K., (1992). Sea Carousel - A benthic, annular flume. *Estuarine Coastal and Shelf Science*, **34** (6), 557-577.

Amos, C.L., Sutherland, T.F., and Zevenhuizen, J., (1996). The stability of sublittoral, fine-grained sediments in a subarctic estuary. *Sedimentology*, **43**, 1-19.

Amos C.L., Feeney T., Sutherland T.F., and Luternauer J.L., (1997). The stability of fine-grained sediments from the Fraser River delta. *Estuarine Coastal and Shelf Science*, **45** (4), 507-524.

Amos, C.L., Li, M.Z. and Sutherland, T.F., (1998). The contribution of ballistic momentum flux to the erosion of cohesive beds by flowing water. *Journal of Coastal Research*, **14** (2), 564-569.

Amos, C.L., Sutherland, T.F., Cloutier, D. and Patterson, S., (2000). The impact of saltating littorinid shells on the erosion of subaquaeous cohesive beds. *Continental Shelf Research*, **20**, 1291-1315.

Amos, C.L., Droppo, I.G., Gomez, E.A., and Murphy, T.P., (2003). The stability of a remediated bed in Hamilton Harbour, Lake Ontario, Canada. *Sedimentology*, **50**, 149-168.

Bagnold, R.A., (1954). Experiments on a gravity-free dispersion of large solid spheres in a Newtonian fluid under shear. *Philosophical Transactions of the Royal Society London (A)*, **225**, 49-63.

Bagnold, R.A., (1955). Some flume experiments on large grains but little denser than the transporting fluid and their implications. *Proc. Instn Civ. Engrs,* **4**, 174-205.

Bagnold, R.A., (1966). An approach to the sediment transport problem from general physics. *USGS Professional Paper*, 422-I: 37p.

Bagnold, R.A., (1973) The nature of saltation and of 'bed-load' transport in water. *Phil. Trans. R. Soc. London*, A **332**, 473-504.

Best, J.L., and Leeder, M.R., (1993). Drag reduction in turbulent muddy seawater flows and some sedimentary consequences. *Sedimentology*, **40** (6), 1129-1137.

Bogue, D.C., and Metzner, A.B., (1963). Velocity profiles in turbulent pipe flow. *Industrial and Engrg. Chem. Fund*., **2**, 143.

Bowden, K.F., (1962). Turbulence. In: *'The Sea: Ideas and Observations'* (M.N. Hill, ed.), Vol. III, Interscience, New York.

Burt, T.N., and Game, A.C., (1985). The carousel: Commissioning of a circular flume for sediment transport research. Rep. SR 33, Hydraulic Res., Wallingford, UK.

Caldwell, D.R., and Chriss, T.M., (1979). The viscous sublayer at the sea floor. *Science*, **205**, 1131-1132.

Carder, K.L., Steward, R.G. and Betzer, P.R., (1982). In-situ holographic measurements of the sizes and settling rates of oceanic particulates. *J. Geophys. Res.*, **87**, 5681-5685.

Cloutier, D., LeCouturier, M.N., Amos, C.L., and Hill, P.R., (2003). The effects of suspended sediment concentration on the structure of turbulence in a rotating circular flume. Special issue *Journal of Ecological Progress*.

Coleman, N., (1981). Velocity profiles with suspended sediment. *Journal of Hydraulic Research*, **19**(3), 211-229.

Downing, J.P., (1983). An optical instrument for monitoring suspended particulates in ocean and laboratory. In: *Proceedings of Oceans*, **83**, 199-202.

Dyer, K.R., (1980). Velocity profiles over a rippled sand bed and the threshold of movement of sand. *Estuarine Coastal Mar. Sci*., **10**, 181-199.

Dyer, K.R., (1986). *Coastal and Estuarine Sediment Dynamics*. John Wiley and Sons, Chichester.

Dyer, K.R., (1989) Sediment processes in estuaries: future research requirements. *Journal of Geophysical Research*, **94**C, 14327-39.

Einstein, A., (1906). Eine neue Bestimmung der Molekul dimensionen. *Annalen der Physiek*, Leipzig (4), 19.

Eisma, D., Dyer, K.R. & van Leussen, W., (1997). The in situ determination of the settling velocities of suspended fine-grained sediment-a review. In: *Cohesive Sediments* (eds N. Burt, R. Parker & J. Watts), 17-44. Wiley, New York.

Fortier, J.R. and Scobey, F.C., (1926). Permissible canal velocities. *Trans. Am. Soc. Civ. Eng*., **89**, 940-984.

Francis, J.R.D., (1973). Experiments on the motions of solitary grains along the bed of a water stream. *Proc. R. Soc. London*, **A332**, 443-471.

Fukuda, M.K., (1978). The entrainment of cohesive sediments in fresh water. Ph.D. Dissert., Case Western Reserve Univ., Cleveland, OH.

Fung, A., (1995). Accurate calibration measurements of flow in Lab Carousel under varying lid rotations. Contract No. 23420-5-M083/01-HAL. Halifax, N.S.

Gore, R. A., and Crowe, C. T., (1989). Effect of particle size on modulating turbulent intensity. Int. *J. Multiphase Flow*, **15**, 279-285.

Graf, E.H., (1971). *Hydraulics of sediment transport*. McGraw-Hill Book Co., Inc., New York, 513 pp.

Graham, D.I., James, P.W., Jones, T.E.R., Davies, J.M., and Delo, E.A., (1992). Measurement and prediction of surface shear-stress in annular flume. *Journal of Hydraulic Engineering - ASCE*, **118** (9), 1270-1286.

Graham, D.I., (2000). Turbulence attenuation by small particles in simple shear flows. *Journal of Fluids Engineering Transactions of the ASME*, **122** (1), 134-137.

Grant, W.D., and Madsen, O.S., (1979). Combined wave and current interaction with a rough bottom. *J. Geophys. Res*., **84**, 1797-1808.

Grant, W.D., and Madsen, O.S., (1982). Movable bed roughness in unsteady oscillatory flow. *J. Geophys. Res.*, **87**, 469-481.

Grant, W.D., Williams, A.J. & Glenn, S.M., (1984). Bottom stress estimates and their prediction on the northern California continental shelf during CODE-1: the importance of wave-current interaction. *J. Phys. Oceanogr.*, **14**, 506-527.

Grass, A.J., (1971). Structural features of turbulent flow over smooth and rough boundaries. *J. Fluid Mech*., **50**, 233-55.

Gratiot, N., Mory, M., and Auchere, D., (2000). An acoustic Doppler velocimeter (ADV) for the characterisation of turbulence in concentrated fluid mud. *Continental Shelf Research*, **20**, 1551-1567.

Green, M.O., Rees, J.M., and Pearson, N.D., (1990). Evidence for the influence of wave-current interaction in a tidal boundary layer. *J. Geophys. Res*., **95**, 9629-9644.

Green, M.O., and McCave, I.N., (1995). Seabed drag coefficient under tidal currents in the eastern Irish Sea. *Journal of Geophysical Research*, **100**, NO.C8, 16057-16069.

Gust, G., (1976). Observations on turbulent-drag reduction in a dilute suspension of clay in sea-water. *J. Fluid Mech.*, **75**, 29-47.

Gust, G. and Walger, E., (1976). The influence of suspended cohesive sediments on boundary-layer structure and erosive activity of turbulent sea-water flow. *Mar. Geol.*, **22**, 189-206.

Hesse, R. and Chough, S.K., (1980). The Northwest Atlantic Mid-Ocean Channel of the Labrador Sea: II. Deposition of parallel laminated leveemuds from the viscous sublayer of low density turbidity currents. *Sedimentology*, **27**, 697-711.

Hou, H., and Yang, X., (1983). Effect of fine sediment on the drag reduction in muddy flow. *Proc., 2nd Int. Symp. On River Sedimentation, Water Resources and Power Press*, Beijing, China, 47-80.

Hughes, W.F., and Brighton, J.A., (1967). *Fluid Dynamics*. New York: McGraw-Hill Book Company.

Hunt, J.N., (1954). The turbulent transport of sediment in open channels. *Proc. R. Soc. London*, **A224**, 322-335.

Huntley, D.A., Nicholls, R.J., Liu, C., and Dyer, K.R., (1994). Measurements of semi-diurnal drag coefficient over sand waves. *Continental Shelf Research*, **14**, 437-456.

Ippen, A.T., (1971). A new look at sedimentation in turbulent streams. *J. Boston Soc. Civ. Engrs*, **58**, 131.

James, A.E., and Williams, D.J.A., (1982). Flocculation and rheology of kaolinite/quartz suspensions. *Rheol. Acta*, **21**, 176-183.

Jeffreys, D.J., (1982). Aggregation and break-up of clay flocs in turbulent flow. *Advances in Colloid and Interface Science*, **17**, 213-18.

Jin, Y.C., Zarrati, A.R., Zheng, Y., (2004). Boundary shear distribution in straight ducts and open channels. *Journal of Hydraulic Engineering*, **130**(9), 924-928.

Kamphuis, J.W., (1983). Influence of sand or gravel on the erosion of cohesive sediment. *Canadian Journal of Civil Engineering*, **10**(2), 223-231.

Kamphuis, J.W., (1990). Influence of sand or gravel on the erosion of cohesive sediment. *Journal of Hydraulic Research*, **28**(1), 43-53.

Khiadani, M.H., Beecham, S., Kandasamy, J., Sivakumar, S., (2005). Boundary shear stress in spatially varied flow with increasing discharge. *Journal of Hydraulic Engineering*, **131**(8), 705-714.

Kirby, R. & Parker, W.R., (1983). Distribution and behavior of fine sediment in the Severn Estuary and Inner Bristol Channel, UK. *Canadian Journal of Fisheries and Aquatic Sciences*, **40**, 83-95.

Komar, P.D., (1976). Boundary layer flow under steady unidirectional currents. In: Stanley, D.J., Swift, D.J.P. (Eds.), *Marine sediment transport and environmental management.* John Wiley, New York.

Komar, P.D., (1985). The hydraulic interpretation of turbidites from their grain sizes and sedimentary structures. *Sedimentology*, **32**, 395-408.

Komatina, D., and Jovanovic, M., (1997). Experimental study of steady and unsteady free surface flows with water-clay mixtures. *Journal of Hydraulic Research*, **35**, NO. 5, 579-590.

Lee, D.I., (1969). The viscosity of concentrated suspensions. *Trans. of the Soc. of Rheology*, 13 no.2, 273-288.

Leeder, M., (1999). *Sedimentology and Sedimentary basins: From Turbulence to Tectonics.* Blackwell Science, Oxford.

van Leussen, W., (1997). The Kolmogorov microscale as a limiting value for the floc sizes of suspended fine-grained sediments in estuaries. In: *Cohesive Sediments* (eds N. Burt, R. Parker & J. Watts), 45-62. Wiley, New York.

Li, M.Z. and Gust, G., (2000). Boundary layer dynamics and drag reduction in flows of high cohesive sediment suspensions. *Sedimentology*, **47** (1), 71-86.

Lohrmann, A., Cabrera, R., and Kraus, N.C., (1994). Acoustic-Doppler velocimeter (ADV) for laboratory use. *Proc. Conf. On Fundamentals and Advancements in Hydraulic Measurements and Experimentation*, Buffalo, NY, American Society of Civil Engineers, 351-365.

Ludwick, J.C., (1975). Variations in boundary drag coefficient in the tidal entrance to Chesapeake Bay, Virginia. *Marine Geology*, **19**, 19-28.

Lyn, D.A., (1991). Resistance in flat-bed sediment-laden flows. *Journal of Hydraulic Engineering - ASCE*, **117** (1), 94-114.

Maa, J.P.-Y., (1990). The bed shear stress of an annular sea-bed flume. In: *Estuarine Water Quality Management, Monitoring, Modelling and Research* (ed. W. Michaelis), Coastal and Estuarine Studies, 36, Springer-Verlag, Berlin.

Maa, J.P.-Y., Wright l.D., Lee, C.-H., and Shannon T.W., (1993). VIMS Sea Carousel - A field instrument for studying sediment transport. *Marine Geology*, **115** (3-4), 271-287.

Maa, J.P.-Y., Lee, C.-H., and Chen F.J., (1995). Bed shear stress measurements for VIMS Sea Carousel. *Marine Geology*, **129**, 129-136.

Maa, J.P.-Y., (2001). Discussion on the article 'Numerical modelling of flow characteristics in a rotating annular flume' by Yang, Z., Baptista, A., Darland, J. [Dyn. Atmos. Oceans 31 (2000) 271-294]. *Dynamics of Atmospheres and Oceans*, **33**, 321-323.

Maude, A.D. and Whitmore, R.L., (1958). A generalised theory of sedimentation. *Brit. J. Appl. Phys*., **9**, 477-482.

McCave, I.N., (1973). Some boundary layer characteristics of tidal currents bearing sand in suspension. *Mem. Soc. Roy. Sci. Liege*, 6th Ser., **6**, 187-206.

McCave, I.N. and Swift, S.A., (1976). A physical model for the rate of deposition of fine-grained sediments in the deep sea. *Bull. Geol. Soc. Am.,* **87**, 541-546.

McCave, I.N., (1979). Suspended sediment. In: Dyer, K.R. (Ed.), *Estuarine Hydrography and Sedimentation*, Cambridge University Press, Cambridge, 131-185.

McCave, I.N., (1984). Erosion, transport and deposition of fine-grained marine sediments. In: *Fine-Grained Sediments: Deep Water Processes and Facies* (Ed. by D.A.V. Stow and D.J.W. Piper), *Spec. Publ. Geol. Soc. London,* **15**, 35-69.

Mehta, A.J., (1989) On estuarine cohesive sediment suspension behaviour. *Journal of Geophysical Research*, **94**, 14303-14.

Mehta, A.J. and Dyer, K.R., (1990). Cohesive sediment transport in estuarine and coastal waters. In: *Sea*, vol. **9** (Eds B. Le Mehaute and D.M. Hanes), 815-839. John Wiley and Sons, Chichester.

Mehta, A.J. and Li, Y., (1998). Principles and process-modelling of cohesive sediment transport. University of Florida.

Metzner, A.B., (1961). In: V.L. Streeter (Editor), *Handbook of Fluid Dynamics*. McGraw-Hill, New York, N.Y.

Migniot, C., (1968). Etudes proprietes physique de differer sediments tres fins et de leur comportement sous des action hydrodynamiques. *Houille Blanche,* **23**, 591-620.

Nezu, I., and Rodi, W., (1986). Open channel flow measurements with a laser Doppler anemometer. *J. Hydraul. Eng*., **112**, 335-355.

Nikuradse, J., (1950). Laws of flow in rough pipes. *Nat. Advisory Comm. Aeronautics, Tech. Mem.*, **1292**, 1-62.

Nowell, A.R.M., McCave, I.N., Hollister, C.D., (1985). Contributions of HEBBLE to understanding marine sedimentation. *Marine Geology*, **66**, 397-409.

Odd, N.V.M., (1982). The feasibility of using mathematical models to predict sediment transport in the Severn Estuary. In: *The Severn Barrage*, Thomas Telford Ltd, London, 195-202.

Owen, M.W., (1970). A detailed study of settling velocities of an estuary mud. *Hydraulics Research Station, Report INT 78*.

Owen, M.W., (1971). The effect of turbulence on the settling velocities of silt flocs. *Proc. 14th Cong. Int.Ass. Hydraul. Res.*, 27-32.

Pantin, H.M.P. & Leeder, M.R., (1987). Reverse flow in turbidity currents: the role of internal solitons. *Sedimentology*, **34**, 1143-55.

Partheniades, E. and Paaswell, R.E., (1970). Erodibility of channels with cohesive boundary. *Proc. Am. Soc. Civ. Eng., J. Hydraul. Div.*, **96**, 755-771.

Partheniades, E., (1986). A fundamental framework for cohesive sediment dynamics. In: *Estuarine Cohesive Sediment Dynamics* (ed. Mehta A.J.), Lecture Notes on Coastal and Estuarine Studies, 14, Springer-Verlag, New York.

Paterson, D.M., (1997) Biological mediation of sediment erodibility: ecology and physical dynamics. In: *Cohesive Sediments* (eds N. Burt, R. Parker & J. Watts), 215-29. Wiley, New York.

Radin, I., Zakin, J. & Patterson, G.K., (1973). Drag reduction of solid-liquid suspensions in pipe flow. *Nature*, **246**, 11.

Richardson, J.F. & Zaki, W.N., (1958) Sedimentation and fluidization. *Transactions Institute of Chemical Engineers*, **32**, 35-53.

Schlichting, H., (1951). *Boundary-Layer Theory*. New York: McGraw-Hill.

Schlichting, H., (1979). *Boundary Layer Theory*. McGraw-Hill, New York.

Shames, I., (1962). *Mechanics of Fluids*. McGraw-Hill Book Company, New York.

Simpson, J.E., (1997). *Gravity currents in the environment and the laboratory*. Second edition, Cambridge University Press.

Sleath, J.F.A., (1984) *Sea Bed Mechanics*. Wiley, New York.

Smith, J.D., and McClean, S.R., (1977). Boundary layer adjustments to bottom topography and suspended sediment. In: *Bottom Turbulence, Proceedings of the 8th International Liege Colloquium on Ocean Hydrodynamics*, Nihoul, J.C.J. (ed.), 123-151, Elsevier, Amsterdam.

Soulsby, R.L., (1980). Selecting record length and digitisation rate for near bed turbulence measurements. *Journal of Physical Oceanography*, **10**, 208-219.

Soulsby, R.L., (1983). The bottom boundary layer of shelf seas. In: Johns, B. (Ed.), *Physical Oceanography of Coastal and Shelf Seas*, Elsevier Oceanography Series, **35**, Amsterdam, Ch.5B.

Soulsby, R.L., and Humphrey, J.D., (1989). Field observations of wave and current interaction at the sea bed. In: Torum, A. (Ed.), *Proc. Of NATO Advanced Research Workshop of Water Wave* Kinematics, Norway, Pub. B. V., Dordrecht, The Netherlands.

Soulsby R.L., Atkins R., Salkield A.P., (1994). Observations of the turbulent structure of a suspension of sand in a tidal current. *Continental Shelf Research*, **14** (4), 429-435.

Sternberg, R.W., (1968). Friction factors in tidal channels with differing bed roughness. *Marine Geology*, **6**, 243-260.

Sternberg, R.W., (1972). Predicting initial motion and bedload transport of sediment particles in the shallow marine environment. In Swift, D.J.P., Duane, D.B. and Pilkey, O.H. (Eds), *Shelf Sediment Transport: Process and Pattern*, Dowden, Hutchinson and Ross, Stroudsburg, 61-82.

Sternberg, R.W., Kineke, G.C., Johnson, R., (1991). An instrument system for profiling suspended sediment, fluid, and flow conditions in shallow marine environments. *Continental Shelf Research*, **11**(2), 109-122.

Stow, D.A.V. and Bowen, A.J., (1980). A physical model for the transport and sorting of fine-grained sediment by turbidity currents. *Sedimentology*, **27**, 31-46.

Tennekes, H. and Lumley, J.L., (1971). *A first course in turbulence*. MIT Press, Cambridge, Mass.

Tennekes, H., (1973). The logarithmic wind profile. *J. Atmos. Sci*., **30**, 234-238.

Terwindt, J.H.J., Breusers, H.N.C. & Svasek, J.N., (1968). Experimental investigation on the erosion-sensitivity of a sand-clay lamination. *Sedimentology*, **11**, 105-114.

Thompson, C.E.L., Amos, C.L., Jones, T.E.R. and Chaplin, J., (2003). The manifestation of fluid-transmitted bed shear stress in a smooth annular flume - a comparison of methods. *Journal of Coastal Research*, **19**(4), 1094-1103.

Thompson, C.E.L., Amos, C.L., Lecouturier, M., and Jones, T.E.R., (2004). Flow deceleration as a method of determining drag coefficient over roughened flat beds. *Journal of Geophysical Research*, **109**, C03001, doi: 10.1029/2001JC001262.

Thompson, C.E.L., Amos, C.L., Angelaki, M., Jones, T.E.R, Binks, C.E., (2006). An evaluation of bed shear stress under turbid flows. *Journal of Geophysical Research*, **111**, C04008, doi: 10.1029/2005JC003287.

Toms, B.A., (1948). Some observations on the flow of linear polymer solutions through straight tubes at large Reynolds numbers. *Proc., 1st Int. Congr. on Rheology*, Vol.**II**, 135-141.

Van Rijn, L.C., (1993). *Principles of sediment transport in rivers, estuaries and coastal seas.* Aqua Publications.

Van Tassell, J., (1981). Silver abyssal plain carbonate turbidite; flow characteristics. *J. Geol.*, **89**, 317-333.

Virk, P.S., (1971). An elastic sublayer model for drag reduction by dilute solutions of linear macromolecules. *J. Fluid Mech*., **45**, 417.

Wan, Z., (1982). Bed material movement in hyperconcentrated flows. *Inst. Hydrodynamics and Hydraulic Eng., Tech. Univ. Denmark. Series Paper*, **31**.

Wang, Z.Y., Larsen P., Nestmann F., and Dittrich A., (1998). Resistance and drag reduction of flows of clay suspensions. *Journal of Hydraulic Engineering - ASCE*, **124** (1), 41-49.

Whitehouse, U.G., Jeffrey, L.M. and Debrecht, J.D., (1960). Differential settling tendencies of clay minerals in saline waters. *Proc. 7th Conf. Clays Clay Mins.*, 1-79.

Widdows, J., Brinsley, M.D., Salkeld, P.N., and Elliot, M., (1998). Use of annular flumes to determine the influence of current velocity and bivalves on material flux at the sediment-water interface. *Estuaries*, **21**(4A), 552-559.

Winterwerp, J.C., Cornelisse, J.M., and Kuiper, C., (1991). The behaviour of mud from the Western Scheldt under tidal conditions. Delf Hydraulics, The Netherlands, Rep. Z161-37/HW/paper 1wm, 14pp.

de Wit, P., and Kranenburg, C., (1996). On the effects of a liquefied mud bed on wave and flow characteristics. *Journal of Hydraulic Research*, **34**(1), 3-18.

Wood, W.H., Granquist, W.T., and Krieger, I.M., (1955). Viscosity studies on dilute clay mineral suspensions. In *Proceedings 1st-15th, 1952-1966 National Conference on Clays and Clay Minerals,* Pergamon Press 456: 240-250.

Yalin, M.S., (1972). *Mechanics of sediment transport*, 290 pp., Pergamon Press, Oxford.

Yang, Z., Baptista, A., Darland, J., (2000). Numerical modelling of flow characteristics in a rotating annular flume. *Dynamics of Atmospheres and Oceans*, **31**, 271-294.

Young, R.N. and Southard, J.B., (1978). Erosion of fine-grained marine sediments: Sea floor and laboratory experiments. *Geological Society of American Bulletin*, **89**, 663-672.

Zandi, I., (1967). Decreased heat losses in raw water conduits. *J. Am. Waterworks Ass.*, **59**, 213.